Ultrasound imaging in joint and soft tissue inflammation

A thesis submitted for the degree of Doctor of Philosophy
in the Faculty of Medicine of the University of Glasgow

by

©Péter Vince Bálint M.D.

July 2002

Centre for Rheumatic Diseases, University Department of Medicine,
Glasgow Royal Infirmary, University of Glasgow

Acknowledgments

I am deeply indebted to the expertise of my supervisor Professor Roger D Sturrock. He has instilled a level of professionalism in my scientific research that I will carry with me in my future scientific career. It has been a privilege to be a part of the Centre for Rheumatic Diseases for the past few years. During my residency in Scotland I had the opportunity to establish with Professor Sturrock and with the financial help of the McLeod Bequest the first ultrasound laboratory in a Rheumatology Department in the United Kingdom. I hope this dedicated musculoskeletal ultrasound lab will flourish even further in the future. I also hope that we can maintain our links through collaborative projects for the benefit of our patients and nations.

During my Ph.D. work we built up a close relation with the Centre for Ultrasonic Engineering at the University of Strathclyde. Professor Gordon Hayward was always open to new ideas and introduced me to the fantastic scene of ultrasound engineering. I also would like to say thank you for his colleagues' support, especially to Stephen Kelly and Walter Galbraith for their help in the every day problems. I also hope that eventually we will be overcome the problem of observer variation for scanning healthy, normal and rheumatoid hands with our current research and we can build up a new water-bath hand scanner with collaboration not only between Glasgow and Budapest but also with the medical physics and medical engineering expertise of Professor Norman McDicken at University of Edinburgh.

In Budapest I have enjoyed the invaluable support of Lajos Patonay and Professor Miklós Réthelyi during the preparation of the anatomical sections and hopefully this high quality work will be published not only in my thesis but also as a separate chapter in a new rheumatological musculoskeletal ultrasound book. In Glasgow John Shaw-Dunn helped us with enthusiasm in our airborne ultrasound study. For this research he supplied us with an articulated bony hand specimen.

Dr David Kane was my "special student" during my Ph.D. course. David, your questions inspired me to think over and over again the potential of ultrasonography in rheumatology research. We worked shoulder to shoulder to finish more studies. Thank you for all your efforts. I am also grateful to my other colleagues especially to Max Field, Iain McInnes and Hilary Wilson who requested many ultrasound scans not for research but for diagnostic purposes and for a higher level of care of their patients.

I worked in close contact with Bill Ferrell, Colin Egan and John Lockhart in the power Doppler study. Bill was always ready to help with statistics during my planning and writing up period of this thesis and I learned many interesting facts from Bill not only about laser Doppler but statistics as well.

A special thanks to Alastair Gracie, Dániel Feszty and Andy Jenkins for their technical advice in computing and picture editing and to Colin Perry who kindly allow his recently accepted Ph.D. thesis's structure as a guide for my thesis.

John Fleming who worked in the past with Ian Donald in Glasgow and who is now the Curator of the Historical Collection of BMUS (The British Medical Ultrasound Society) was kind enough to provide me with historical papers about Glasgow's contribution to medical ultrasonography.

The Robertson Centre for Biostatics helped with statistical guidance in the first study of observer variation, also special thanks to the librarians who were always very helpful at the University of Glasgow Library and at the Royal Infirmary Library.

I highly appreciate the support of my home country Hungary and my principals at the National Institute of Rheumatology and Physiotherapy especially to Ágnes Megyeri, Géza Bálint, Zsolt Balogh, László Hodinka and Gyula Poór.

I am also grateful to my radiologist colleagues especially to Károly Földes, Pál N Kaposi and Alistair W Forrester; they fostered my love of musculoskeletal ultrasonography.

Finally, I want to thank my parents Elvira and Géza for their infinite support throughout my career, and to my wife Ágnes for her endurance and love and to my children Dóra, Boldizsár and Júlia for their patience and their entertainment during this exhausting but rewarding period of my life.

Abstract

The economical and social burden of musculoskeletal diseases is steadily increasing. The World Health Organisation declared "The Bone and Joint Decade 2000-2010" to focus the attention of the public, professionals and governments on musculoskeletal conditions. Musculoskeletal ultrasound (US) is mentioned in this declaration as a possible new diagnostic tool related to musculoskeletal diseases.

History and physical examination are the two main pillars concerning the diagnosis of rheumatological conditions. Diagnostic ultrasonography may be regarded as a tool for extended physical examination. The main argument against the acceptance of the musculoskeletal US is the significant concern regarding observer variation. However this concern is solely based on qualitative pathological ultrasound studies. Obtaining reproducible images with measurable parameters is fundamental and emphasises the importance of a standardized imaging technique. Standardized imaging techniques need to be based on human anatomy but comprehensive comparison of human anatomy and musculoskeletal ultrasound anatomy is absent from the musculoskeletal ultrasound literature.

When a method is standardized, it is essential to measure its intra- and interobserver variability, sensitivity, specificity and predictive values before it is widely used in clinical practice. The use of ultrasound as an extended and more objective investigation performed as an extension of physical examination has a potential role in studying inflammation in different rheumatic diseases such as rheumatoid arthritis (RA) and spondylarthropathy (SpA). Rheumatoid arthritis is a chronic

disease causing joint inflammation and destruction. Metacarpophalangeal (MCP) joint involvement is one of the earliest and most permanent signs of RA. US has been used to detect synovitis and erosions in MCP joints with high accuracy when compared to X-ray and magnetic resonance imaging (MRI). In RA joints, power Doppler has been used to detect increased blood flow as a potential sign of inflammation but gray-scale and power Doppler ultrasonography was not compared to another method to detect increased blood flow in MCP joints. After RA the next most common inflammatory group of diseases are the seronegative spondylarthropathies. In SpA joint inflammation and ankylosis occur in addition to periarticular enthesitis, which is one of the major hallmarks of the disease and has been poorly studied by ultrasonography.

In order to reduce observer variation in musculoskeletal ultrasound examination to the level of other imaging methods it is necessary to avoid direct contact between the observer and the subject. This problem has been addressed in the aerospace industry and led to the development of air-coupled non-destructive testing. Air-coupled ultrasonography has the potential in medical imaging to exclude observer variation if it is able to depict human anatomy. There are currently no data regarding airborne ultrasound in the musculoskeletal ultrasound literature.

As an overview of the experimental chapters:

i) **Chapter 2. Standardized ultrasound examination of normal adult human musculoskeletal tissue and joints. Correlation with human anatomy.**

Fresh frozen human cadaver sections - corresponding with the planes used in musculoskeletal ultrasound examination - were prepared, photographed and compared to ultrasound images of living human tissues in the same planes. Skin, subcutaneous tissue, fat pad, muscle, tendon, tendon sheath, fascia, aponeurosis, ligament, joint capsule, retinaculum, bursa, hyaline cartilage, fibrocartilage, bone surface, lymph node and nerve were studied. The photo-images of anatomical structures corresponded well with ultrasound images of living human tissues examined in the same plane. Normal ultrasound characteristics, standardized planes and positions were described.

ii) **Chapter 3. Intraobserver repeatability and interobserver reproducibility in musculoskeletal ultrasound imaging measurements**

After the description of normal tissue ultrasound characteristics and standardization, intra- and interobserver variation of musculoskeletal ultrasonography was measured on a living subject and on a phantom. Two independent investigators were blinded to their own and each other's results and measurement error, correlation coefficient and Bland–Altman graphic technique were calculated and illustrated. In this way it was proven, that in measuring distances of ultrasound images both intra- and interobserver variations were acceptable even if the second investigator was relatively inexperienced in the use of musculoskeletal US.

iii) Chapter 4. Ultrasonography of lower limb entheseal insertions in spondylarthropathy

Lower limb enthesitis is a characteristic finding in SpA. For assessing SpA different clinical enthesitis indices are used. Using standardized ultrasound method for entheses of the lower limb was found that ultrasound was significantly superior to clinical examination, regarding both sensitivity and specificity. The intraobserver reliability of the re-evaluation of the stored images was high. This work showed that ultrasound can be used for detecting subclinical enthesitis in SpA.

iv) Chapter 5. Power Doppler and gray - scale ultrasound imaging of inflammatory hyperaemia in MCP joints

Assessing inflammatory activity of individual joints by non-physical examination methods is an unsolved problem in RA. Inflammation is characterized by joint swelling due either to synovial proliferation or synovial effusion or both. Measuring increased blood flow or hyperaemia in a joint provides a surrogate marker for inflammation especially when hyperaemia of the overlying tissues (i.e. skin) can be excluded. We studied blood flow of the 2^{nd} and 3^{rd} MCP joints comparing laser Doppler imaging (LDI), gray-scale and power Doppler US. It was found that the LDI measured hyperaemia did not correlate with power Doppler imaging of the same joints, but gray scale ultrasound showing characteristics of synovitis did correlate with LDI.

v) **Chapter 6. Air-coupled ultrasonography of the skeleton of the human hand**

In order to reduce observer variation in musculoskeletal ultrasound examination air coupled ultrasonography was used to avoid any observer variation and to depict human anatomy. An ultrasonic system that was designed originally for testing in the aerospace industry was modified and used to depict the skeleton of human hand. The scan showed the outline of the hand bones but no internal structure. Acquisition time was long and we cannot obtain a real tomographic view of the hand bones.

Conclusions

From the above experimental chapters, several conclusions can be made

i) Ultrasound can depict normal musculoskeletal tissues, which correlate with the anatomical structures.

ii) Where an acoustic window allows the use of ultrasound it is possible to depict normal peripheral joint structure according to the well-known anatomical structures in standardized anatomical planes.

iii) With well-defined anatomical landmarks and with pre-determined criteria, acceptable intra- and interobserver variation was obtained when musculoskeletal ultrasound was performed by two different observers.

iv) A rheumatologist with experience of US imaging can train a novice within a relatively short space of time to produce acceptable musculoskeletal ultrasound images.

v) Ultrasound detection of enthesitis is more sensitive and more specific than clinical examination and considerable sub-clinical enthesitis can be detected in SpA.

vi) With the present US equipment, laser Doppler imaging is more sensitive in measuring blood flow of MCP joints in RA than power Doppler imaging.

vii) Laser Doppler images correlated with gray-scale ultrasound images of MCP joint synovitis. There was no correlation between gray-scale US and power Doppler ultrasound images in relation to MCP joint synovitis.

viii) Airborne ultrasound is able to depict the surface of the skeleton of a human hand in an experimental study but cannot obtain a real tomographic view of the hand bones.

Contents

List of figures

Chapter 1

Chapter 2

List of tables

Chapter 4

Chapter 5

List of abbreviations

ARA	American Rheumatism Association
AS	Ankylosing Spondylitis
ATL	Advanced Technology Laboratories
CE	Clinical Examination
CGE	Colin G Egan
CL	Compact Linear
cm	Centimetre
CRP	C-Reactive Protein
CT	Computed Tomography
dB	Decibel
ESR	Erythrocyte Sedimentation Rate
ESSG	European Spondylarthropathy Study Group
EULAR	European League Against Rheumatism
GUESS	Glasgow Ultrasound Enthesitis Scoring System
HDI	High Definition Imaging
HLA	Human Leukocyte Antigen
Hz	Herz
ILAR	International League of Associations for Rheumatology
JIA	Juvenile Idiopathic Arthritis
KHz	Kilohertz
L	Linear
LP	Lajos Patonay
LDI	Laser Doppler perfusion Imaging
MB	Megabyte
MCP	Metacarpophalangeal
MHz	Megahertz
mm	Millimetre
μm	Micrometer
MRI	Magnetic Resonance Imaging
MUS	Musculoskeletal Ultrasonography
n	Number of observations
NDE	Non-Destructive Evaluation
NIR	Near- InfraRed
NJ	New Jersey
nm	Nanometer
p value	Probability value
PD	Power Doppler sign
PIP	Proximal interphalangeal
PTFE	Polytetrafluoroethylene
PU	Perfusion Unit
PVB	Peter V Balint
RA	Rheumatoid Arthritis
RAF	Royal Air Force
ROI	Region Of Interest
RDS	Roger D Sturrock
S.D.	Standard Deviation

S.E.M.	Standard Error of the Mean
SpA	Spondylarthropathy
ST	Soft Tissue
s_W	Within-subject standard deviation
TNF	Tumour Necrosis Factor
UK	United Kingdom
US	Ultrasound
USA	United States of America
VAS	Visual Analogue Scoring
WI	Wisconsin
WRF	William R Ferrell

Publications and Presentations (1999-2002)

i) Book Chapter

Forrester AW, **Balint PV,** Sturrock RD, Crystal arthropathies In: Isenberg D, Renton P. eds. Imaging in Rheumatology Oxford University Press, 2002 (in press).

ii) Original Articles

Balint P, Kane D, Wilson H, McInnes I, Sturrock R: Ultrasonography of lower limb entheseal insertions in spondylarthropathy Ann Rheum Dis (in press).

Balint PV, Kane D, Hunter J, McInnes IB, Field M, Sturrock RD. A comparison of ultrasound-guided with conventional joint aspiration in rheumatology practice – a pilot study. J Rheumatol (in press).

Balint PV, McEntegart A, Jackson R, Forrester AW, Simpson RG: Epitrochlear lymphadenopathy in rheumatoid arthritis caused by silicone particles J Rheumatol 2002; 29: 1097-9.

Hatton M, Gupta M, **Balint P**, Field M: Septic discitis presenting following intravenous cannulation. QJM 2002; 95: 189-91.

Balint PV, Kane D, Sturrock RD: Modern patient management in rheumatology: interventional musculoskeletal ultrasonography. Osteoarthritis Cartilage 2001; 9: 509-11.

Ferrell WR, **Balint PV**, Egan CG, Lockhart JC, Sturrock RD: Metacarpophalangeal joints in rheumatoid arthritis: laser Doppler imaging—initial experience. Radiology 2001; 220: 257-62.

Balint PV, Sturrock RD. Intraobserver repeatability and intraobserver reproducibility in musculoskeletal ultrasound imaging measurements. Clin Exp Rheumatol 2001; 19: 89-92.

Balint PV, Sturrock RD. Inflammed retrocalcaneal bursa and Achilles tendonitis in psoriatic arthritis demonstrated by ultrasonography. Ann Rheum Dis 2000; 59: 931-4.

Ferrell WR, **Balint PV,** Sturrock RD. Novel use of laser Doppler imaging for investigating epicondylitis. Rheumatology 2000; 39:1214-17.

Hamilton J, **Balint P,** Field M, Sturrock RD. A concealed cause of recurrent renal failure in a patient with juvenile chronic arthritis. Ann Rheum Dis 1999; 58: 396-8.

iii) Abstracts

Balint PV, Kane D, Hunter J, McInnes IB, Field M, Sturrock RD. A comparison of ultrasound-guided with conventional joint aspiration in rheumatology practice – a pilot study. Rheumatology 2002;41 Abstracts Supplement 1, Abstract 328 ,p 118.

Kane D, **Balint P,** Sturrock D: Comparison of ultrasonography with clinical examination in the diagnosis of soft tissue of the knee in rheumatoid arthritis. Rheumatology 2002;41 Abstracts Supplement 1, Abstract 176 ,p 76.

Balint P, Kane D, Wilson H, McInnes I, Sturrock R:The majority of lower limb enthesopathy in seronegative spondylarthropathy is underestimated by clinical examination: an ultrasonographic study. ACR 65th Annual Scientific Meeting 2001, Arthritis Rheum 2001; 44: Supplement, S93, p 244.

Kane D, **Balint P,** Sturrock D: Clinical examination underestimates synovitis of the knee in rheumatoid arthritis: a comparison with ultrasonography ACR 65th Annual Scientific Meeting 2001, Arthritis Rheum 2001; 44: Supplement, S223, p 1024.

Balint P, Kane D, Wilson H, McInnes I, Sturrock R: Ultrasonography of lower limb entheses in seronegative spondylarthropathy J Rheumatol 2001; 28: Supplement 63, Abstract M113, p 31.

Kane D, **Balint P,** Sturrock D: Ultrasonography of the knee in rheumatoid arthritis J Rheumatol 2001; 28: Supplement 63, Abstract M 112, p 30.

Balint P, Kane D, Wilson H, McInnes I, Sturrock R: Ultrasonography of entheseal sites in spondylarthropathy Rheumatology 2001; 40: Abstracts Supplement 1, Abstract 120, pp 41-42.

Balint PV, Sturrock RD Intraobserver repeatability and interobserver reproducibility in ultrasound measurements of human hips and phantom RMI 403GS ACR 64th Annual Scientific Meeting 2000, Arthritis Rheum 2000; 43: Supplement, S219, p914.

Ferrel WR, **Balint PV,** Egan CG, Lockhart JC, Sturrock RD Comparison of laser and power Doppler ultrasound imaging techniques in the assessment of joint hyperaemia in rheumatoid hands ACR 63rd Annual Scientific Meeting 1999, Arthritis Rheum 1999; 42:Supplement, S347, p 1656.

Balint P, Sturrock RD Intra and inter-observer variability in ultrasound measurements of adult human hips: pilot study XIV-th EULAR Congress (Glasgow, 1999) Ann Rheum Dis 1999; Abstract 66, p 27.

Balint P, Hamilton J, Sturrock RD Posterior humeral head bone defects in rheumatoid arthritis XIV-th EULAR Congress (Glasgow, 1999) Ann Rheum Dis 1999; Abstract 67, p 27.

iv) Presentations as invited speaker for international audience

"Correlating the ultrasound image with anatomy"

The 20th Congress of the International League of Associations for Rheumatology (ILAR), Edmonton, Alberta, Canada, August 2001.

"Anatomy of a normal joint in ultrasounds: skin, muscles, fascias, tendons, ligaments, cartilage, bone, synovium and nerves"

ECHORHUM, Paris, France, January 2002.

"Correlating the ultrasound image with musculoskeletal tissue anatomy" European League Against Rheumatism (EULAR) 4th Sonography Course, Madrid, Spain, April 2002.

Declaration

We declare that Péter V Bálint has composed this thesis and it is a record of work performed by him. It has not been submitted previously for a higher degree.

The work described in this thesis was carried out under the supervision of Professor Roger D Sturrock, Centre for Rheumatic Diseases, University Department of Medicine, University of Glasgow.

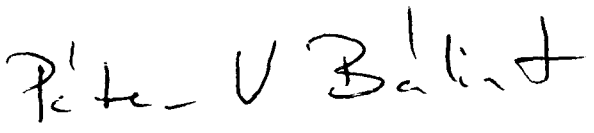

Péter V Bálint

Roger D Sturrock

July 2002,Glasgow

Chapter 1. Introduction

1.1 Spallanzani's bat problem

Human ears can perceive sound waves between 20 Hz and 20 kHz frequencies. High frequency, non-audible sound waves over 20 kHz are termed ultrasound and have existed in nature for more than 1 million years. In the animal kingdom grasshoppers, bats, porpoises and others use ultrasound emission and reception to locate obstacles, food sources and perhaps for communication. Certain types of moths may emit ultrasound waves -as a defence system- disturbing ultrasound waves emitted by hunting bats. This form of "anti-reconnaissance" jamming activity allows them to successfully survive bat attacks.

For centuries mankind did not know this type of inaudible sound. The first – detailed experiments, indicating that non-audible sound might exist, were done by Lazzaro Spallanzani (1729-1799) an Italian priest and physiologist in Pavia. He became interested in the spatial orientation of bats in darkness (1). He noticed that his owl was totally helpless and disorientated in full darkness, in spite of the widely told belief that owls could see in total darkness. He demonstrated, that bats orientate very well with blinded eyes, but that they bumped against obstacles, when their mouths were covered. He also ruled out the role of the sense of touch in bats' orientation by plastering their bodies with varnish and paste. This did not effect the spatial orientation of the bats in flight (2). A Geneva scientist, Charles Jurine reproduced Spallanzani's experiments, with the same results. He also noticed that the bat's orientation was blocked when their

ears was plugged (2). Spallanzani sought to explain the unbelievable. Finally he stated "The ear of the bat serves more efficiently for seeing, or at least for measuring distances..." "Can it then be said that ...their ears rather then their eyes serve to direct them in flight?" (2). In the 1790's the idea that bats "see" by hearing was scientific heresy. Neither Spallanzani nor Jurine deducted the existence of inaudible sounds. Although piezoelectricity was discovered by Pierre and Jacques Currie in 1880, the "Spallanzani's Bat Problem" was not solved for another sixty years.

In 1938 Professor G.W Pierce of Harvard Physics Department was experimenting with "his sonic detector" which transposed ultrasonic vibrations down to audible frequencies. A young Harvard student, Donald R. Griffin who was studying the habits of bats approached the professor with the suggestion that they might use the apparatus to listen to bats. The sonic detector was placed before a cage full of bats, and a chorus of clicks, sputters and pops poured from the loudspeaker. But to Pierce's and Griffin's disappointment, when some bats were released from the cage, the detector remained nearly mute. Pierce and Griffins deducted, that bats produced ultrasonic sounds only occasionally, probably as a sort of call rather than a means of orientation (3).

Solving "Spallanzani's Bat Problem" was nearly missed again. But in the following year Griffin with another physiology undergraduate -a Hungarian descendant- Robert Galambos, restarted the research on bats' orientation. They discovered that bats' ultrasonic emissions were directional and tended to focus in a beam directly forward from the bat's head. The sounds could be detected only

when the bats flew towards the microphone (4-6). With a number of well-designed experiments Griffin and Galambos proved beyond any doubt, that bats navigate by sending out ultrasonic noises and listening for the echoes. The returning echoes are received and interpreted by a specialised area of the brain thus enabling the bat to perceive the size and shape of it's target and know its exact position.

1.2 Discovery of piezoelectricity, military and industrial applications

The Curie brothers Pierre and Jacques discovered piezoelectric phenomena in 1880 during their study on crystallography (7). "Piesis" means pressing or squeezing in Greek and piezoelectricity means that when certain crystals are subjected to mechanical stress, electricity is induced. The Curies observed that electricity was induced when mechanical pressure was applied on a quartz crystal such as the Rochelle salt (sodium potassium tartrate tetrahydrate, KNaC4H4O6.4H2O). In the first instance they did not consider the reciprocal effects. Next year the mathematician-physicist Gabrial Lipmann hypothesised, by deduction from thermodynamic principles, that the converse piezoelectric effect existed, in other words if an electric charge were applied to the same crystals, mechanical oscillations of the crystal would result. Some crystalline materials (some ceramics and polymers as well) contain dipolar molecules, which have a positive and negative charge at the ends. In the natural state these dipolar molecules are randomly arranged in a fixed position in the crystals. If the material is heated above a specific temperature (Curie temperature, which depends on the characteristics of the material) these molecules can move freely. When an electrical charge is applied across the crystal in this state and the crystal cools below the Curie temperature each positive region of the molecules will align towards the negative plate and each negative region will point toward the positive plate. When voltages are applied to the conducting plates, -which are now placed on the opposite sides of the crystal- the molecules will twist to align themselves towards the appropriate electrodes. This will cause a thickening of the crystal. Changing polarity will cause an opposite effect and will decrease the thickness of the crystal.

This expansion (rarefraction of the molecules) and contraction (compression of the molecules) of the crystal causes mechanical vibrating motions (pressure waves), which will generate sound waves. In 1882 the Curie brothers succeeded in producing mechanical pressure waves using this technique and the eternal physical law of reciprocity was finally verified.

Echolocation (echo* means a returned sound in Greek) with audible sound was well known by the ancient Phoenician fishermen who made loud noises and then listened for echoes to gauge distances to land obscured by fog.

Figure 1.1. **"Echo and Narcissus"** painted in 1903
by John William Waterhouse (1849-1917),
Walker Art Gallery, Liverpool, England, UK
(oil on canvas; 109 x 189 cm)

---

* Echo: In Greek mythology, a nymph of whom several stories are told. Either she was beloved by Pan and was torn to pieces, only her voice surviving; or she was punished by Hera so that she could only repeat that last words of another speaker. She loved Narcisuss (Figure 1.1.), who rejected her, so that she wasted away to a voice (8).

After the disastrous collision of the Titanic, Lewis F Richardson (in Britain) and the Canadian Reginald A Fessenden (in the USA) patented devices using active echolocation in 1912. Fessenden's Sonar (**SO**und **NA**vigation and **R**anging) apparatus was built in 1914 and detected an iceberg two miles away.

Beside this important and peaceful application of ultrasound, a hydrophone (passive listening machine) was developed and used for other purposes as well. Echolocation was the focus of a very important military program in World War I., when the Allies (Entente) used this to locate German submarines. Paul Langevin -a previous co-worker of Pierre Curie- and Constantin Chilowsky constructed an underwater sandwich sound generator using quartz crystals and two steel plates (9). Langevin's device was the forerunner of the modern ultrasound devices. The first recorded detection and subsequent sinking of a German U-boat using a hydrophone was 23 of April in 1916 (10).

Between the two world wars another technical use was developed using ultrasound – but this was entirely peaceful. In the USSR Sokolov developed an ultrasound technique in 1928 to detect flaws in metal. Later many other countries (USA, Great Britain, Germany, Austria) also developed similar machines called reflectoscopes (11,12). These unidirectional machines emitted and received unidirectional high frequency sound waves- in one line only. Sokolov also calculated, that at 3 GHz frequency the sound waves' wavelength in water would be equal with the green light's wavelength. At that time, it was not possible to develop such high frequency equipment but theoretically he had opened the door

to the development of the acoustic microscope, which is now being operated in many places worldwide (13).

Ultrasound applications are now widespread in many different areas of human activity and in different areas of science (14). For example ultrasound is used for mapping sea beds, locating objects within the muddy seabed or testing railway tracks for metal flaws. Airborne ultrasound may be helpful for detecting flaws of aircraft wings (15). The military and industrial applications of ultrasound led to the development of medical diagnostic ultrasound.

1.3 Medical ultrasound imaging

The first physician to use ultrasound as a diagnostic tool was Karl Theodore Dussik, a neurologist at the University of Vienna. In 1942, he attempted to locate brain tumours and the cerebral ventricles by measuring the transmission of ultrasound beams through the head (16,17). He worked with his physicist brother Friederich on the "hyperphonography of the brain". Interestingly they misinterpreted their results and described a number of structures of the brain that were later proved to be simple artifacts. But their "discovery" was enough to arouse interest on the other side of the Atlantic in the potential medical use of ultrasound imaging.

The first pioneers in the United States -George Ludwig and WF Struthers- worked on the detection of gallstones and foreign bodies in animals (18). At the Massachusetts Institute of Technology, George Ludwig, RT Bolt, HT Ballantine and Theodor Heuler determined the velocity of sound transmission in animal soft tissues and found it to be between 1500 and 1600 m/sec (19, 20). At the same time Ludwig also demonstrated that two-dimensional images of soft-tissues could be obtained.

John Julian Wild, a Cambridge medical graduate is considered as one of the first true founders of ultrasonic tissue diagnosis (21-24). In collaboration with an engineer, Donald Neal, he first published unidirectional A-mode (amplitude mode) ultrasound investigations into the thickness of surgical intestinal material and later on in the diagnosis of intestinal and breast malignancies. Wild later

worked with another engineer, John Reid and they soon developed a linear handhold B (Brightness)- mode instrument. As early as 1953 they produced real-time images at 15MHz of a 7mm cancerous growth of the breast. They named this method echography and echometry. Wild and Reid also described the use of endoscopic (transrectal and transvaginal) A- mode scanning transducers in 1955 (25, 26).

The other great pioneer of ultrasound diagnostics was Douglas Howry, a radiologist at the Veteran's Administration Hospital in Denver. In 1951 with two engineers, William Roderic Bliss and Gerald L Posakony he produced the first two dimensional B - mode or plan position indication (PPI) - mode in an immersion tank. They later developed a motorised somascope in 1954. The transducer of the somascope was mounted around the rim of a large metal immersion tank filled of water. The machine was able to make compound scans of an intra-abdominal organ from different angles with a circumferential scanner (27-31). His sonographic images were referred to as somograms. Meanwhile LA French, JJ Wild and D. Neel worked on detection of cerebral tumours (32), William Fry and his co-workers used an ultrasound beam to accurately ablate brain tissue (33-35) and Karl Leksell of Sweden described midline echoencephalography in 1956 (36).

M (motion)-mode was described by Inge Edler and Carl Hellmuth Hertz (son of the Nobel Prize Laurate Gustav Ludwig Hertz) in Sweden in 1954 using a modified Siemens metal flaw detector showing cardiac valve motion (37-40). In Japan Shigeo Satomura was the first to use ultrasonic Doppler techniques to

study peripheral blood vessel pulsation (41). In 1966 Kanemasa Kato and T Izumi developed the direct flow meter. However in 1964 in Seattle (USA) a team led by Robert Rushmer pioneered continuous-wave flow and described spectral analysis. A member of the Seattle team, Donald Baker (in the same time with Japanese colleagues) developed the first pulsed-Doppler scanner in 1970. Frank Barber and others also developed the first duplex Doppler scanner in Seattle in 1974 (42, 43). The next major address were the introduction of a 2D color flow imaging in 1978 by the Seattle group and the first real-time color flow imaging scanner in Japan by Aloka company in 1985. A few years later AngioDynography was pioneered in Issaquah, Washington. From this application Color Power Imaging – what now we call Power Doppler imaging - was developed (25, 44).

1.4 Ian Donald's and Glasgow contribution

One of the major advances in medical ultrasound diagnostics occurred in Glasgow in the second half of fifties and the first half of the sixties under the leadership of Professor Ian Donald, Professor of Obstetrics. Donald titled his paper "Sonar-The story of an experiment" he wrote: "My own great fortune lay in the fact that I approached the subject through engineering channels...in the detection of flaws in metal structures there was no question of tank work, but probes coated with oil were applied directly to the material under test ...Glasgow, with its technical know-how has proved the ideal city in which to work" (45).

Ian Donald (1910-1987) was educated in Scotland, South Africa and England. After his medical graduation in London he stayed in the city and was deeply interested in different technical problems and machines in his early careers. In 1939 he joined the RAF (Royal Air Force) where his technical knowledge and skills further expanded and gathered expertise in radar and sonar technique. After World War II he specialised in obstetrics and gynaecology. His enthusiasm for technical innovations was undiminished. He was introduced to Dr John Julian Wild while he was at Hammersmith in London and was impressed by his work on ultrasound. He was aware that human ultrasound images could be obtained by immersing patients in a large tank water but that this was unsuitable in clinical practice. Besides his outstanding medical and personal qualities he was an excellent lecturer. The trademark of his teaching capability was the well-known motto that " The art of teaching is the art of sharing enthusiasm" (46). His

clinical work, research interest and teaching ability gave him the capability to continue his work in a higher academic level. He returned to Scotland as the Regius Professor of Midwifery of the University of Glasgow in 1954. He took with him some rudimentary knowledge of radar and sonar from his days in the Royal Air Force, Dr Wild's ultrasound research results and his "childish" interest in machines.

In 1957 Ian Donald and co-workers began to study pregnancy by first identifying the foetal head. That was pioneered by the Staff Nurse, Marjory Marr who used the machine to locate the position of the foetal head in cases where it was difficult to determine by palpation. With the further help of Kelvin Hughes Ltd. research workshop, Ian Donald and Tom Brown developed their first two dimensional scanner. His work was always tightly connected with engineers not only with Tom Brown but also with John Fleming and Tom Duggan (47, 48). In 1958 Donald, MacVicar and Brown published their findings in the Lancet, which Donald regarded as his most important paper, but was also a major milestone in medical ultrasound (49).

In 1960 they developed an automatic scanner, which was used to diagnose two cases of placenta previa a condition that had not been diagnosed ante-partium before. James Willocks and Donald also developed the method for measuring biparietal diameter of foetal head with great accuracy (+/- 1mm) in 1962. Later in 1968 the method was refined by Stuart Campbell and fetal cephalometry was the first medical ultrasound measurement which became a standard method for studying intrauterine human development and first ultrasonic anthropology measurement (50).

In 1963 Donald noticed that if the patient had a full bladder it was possible to obtain a more accurate image of the foetal head. This method allowed the detection of very early pregnancy of about 6-7 weeks gestation (51). Now the whole course of pregnancy could be followed by ultrasound. The Holmes's group in the States published the first report of placentography in 1966. Ian Donald with his Iraqi assistant Usama Abdulla also worked on placentography and on a method of placental localization (52). Ian Donald in co-operation with Malcolm Ferguson-Smith tested the safety of ultrasound in cell research (53). Looking back at what Donald's work achieved, we can say that he introduced ultrasound imaging to everyday clinical practice and that he and his engineer co-worker Tom Brown introduced the first compound B-mode contact scanners for medical investigations. The immersion tank was no longer relevant in clinical practice. Tom Brown was the first to describe the possibility of 3D ultrasonic imaging but due to the technical limitations at that time he did not build a 3D scanner. Donald's earned him national and international acclaim. He was invited to an audience in Rome with the Pope in recognition of his influential impact in the antenatal detection of life. After his death the Ian Donald Inter-University School of Medical Ultrasound was opened in Dubrovnik, Croatia in 1989. The Ian Donald Gold Medal was also established to acknowledge his major contribution to obstetrical and gynaecological ultrasonography.

1.5 Further development of medical ultrasound imaging and biological effect of ultrasound

After the 60-s the ultrasound technology rapidly developed. Jan C Somer in the Netharlands described and produced the first phased array; W. Krause and Richard Soldner invented the first real-time machine, which was manufactured by Siemens in Germany under the name of Vidoson. The development of the analog scan converter and later gray scaling by George Kossoff group in Australia dramatically improved the quality of obtained images in the early 70's (54-57). A decade later digital scan converters replaced them in the early 80's (58). Computer technology also helped to improve measurement accuracy and tissue phantoms became available for testing the quality and the accuracy of ultrasound machines (25).

The transducer technology also improved. James Griffith and Walter Henry designed the first mechanical oscillating scanner; Norman W McDicken in Edinburgh developed a membrane-oil coupling mechanical oscillating scanner and the first circular rotating system was introduced by the KretzTechnik. Electronic arrays were first described in an ophthalmologic examination in the mid 60's by Werner Buschmann in Berlin and in the late 70's electronic arrays became available for other applications. Jan C Somer and Nicolaas Bom in the Netherlands introduced the phased array and linear array transducers in 1968 and in 1971. In Japan, Aloka with Rokuro Uchida developed the first prototype of linear array scanner. Crystal stepping techniques experiments performed by Nicolaas Bom, Donald L King, Tony Whittingham and others led the

development of multi-element sequential-firing scanning systems. In 1975 the Acoustic Diagnostic Research Corporation (ADR) under the leadership of Martin H Wilcox developed the first variable focus transducer. In the same time steered-beam phased array and annular array technology improved cardiac ultrasound facilities. In the mid 80's real time scanners replaced static scanners in clinical practice and curvilinear (convex) sector array transducers were referred for abdominal examination (25)

Alfred Kratochwill in Austria was the first physician to use ultrasonography for injection guidance (59). He was also influential in the technical developments of the Austrian ultrasound scanner manufacturer KretzTechnik Company and he published over 100 ultrasound papers in obstetrics and gynaecology. Interventional ultrasonography was further developed by Hans Henrik Holm (60) in Copenhagen and Barry Goldberg (61, 62) in the States. Another Hungarian descendent Lajos von Micsky was one of the first physicians to introduce endoscopic sonographic (intravesical, rectal) equipment in the early 60's while working at the St Luke's Medical Center in New York (63, 64). Due to the new transducer technology and computer development the next major technological advance was in the early 90's. Broadbrand wide aperture, multi-channel, high dynamic range transducers, fully digitalized signal processing created improved resolution. In the last few years the image quality improved even further with the introduction of tissue harmonic imaging and contrast agents. Tissue harmonic imaging technique allows using lower insonation frequency to improve the penetration and processing only the received higher frequency inherent harmonic frequencies from the tissues (65). In this way not only less artifacts will be but

also better contrast resolution between different tissues. Tom Brown's imagination finally also became reality and 4D (3D in real-time) ultrasonography is now commercially available (66).

The biological effects of ultrasound were first demonstrated by Paul Langevin. He killed small fish by exposing them to ultrasound and he also experienced pain on exposing his hands to ultrasound (67). RW Wood, EN Harvey and AL Loomis published the first papers about the biological effects of ultrasound (68, 69) and Nobel Prize winner Albert Szent-Györgyi mentioned first that ultrasound was tried to destroy cancer cells (70, 71). Ultrasound can cause thermal effects and cavitations as bioeffects. These bioeffects now are well studied (72-76). The therapeutic benefits of ultrasound bioeffects are utilised in physiotherapy. High-intensity focused ultrasound (HIFU) may play a significant role in ablative therapy of cancers. MRI-guided experimental HIFU synovectomy of the rabbit knee has been successfully performed and the method is patented in the USA (77, 78). A further interesting research application of ultrasound is in the potential safe drug delivery to target tissues hereby reducing drug side-effects (79). Other established methods, such as the "extended field of view" technique (80), lithotripsy (81) and quantitative ultrasound (QUS) as a method studying bone fracture risk (82) have also been demonstrated to be safe in humans. In diagnostic imaging, ultrasound is deemed to be safe and sonographers practice according to the ALARA (**A**s **L**ow **A**s **R**easonably **A**chievable) principle (83).

1.6 Musculoskeletal ultrasonography

Interestingly the first report of musculoskeletal ultrasonography goes back more than forty years. The first paper associated to this field was published by Karl T Dussik -who was the first in 1942 to use ultrasound as a medical diagnostic tool. In this article, he examined different articular and periarticular tissues such as skin, adipose tissue, muscle, tendon, articular capsule, articular cartilage and bone (84). He measured the acoustic attenuation constants of these tissue, described fibre- anisotropy and proposed a number of different pathological influences on sound attenuation:

1. Hydration decreases, dehydration increases the attenuation constants.
2. Inflammation leading to edema formation decreases the values but if cellular filtration occurs, values may be increased.
3. Fatty infiltration decreases the attenuation constants.
4. Cirrhotic changes increase the attenuation constants.
5. The effect of pathological new growth in structures can either be a decrease in the case of cyst formation or an increase of attenuation constants if cellular infiltration and the increased production of intercellular substances prevail.
6. Some observations corroborate the assumption that aging of tissues tends to increase the attenuation value as a results of the gradually increased relative amount of intercellular substances and the progressive loss of fluid (84).

Many of these statements are still valid.

The first B-scan image of a human joint was published thirty years ago in 1972 by Daniel G. McDonald and George R Leopold in the British Journal of Radiology (85). They described the use of ultrasound imaging to differentiate of Baker's cyst and thrombophlebitis. Spurred by McDonald and Leopold many investigators looked at other joints and described different musculoskeletal applications such as shoulder (86-88), elbow (87, 89, 90), wrist (91-93), small joints (91, 94-96), hip (87,97-99), knee (100-102), ankle (103-105) and soft-tissue ultrasound examination such as tendon (106-110), hyaline cartilage (111-121). The literature of musculoskeletal ultrasonography has expanded exponentially over the last twenty years. Despite these extensive studies of different regions and different diseases musculoskeletal ultrasonography has not yet become the "gold" standard of musculoskeletal examination. The only exception is the neonatal hip examination described by Graf and Harcke (122, 123).

Through the work of the radiologists, -especially Bruno Fornage (124) and Marnix van Holsbeeck (125) - rheumatologists become interest in musculoskeletal ultrasonography. Many of them felt that ultrasonography was a logical extension of physical examination of their patients. They followed the same route of their colleagues in Obstetrics and Gynaecology, Cardiology and other specialities. Radiologists trained them or they simply were self-trained. As the image resolution and quality dramatically improved ultrasonography began to rival other radiology modalities such as MRI examination and X-ray in a number of musculoskeletal imaging applications (126-128). However the main argument against the acceptance of the musculoskeletal US remains the

significant concerns regarding observer variation. However these concerns are solely based on qualitative pathological studies (129-136). In other specialities intraobserver and interobserver error measurement experiments were implemented to prove the reliability and repeatability of ultrasound study. This is not the case in human adult musculoskeletal ultrasound, where only non-blinded studies have been performed (99). For measuring musculoskeletal parameters and to obtain reproducible images the importance of a standardized image technique is fundamental. Standardized image techniques need to be based on human anatomy and this type of wide-ranging comparison of human anatomy and musculoskeletal ultrasound anatomy is absent from the musculoskeletal ultrasound literature.

The use of ultrasound (US) as an extended and more objective investigation performed after physical examination has a potential role in the study of inflammation in different rheumatic diseases such as rheumatoid arthritis and spondarthritides. Rheumatoid arthritis is a chronic inflammatory disease, which leads to joint inflammation and destruction. MCP joint involvement is one of the earliest and most permanent signs of rheumatoid arthritis. US has been used to detect synovitis and erosions in MCP joints with high accuracy when compared to X-ray and MRI (128). In RA joints power Doppler has been used to detect increased blood flow as a potential sign of inflammation (137) but gray-scale and power Doppler ultrasonography were not compared to other methods to detect increased blood flow in MCP joints. After rheumatoid arthritis the next largest inflammatory disease group is seronegative spondylarthropathy (SpA). In SpA joints inflammation and ankylosis occur in addition to periarticular enthesitis,

which is one of the major hallmarks of the disease. Three studies of US of the lower extremities in SpA suggest a discrepancy between clinical and sonographic enthesitis. These studies do not provide an exact description of the different imaging features of enthesitis such as erosion, enthesophyte and thickness of tendon, ligament or aponeurosis nor do they report intraobserver variability or specificity and sensitivity of the relative examination techniques (138-140).

In order to reduce observer variation in musculoskeletal ultrasound examination it is necessary to avoid direct contact between the observer and the subject. This problem has been addressed in the aerospace industry and led to the development of air-coupled non-destructive testing (NDE) (15). Air coupled ultrasonography has the potential in medical imaging to exclude any observer variation if it is able to depict human anatomy. There is no such data available about airborne ultrasound in the musculoskeletal ultrasound literature.

1.7 Aims of this thesis

1. The determination and description of the normal US images of periarticular and intraarticular tissues and standardization of the musculoskeletal ultrasound anatomy and examination.
2. Determination of the magnitude of inter- and intraobserver errors using US imaging of an unselected group of normal controls and patients with inflammatory joint disease.
3. Comparison of clinical examination and ultrasonography in the detection of enthesitis of the lower limbs in SpA.
4. To establish whether increased blood flow associated with active rheumatoid arthritis of the 2^{nd} and 3^{rd} MCP joints as detected by ultrasonography correlates with independent methods such as laser Doppler imaging.
5. Testing the hypothesis that airborne non-contact imaging apparatus could provide a satisfactory image of a large structure such as the skeleton of the human hand.

Chapter 2. Standardized ultrasound examination of normal adult human musculoskeletal tissue and joints. Correlation with human anatomy.

2.1. Introduction

Musculoskeletal ultrasonography is not a standard medical diagnostic technique. Due to technical advances the resolution of ultrasonography, allows the detection of smaller and smaller anatomic structures (141). US has the advantage, that it can be performed in a number of different planes, but has the disadvantage, that the image is not panoramic and not fully tomographic. When assessing plain radiographs and MRI or CT scans it is usually possible to recognize the depicted part of the body. The sonographic image is often not easily recognizable by a non-ultrasonographer, who does not know in which plane the image has been depicted. Besides its technical advantages, musculoskeletal ultrasonography also has other disadvantages. One disadvantage is that only anatomical regions, having a suitable "acoustic window" can be examined. That means, that the region should not be covered by bone, which completely reflects the sound beam. Interestingly after nearly 30 years of development of musculoskeletal ultrasonography there is still only a few published articles comparing normal adult human articular and periarticular tissue anatomy and ultrasound images (142-154) despite numerous articles and books published over the last decade in English (124,125,155-159). My aim was to compare the anatomy and ultrasound image to develop possible guidelines for standardizing human joint ultrasound examination.

2.2. Materials and methods

Cadaver preparation

The biological specimens used for inspection were different musculoskeletal parts of articulated joints detached from a "fresh" frozen human cadaver supplied for anatomical teaching. In selected planes (sagittal, coronal, transverse and in some cases also oblique sagittal) tomographic slices were obtained by using a sawing machine. The planning, the plane selection and the quality control was completed by PVB. LP who is an expert in anatomical sawing implemented the cutting as a highly dangerous operation. After manufacturing the appropriate tomographic slices, a digital camera was used to acquire images for comparison with ultrasound images of living human tissue. Damaged or age-related degenerative tissue structures were excluded during the selection and in this way only "normal" anatomical structures were used for tissue comparison and for standardization.

Ultrasound examination

A number of objective obstacles were encountered earlier when comparing identical anatomical sections with the corresponding cadaver ultrasound image. Firstly we had no dedicated US machine in the Anatomy Department. Secondly, the quality of cadaver ultrasound images was poor compared to ultrasound imaging of a living human subject. Thirdly, obtaining and maintaining an

appropriate body and joint position in a cadaver is much more difficult than in a healthy subject. Therefore we used living human controls in this study. Middle-aged persons (one female and one male) were used as "healthy" controls. Their medical history did not revealed any major musculoskeletal tissue injuries or any other type of musculoskeletal diseases. They had no musculoskeletal complaints or any signs or symptoms of musculoskeletal disease during the study period. Sagittal, coronal, transverse and in some cases oblique sagittal two-dimensional, gray-scale, and in some cases also power Doppler images were obtained of the peripheral human joints with an ATL HDI 3000 (Advanced Technology Laboratories, High Definition Imaging 3000; Bothell, Washington, USA) US machine with a compact linear (CL) 10-5 MHz, 26-mm footprint probe and a linear (L) 7-4 MHz, 38- mm footprint probe. During the observation of gray-scale sonographic characteristics of the human tissues real-time information (tendon movement, blood flow etc.) and audible information (blood flow) was also obtained and included in the study results as complementary information. Obviously this information was not available on cadavers and this way it was not controlled. Sonographic images were stored on magneto-optical disks (Sony Magneto Optical Disk 128MB, Sony Electronics Inc, Recording Media & Energy Products Group, 680 Kinderkamack Rd, Oradell, NJ 07649, USA) for off-line analysis. After the tissue characteristics correlation, joint US image standardization was attempted. During this standardization the ultrasound image anatomical spatial position (coronal, sagittal, transverse and parasagittal oblique), the body and joint position and specified anatomical landmarks were recorded. The ultrasound transducer position and body position on digital image (Ricoh Digital Camera, RDC-300Z, Ricoh Company, LTD, Taiwan) was also

recorded. Standardized ultrasound images were obtained from most peripheral joints including shoulder, elbow, wrist, small hand joints, hip, knee, ankle, midfoot and forefoot joints. In this chapter only a selection of standardized images will be shown. The selection is based on the occurrence of standardized planes in other chapters. These selected standardized planes were:

1. Dorsal sagittal plane through the 2nd MCP joint.
2. Anterior oblique parasagittal plane through the anterior hip recess.
3. Anterior sagittal plane through the superior pole of the patella.
4. Anterior sagittal plane through the inferior pole of the patella.
5. Anterior sagittal plane through the tibial tuberosity.
6. Dorsal sagittal plane through the Achilles tendon.
7. Plantar medial parasagittal plane through the plantar aponeurosis.

The following rules were used for US standardization:

1. Depicting and describing the same anatomical landmarks on ultrasound as well as on macroscopic anatomical sections.
2. Using always the same characteristic anatomical planes to obtain a standard US image (sagittal, transverse, coronal were the most common used anatomical planes).
3. Showing and describing the positions of the examined body part and describing the body position during the scan.
4. Showing and describing the positions of the transducer.

Terminology

In this thesis internationally accepted terminology for human anatomy was used (160). The following definitions of ultrasound terminology were used. The term "anechoic" was used when the biological material allowed the propagation of the ultrasound without reflection and significant loss of energy (no interfaces) appearing on display as an echofree black field. Acoustic enhancement refers to increased echogenicity observed immediately posterior to an anechoic area. Behind the anechoic area there is no acoustic enhancement if a bony surface is present, which reflects sound beams completely or if the anechoic area is very thin. The term "echoic" was used when the propagated ultrasound was reflected and refracted in the biological material (strong echoes create multiple interfaces). Echoic areas appear as grey (slight echogenecity) to white (marked echogenicity). The term "hyperechoic" was used when an area was more echoic than surrounding tissues and the term "hypoechoic" when an area was less echoic than surrounding tissues.

2.3. Results

Ultrasound image of skin and subcutaneous tissue

Comparison of ultrasound image of the skin and subcutaneous tissue to anatomical sample (Figure 2.1.) provided the following results.

1. Epidermis and dermis was a 1.5-4mm thick single hyperechoic line on the ultrasound scan. The thickness was dependent on the region of the body.
2. No blood flow was detected in the epidermis and dermis.
3. Subcutaneous tissue (hypodermis) contained a hypoechoic layer with hyperechoic strands. The hypoechoic area corresponded to subcutaneous fat and loose connective tissue. Curvilinear hyperechoic strands corresponded to fibrous septa.
4. Superficial veins can be detected in the subcutaneous tissue.
5. No focal hypo-,hyperechoic or anechoic area was detected in the skin or in the subcutaneous tissue in healthy subjects.
6. No focal or diffuse thickening or thinning of subcutaneous tissue was detected in comparison with the contralateral side.

Figure 2.1. Ultrasound and anatomical image of the skin and subcutaneous tissue (sample from the anterior thigh region).

E = epidermis and dermis S = fibrous septae H = hypodermis, F = fascia,

M = muscle

Fat pad

Comparison of ultrasound image of fat pads to anatomical sample (Figure 2.2.) provided the following results:

1. Fat pads can be visualised: e.g. anterior elbow fat pad, Hoffa fat pad (knee), Kager fat pad (ankle).
2. Echogenicity of fat pads was dependent on the ratio of fat, loose connective tissue and the presence of fibrous septae. This is the reason why some fat pads were hyperechoic, some were hypoechoic and others were inhomogenously echoic.
3. No blood flow was detected in the fat pads.
4. No focal anechoic, hypo- or hyperechoic area was detected in fat pads of healthy subjects.

Figure 2.2. Ultrasound and anatomical image of fat pad (sample from the anterior elbow region, sagittal section).

F = fat pad, M = muscle, CA = cartilage, H = humerus, R = radius, JS = joint space

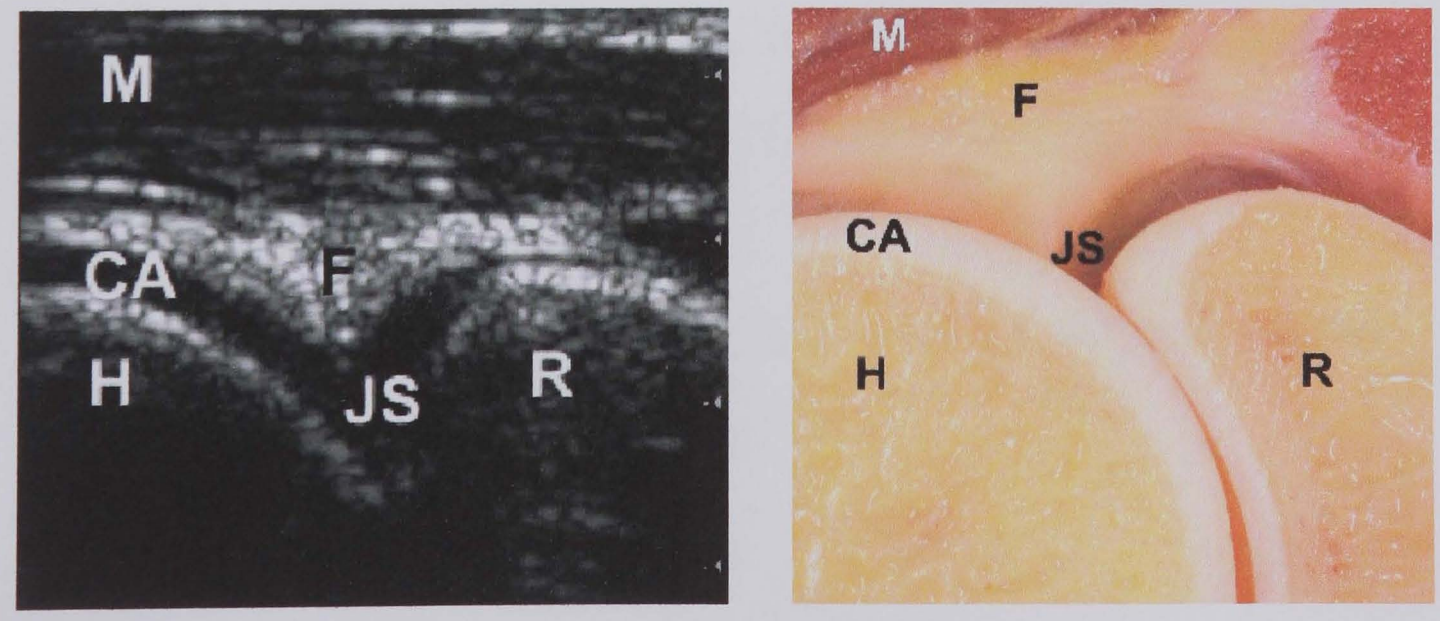

Muscle

Comparison of ultrasound image of muscle tissue to the anatomical sample (Figure 2.3.) provided the following results:

Longitudinal view

1. The epimysium, fibroadipose septa, perimysium were hyperechoic. Epimysium covered the entire muscle. Fibrous intersections were also hyperechoic.
2. Muscle bundles were hypoechoic.
3. The ultrasound patterns showed the same anatomical structures of muscles: eg. unipennate, bipennate, circumpennate.
4. Some vessels could be detected in the muscle.
5. During isometric contraction, the muscle mass is increased and become more hypoechoic.
6. Trained muscle was less hyperechoic due to hypertrophy of muscle bundles.
7. Under pressure of the transducer, echogenicity increased in the muscle
8. No focal anechoic, hypoechoic or hyperechoic intramuscular lesion was detected.
9. At rest, in a standing position or during contraction no muscle structures were detected over the fascia or epimysium.

Figure 2.3. Ultrasound and anatomical image of muscle tissue (sample from the anterior thigh region, sagittal section).

M = muscle, F = fascia

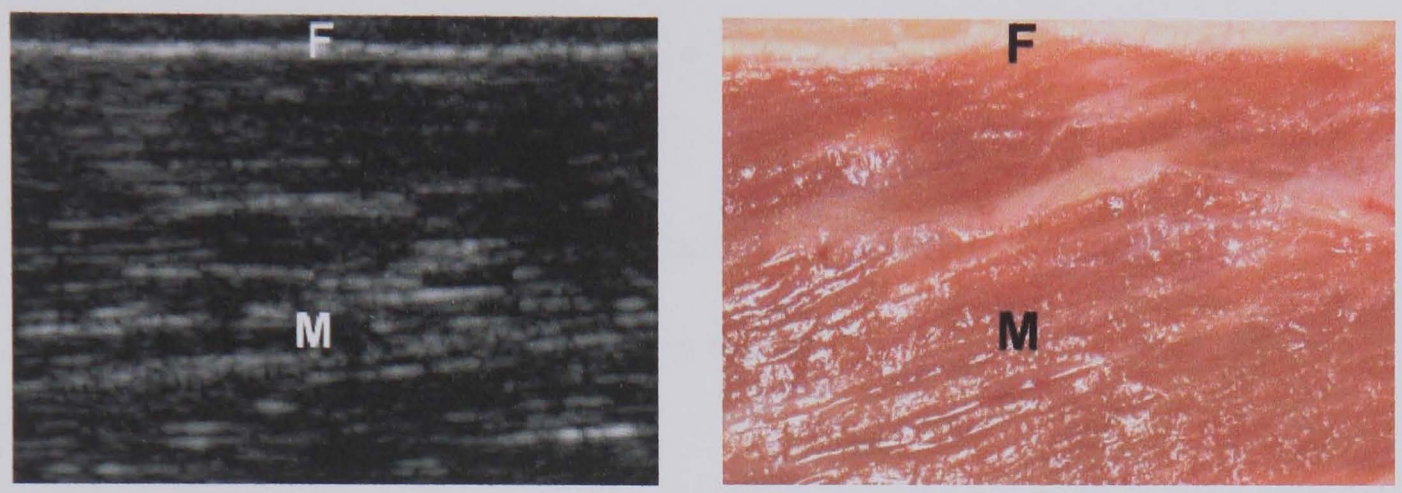

Transverse view (Figure 2.4.)

1. Speckled appearance was observed due to cross-sections of perimysium and vessels.

Figure 2.4. Ultrasound and anatomical image of muscle tissue (sample from the anterior thigh region, transverse section).

M = muscle, F = fascia

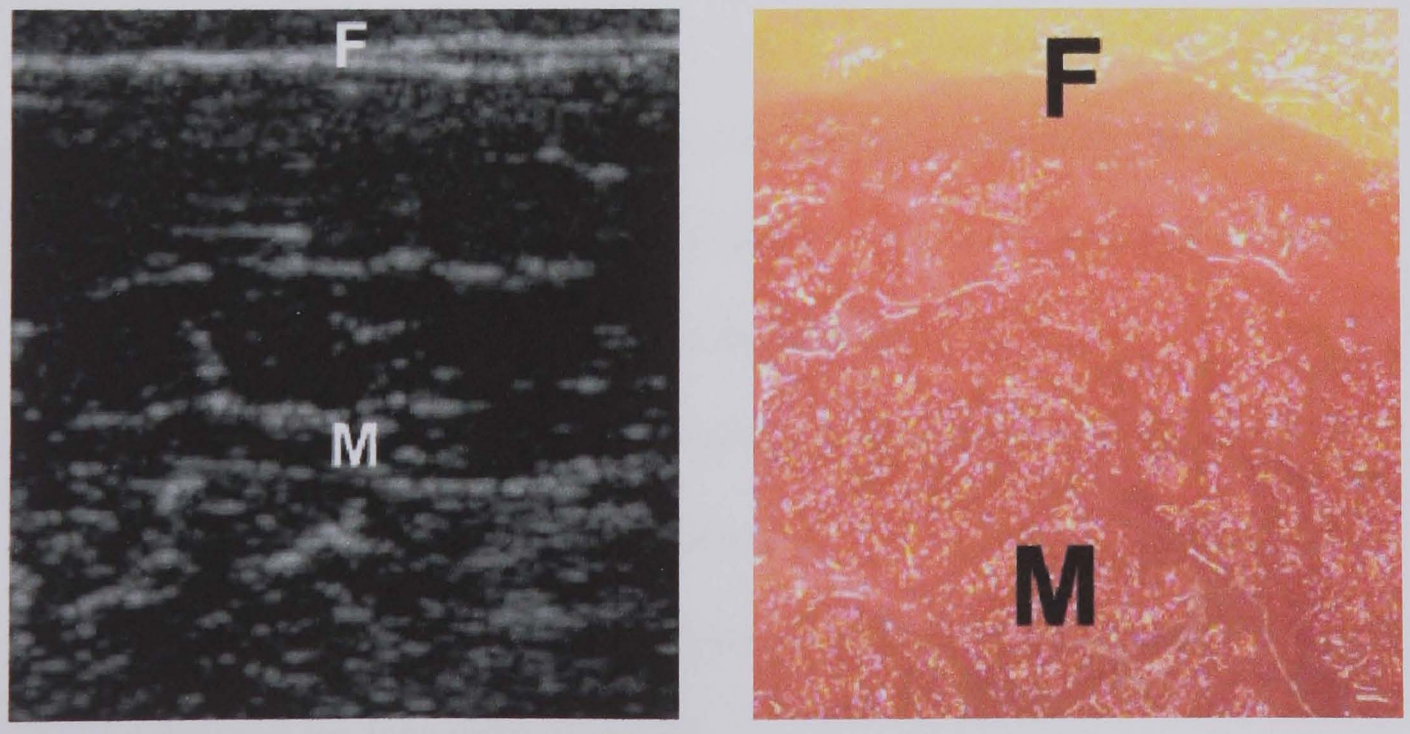

Tendon

Comparison of ultrasound image of tendon tissue to anatomical sample (Figure 2.5.) provided the following results:

Longitudinal view

1. Highly hyperechoic, tightly packed, longitudinally, parallel-orientated fibrillar texture was seen along the axis of the tendon and through the whole width of the tendon.
2. The fibrils ran in the same directions, but crossed each other like a spun pigtail.
3. The straight orientation of fibrillar structure curved only where two tendons blended or the tendon direction was changed.
4. Between the fibrillar structure there was a very small amount of hypoechoic tissue material.
5. No focal hyper-, hyperechoic or anechoic areas were detectable in the tendon, except where sesamoid bones caused different echo patterns in some tendons.
6. No discontinuity of the tendon, no marginal irregularity, no focal flattening or enlargement of the diameter was seen in normal tendons.
7. Vascularity was not detected in the tendon.
8. The same tendon echostructure and size was seen on the contralateral side in the proper anatomic position.
9. During dynamic examination (passive and active movements) freely moving tendons were observed.

Figure 2.5. Ultrasound and anatomical image of tendon tissue (sample from the palmar region of the MCP joint, sagittal section).

T = tendon, B = bone, S = subcutaneous tissue

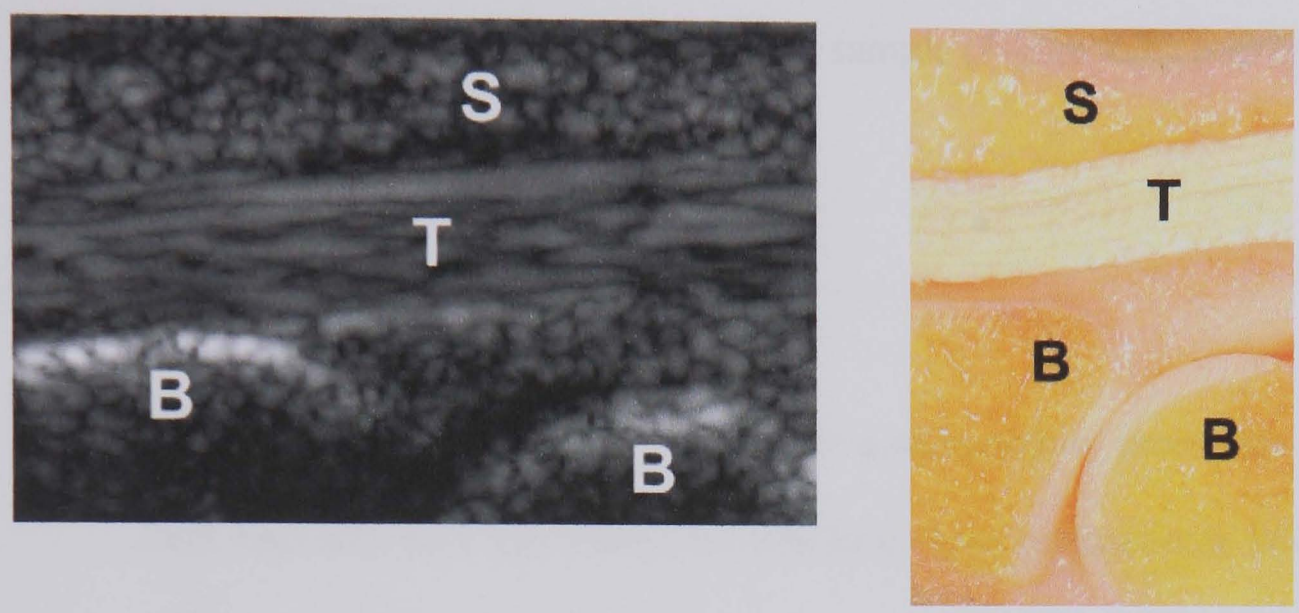

Transverse view (Figure 2.6)

1. A mainly hyperechoic, well-limited shaped structure with densely punctuated pattern (corresponding to the longitudinal fibrillar pattern).
2. Tendon ultrasound cross-section shapes are the same as anatomical shapes: round, oval, flattened or semicircular.

Figure 2.6. Ultrasound and anatomical image of tendon tissue (sample from the palmar region of the MCP joint, transverse section).

T = tendon, B = metacarpal bone, L = deep transverse metacarpal ligament

Tendon sheath, paratenon, extension of the joint capsule

Comparison of ultrasound image of tendon sheath, paratenon or extension of the joint capsule around the tendons to anatomical sample (Figure 2.7.) provided the following results:

Longitudinal view

1. In proper anatomical localisation (under a retinaculum, protrusion of the joint capsule) over the tendon an anechoic layer representing fluid was sometimes observed.

Figure 2.7. Ultrasound and anatomical image of tendon sheath (sample from the palmar region of the MCP joint, sagittal section).

T = tendon, TS = tendon sheath, S = subcutaneous tissue

Transverse view (Figure 2.8.)

1. In proper anatomical localisation around the tendon an anechoic layer (anechoic ring or halo) representing fluid was sometimes observed.

Figure 2.8. Ultrasound and anatomical image of tendon sheath (sample from the palmar region of the MCP joint, transverse section).

T = tendon, TS = tendon sheath, S = subcutaneous tissue

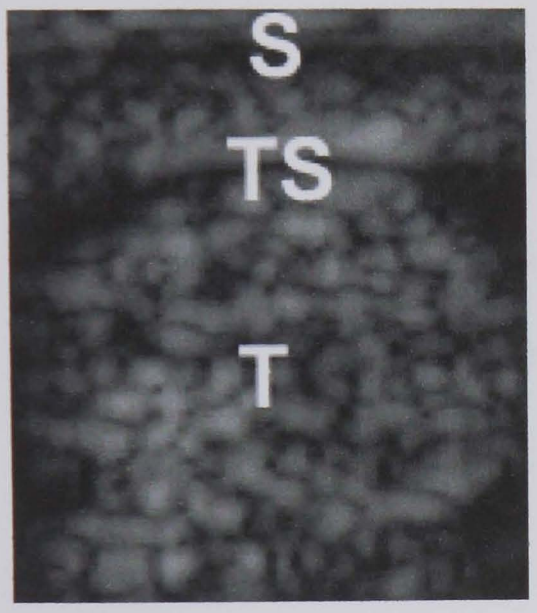

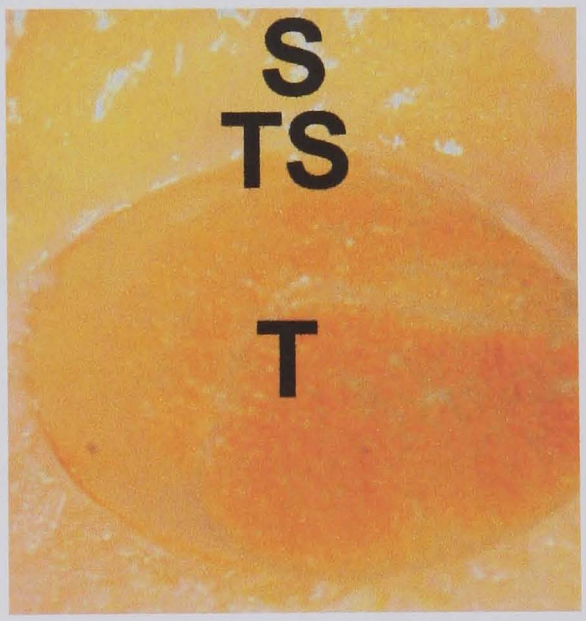

Ligament

Comparison of ultrasound image of ligament to anatomical sample (Figure 2.9.) provided the following results:

1. Ligaments had a hyperechoic parallel structure, similar to that of tendons.
2. Their structures were less regular with less margin definitions than tendons.
3. They were more flattened than tendons.
4. No focal hyper-, hypoechoic or anechoic areas were in the normal ligaments.
5. No discontinuity of the ligament was seen.
6. Vascularity was not detected in the ligament.
7. The same ligament echostructure was seen on the contralateral side.
8. Ligaments were detected in a proper anatomic position between the two bones.

Figure 2.9. Ultrasound and anatomical image of ligament (sample from the iliofemoral ligament at the anterior part of the hip joint, oblique sagittal section).

L = iliofemoral ligament, I = ilopsoas muscle, H = head of the femur, N = neck of the femur

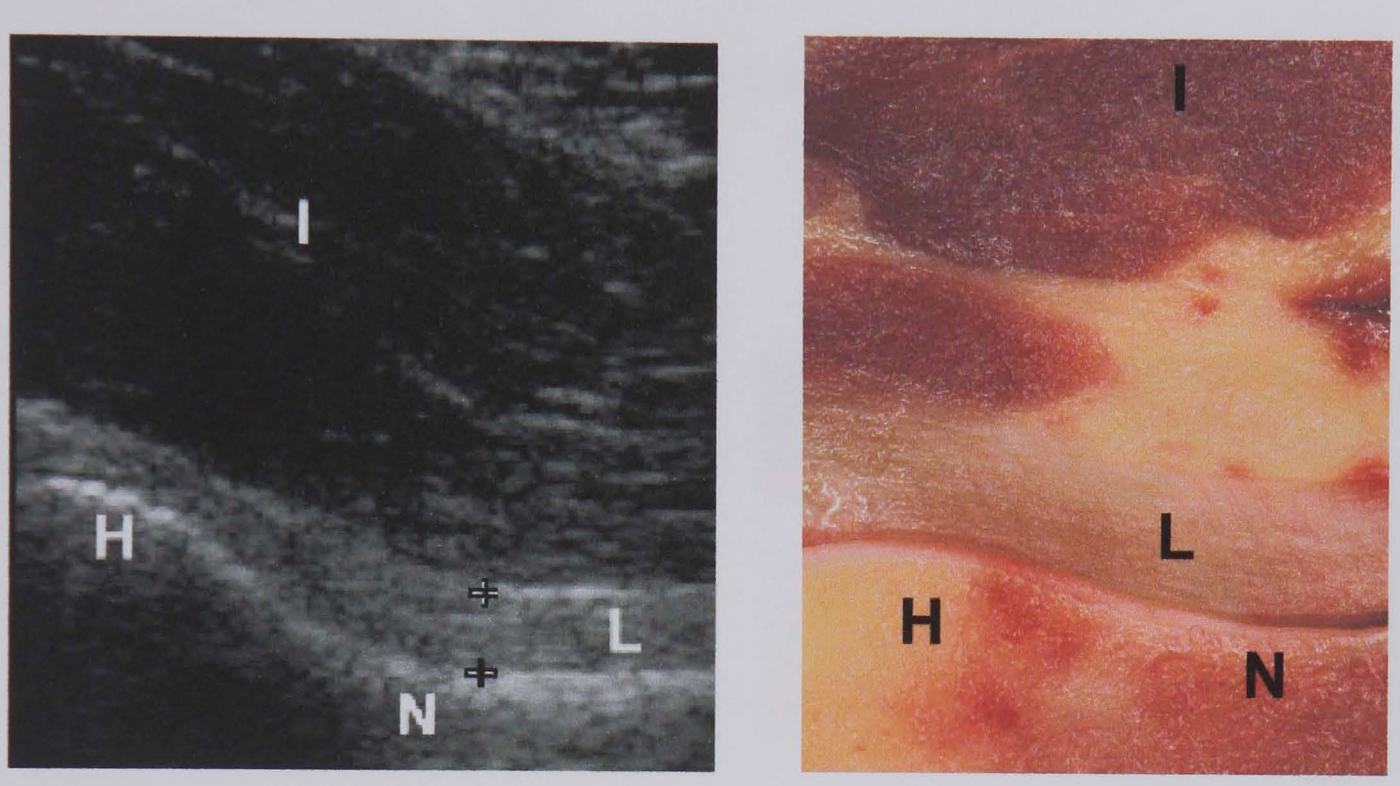

Capsule

Comparison of ultrasound image of capsule to anatomical sample (Figure 2.10.) provided the following results:

1. Capsules very often ran together with the ligaments and they had a similar echostructure and therefore they were not easy to differenctiate from ligaments. Over the bones and cartilage around the joint the first hyperechoic layer was the capsule.
2. Capsular origin and insertion were detected. No sinus or fistula formation was detected in a normal subject.

3. The normal synovial membrane is very thin and is not detectable by ordinary ultrasound equipment.

Figure 2.10. Ultrasound and anatomical image of capsule (sample from the anterior part of the elbow, transverse section).

C = capsule, TH = trochlea humeri, CA = hyaline cartilage, M = muscle

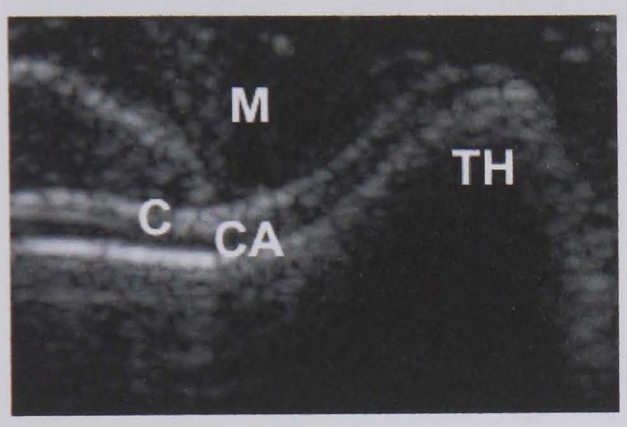

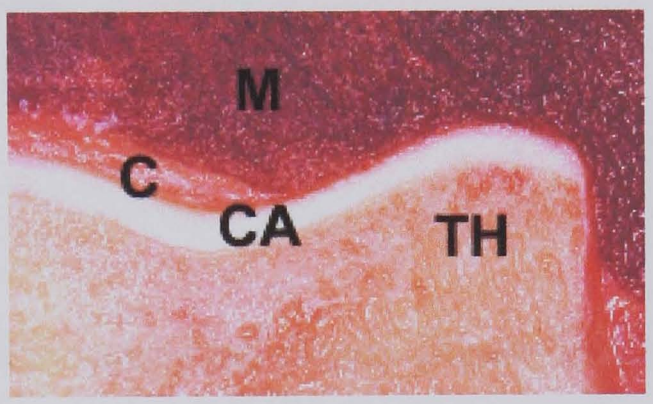

Retinaculum

Comparison of ultrasound image of retinaculum to anatomical sample (Figure 2.11.) provided the following results:

1. The retinaculum was a hyperechoic layer in the proper position.

Figure 2.11. Ultrasound and anatomical image of the flexor retinaculum (sample from the palmar part of the wrist, transverse section).

RE = flexor retinaculum, N = median nerve, T = flexor tendon

Fascia

Comparison of ultrasound image of fascia to anatomical sample (Figure 2.12.) provided the following results:

1. A hyperechoic layer covered the muscle.

Figure 2.12. Ultrasound and anatomical image of fascia (sample from the anterior part of the thigh, longitudinal section).

F = fascia, S = subcutaneous fat, M = muscle

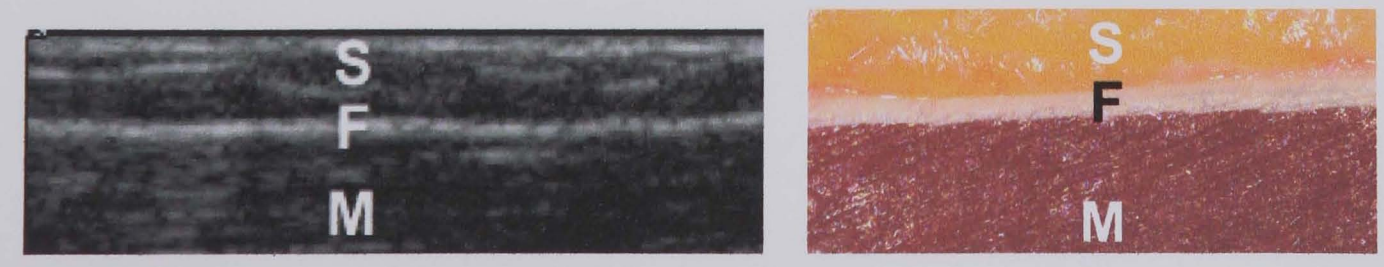

Aponeurosis

Comparison of ultrasound image of aponeurosis to anatomical sample (Figure 2.13.) provided the following result:

1. Hyperechoic layers were detected in the proper anatomical locations.

Figure 2.13. Ultrasound and anatomical image of aponeurosis (sample from the heel, plantar aponeurosis, longitudinal section).

PR = proximal, DI = distal, HFP = heel fat pad, IPF = insertion of the plantar aponeurosis, PF = plantar aponeurosis, CL = calcaneus, FDB = flexor digitorum brevis muscle.

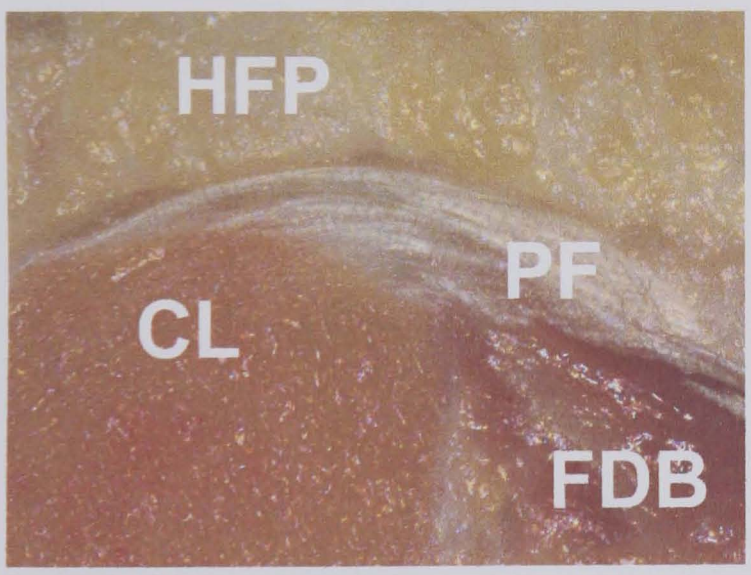

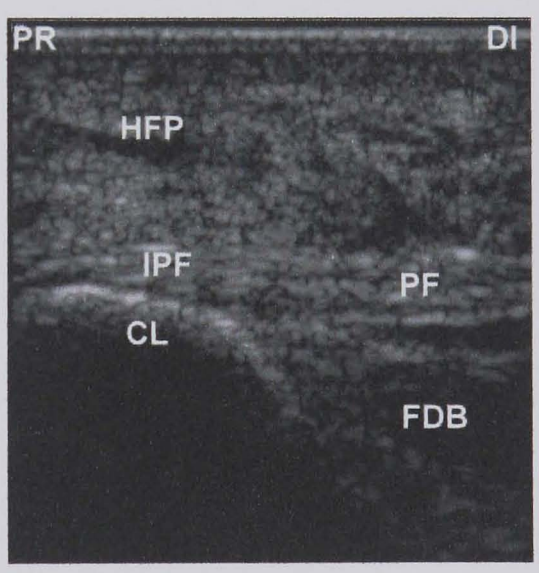

Bursa

Comparison of ultrasound image of bursa to anatomical sample (Figure 2.14.) provided the following results:

1. Normal bursae were not always visualised with the exception of the suprapatellar bursa.
2. The normal bursa had an echoic wall.
3. Between the two walls, there was a small anechoic line representing a fluid film no thicker than 1-2 mm.
4. If there is a communication with the joint, during transducer pressure the anechoic line disappears, because fluid is forced into the joint.
5. No internal echoes were seen in the anechoic layer.
6. Peribursal fat was usually detected around the bursa.
7. Same position (subtendineous, submuscular, subfascial, subcutaneous) and same appearance was observed on the contralateral side.

Figure 2.14. Ultrasound and anatomical image of bursa (sample from the heel, longitudinal section).

PR = proximal, DI = distal, A = Achilles tendon, B = retrocalcaneal bursa, C, CL = calcaneus, K = Kager's fat pad.

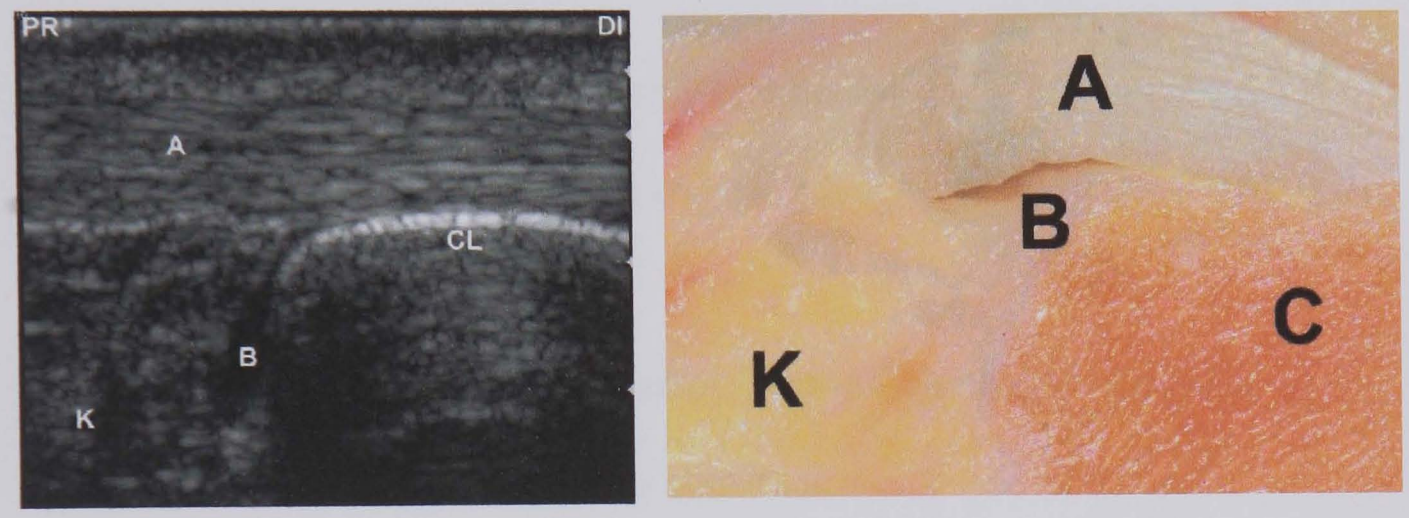

Nerve

Comparison of ultrasound image of nerve to anatomical sample (Figure 2.15.) provided the following results:

Longitudinal view

1. Hypoechoic fascicular pattern was detected.
2. Parallel hyperechoic margin corresponding to the epineurum was observed.
3. No focal hyperechoic or anechoic area was detected in the nerve.
4. No marginal irregularity was observed.
5. No focal flattening or enlargement of the diameter was depicted.
6. Vascularity was not detected in the nerve.
7. Same echostructure and size was detected on the contralateral side.
8. Nerves were detected in the proper anatomic position.

Figure 2.15. Ultrasound and anatomical image of nerve (sample from the median nerve, longitudinal section).

N = median nerve, T = flexor tendon

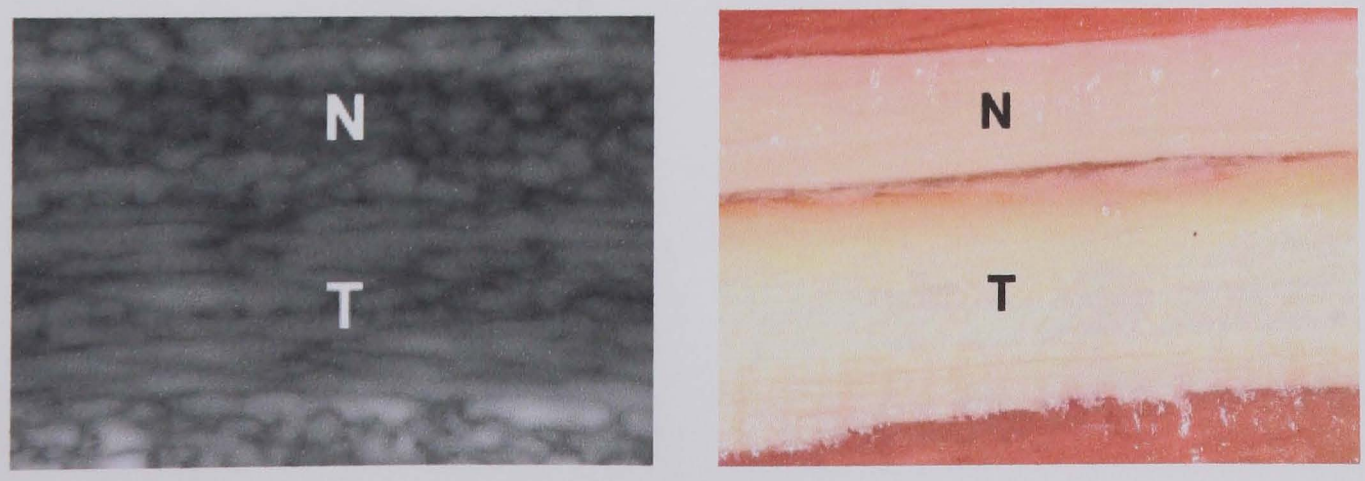

Transverse view (Figure 2.16.)

1. Speckled ovoid or rounded appearance was detected.

Figure 2.16. Ultrasound and anatomical image of nerve (sample from the median nerve, transverse section).

L = lateral, M = medial, RE = retinaculum, N = median nerve, T = flexor tendon, R = radius U = ulna, LI = radiocarpal ligament

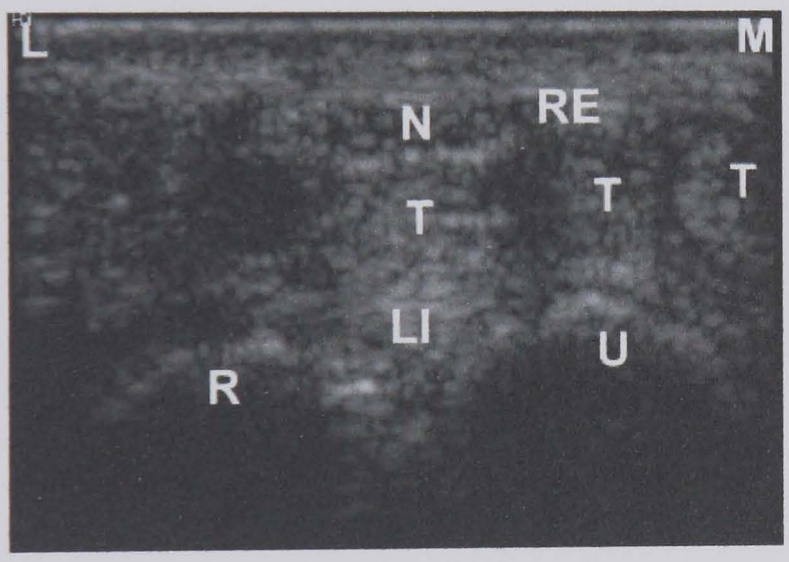

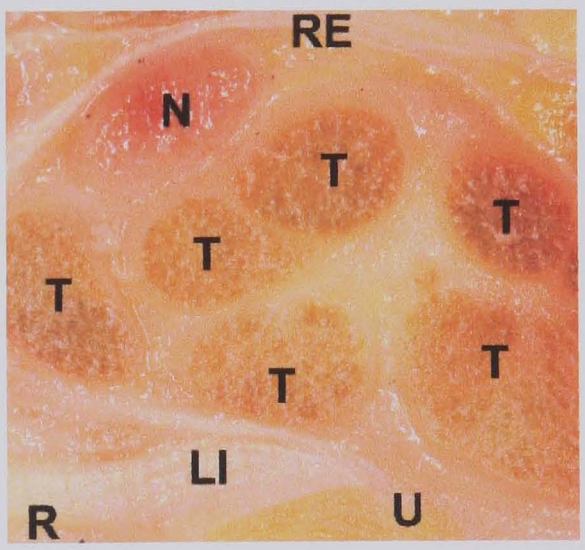

Hyaline cartilage

Comparison of ultrasound image of hyaline cartilage to anatomical sample (Figure 2.17.) provided the following results:

1. Homogeneous anechoic or hypoechoic layers covered the articular bone surfaces.
2. It was not possible to detect the whole convex articular surface.
3. Different bones were covered with a different thickness of cartilage.
4. No marginal irregularities, sharp margins were seen either on articular or bone surfaces.
5. No focal internal echo sign, no vascularity was seen.
6. The same cartilage echostructure and thickness was observed on the contralateral side.
7. The thickest part of the cartilage is centrally over the convexity of bone surface and the thickness decreases continuously towards the margin.

Figure 2.17. Ultrasound and anatomical image of hyaline cartilage (sample from the femoral condyle, longitudinal and transverse section).

C = hyaline cartilage, B = bone, S = skin

Transverse section

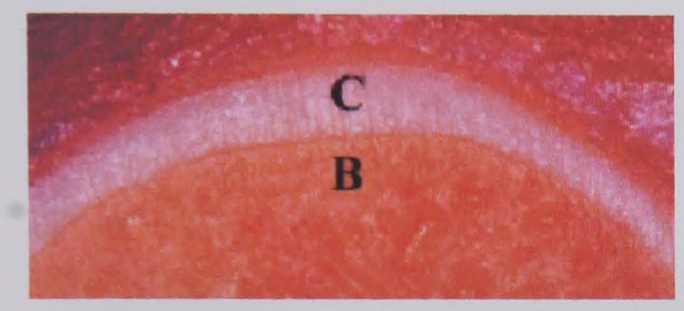

Longitudinal section

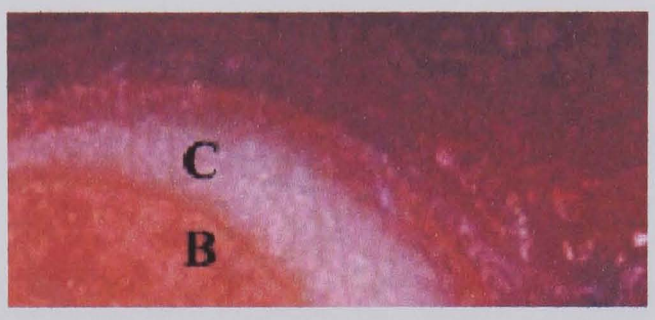

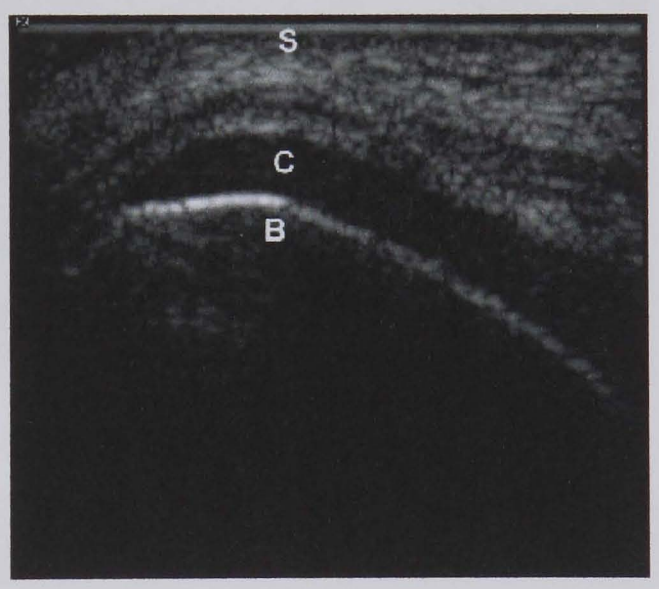

Fibrocartilage

Comparison of ultrasound image of fibrocartilage to anatomical sample (Figure 2.18.) provided the following results:

1. Homogenous hyperechoic structure was detected in a proper anatomical position.

2. The shape was usually triangular or wedge shaped.

3. No vascularity was observed.

4. Normal labrum did not contain anechoic areas.

Figure 2.18. Ultrasound and anatomical image of fibrocartilage (sample from the glenohumeral labrum, transverse section).

H = humeral head, L = labrum, G = glenoid, INF = infraspinatus muscle

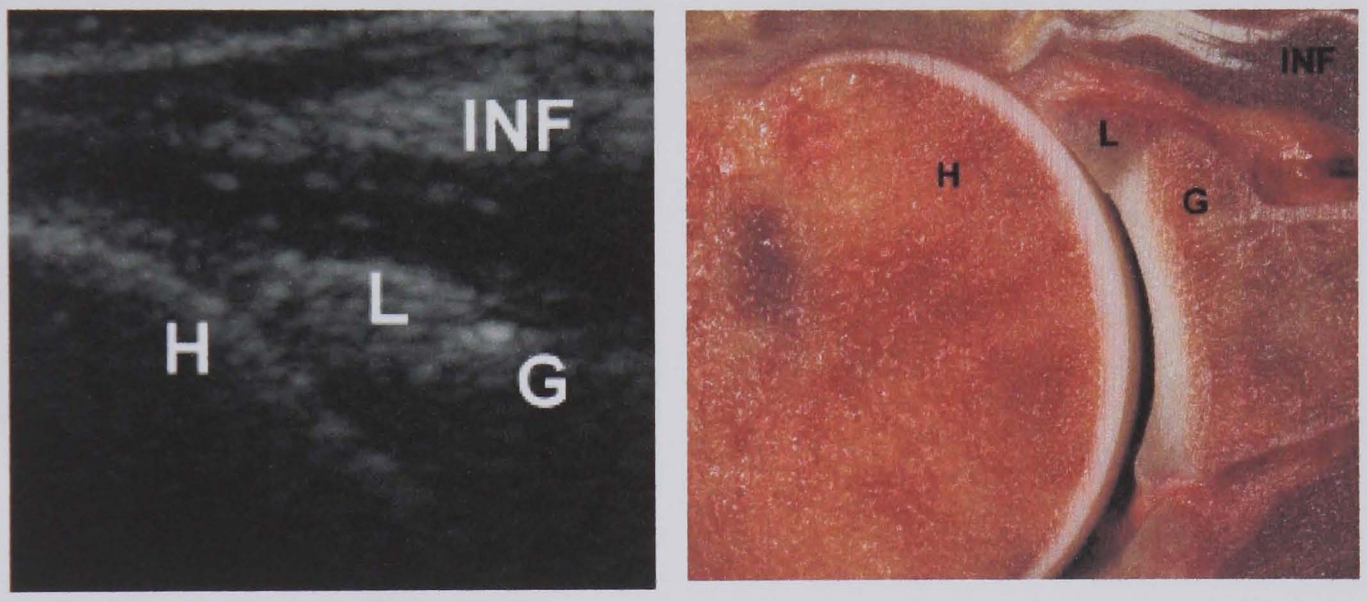

Bone

Comparison of ultrasound image of bone to anatomical sample (Figure 2.19.) provided the following results:

1. Only the bone surface was visible as a hyperechoic line with acoustic shadow.

2. The normal periosteum was rarely detected.

3. The bone surface was smooth and not disrupted except where was groove for tendon attachment, ridge for tendon and muscle attachment and foramen nutrition.

Transverse view

Figure 2.19. Ultrasound and anatomical image of bone (sample from the tibia, transverse section).

S = skin, B = bone, BS = bone surface, M = bone marrow

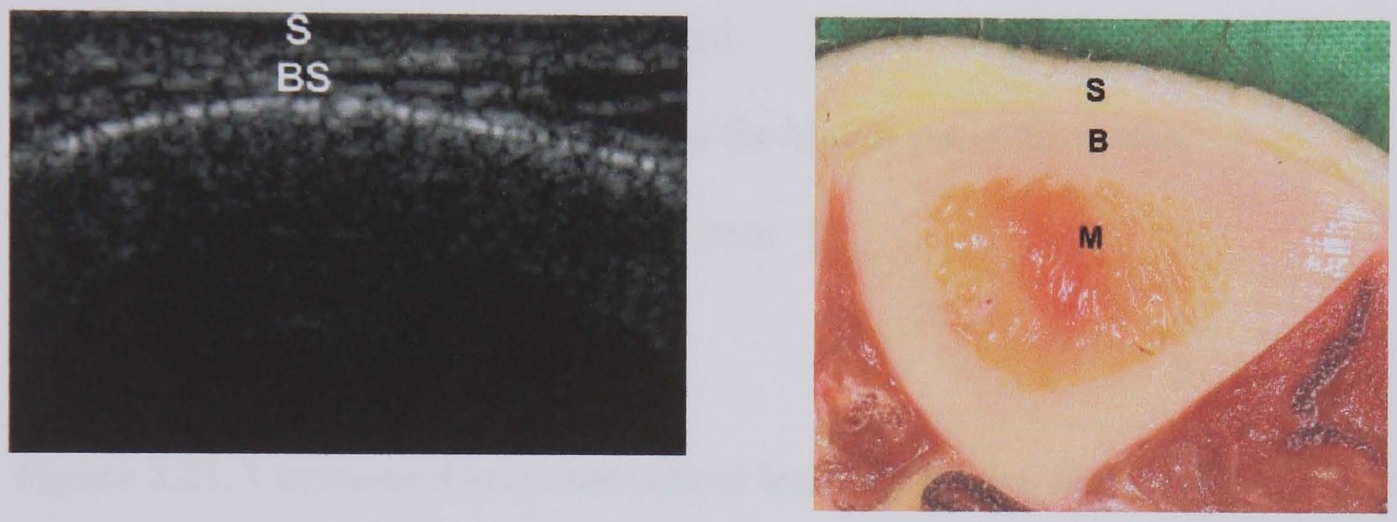

Longitudinal view (Figure 2.20.)

Figure 2.20. Ultrasound and anatomical image of bone (sample from the tibia, longitudinal section).

S = skin, B = bone, BS = bone surface, M = bone marrow

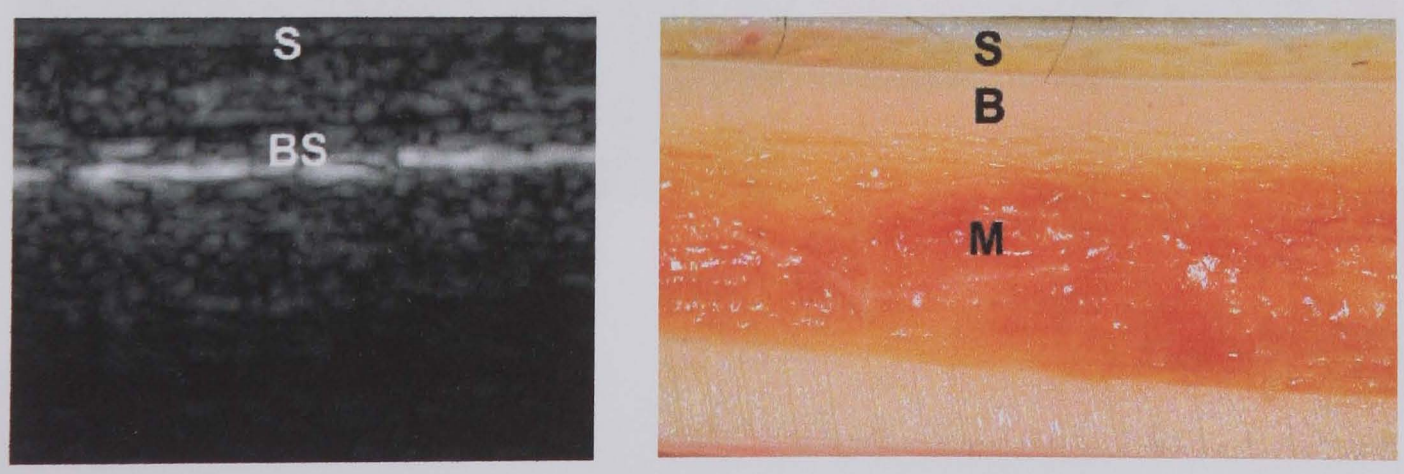

Lymph node

Comparison of ultrasound image of lymph node to anatomical sample (Figure 2.21.) provided the following results:

1. Oval shaped lymph nodes were detected. Longitudinal diameter was parallel with the skin. They were often detected around the blood vessels.
2. Hyperechoic central hilum was seen.
3. Hypoechoic cortex was detected.
4. Hyperechoic capsule was detected.
5. Blood flow was observed only at the hilum, not in the cortex.
6. No extracapsular extension was seen.

Figure 2.21. Ultrasound and anatomical image of lymph node (sample from the groin, longitudinal section).

S = skin, H = hilum, C = cortex, CA = capsule, F = fascia

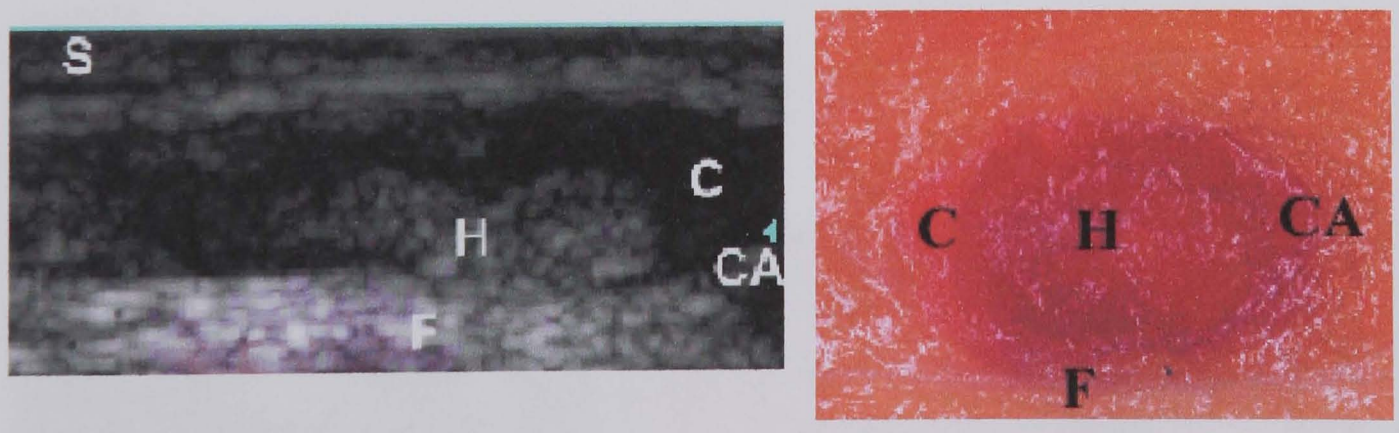

Joint

Comparison of ultrasound image of joint to anatomical sample (Figure 2.22.) provided the following results:

1. The edges of both bones were visualised, which made up the joints.
2. Other parts of the joint (cartilage, intra-articular disc, meniscus, intra-articular ligament, fat pad) were also visualised.
3. Proximal and distal capsule attachment were visualised.
4. No blood flow was detected inside the joint.
5. Movement of the bones were visualised during the movement of the joints.
6. In transverse section we usually could not visualise the edges of both bones, which made up the joints.

Figure 2.22. Ultrasound and anatomical image of joint (sample from the elbow joint, longitudinal section).

B = bone surface, CA = cartilage F = fat pad, JS = joint space, C = capsule, M = muscle

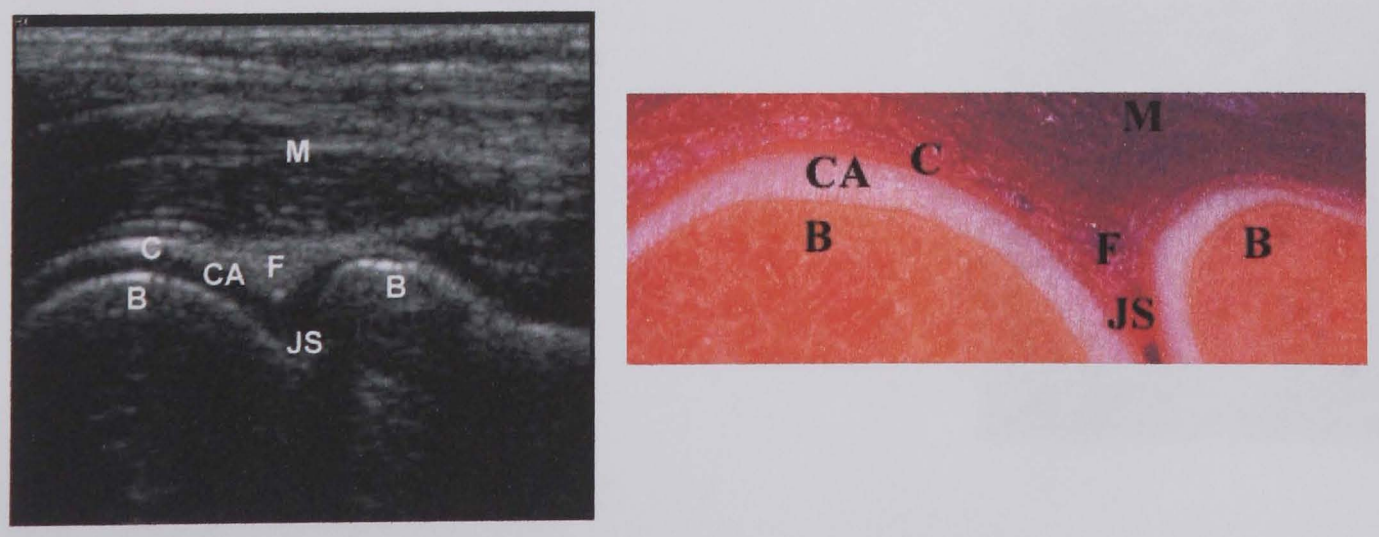

Standardized dorsal sagittal plane through the 2nd MCP joint.

Figure 2.23. Transducer position. Clinical photo.

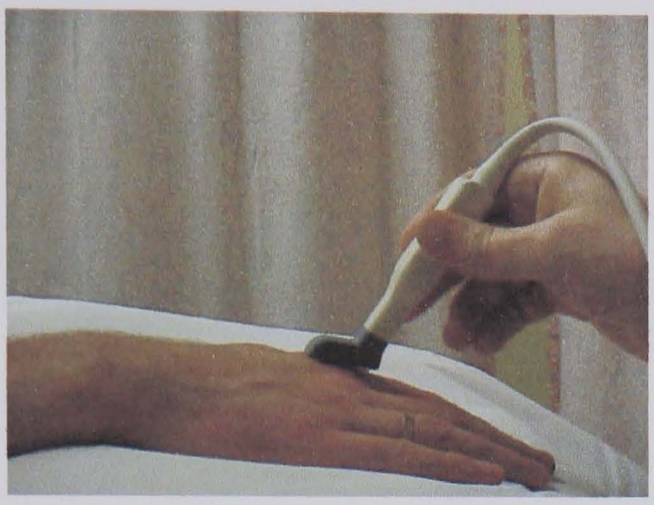

Transducer position

Dorsal aspect, sagittal plane through the MCP joint.

Body position

Extended or flexed elbow, wrist in neutral position, hand and forearm in pronation on the examination table.

Normal anatomical reference landmarks

(M)	Metacarpal head	(P)	Phalangeal base
(JS)	Joint space	(ET)	Extensor tendon
(C)	Cartilage	(FP)	Central slip

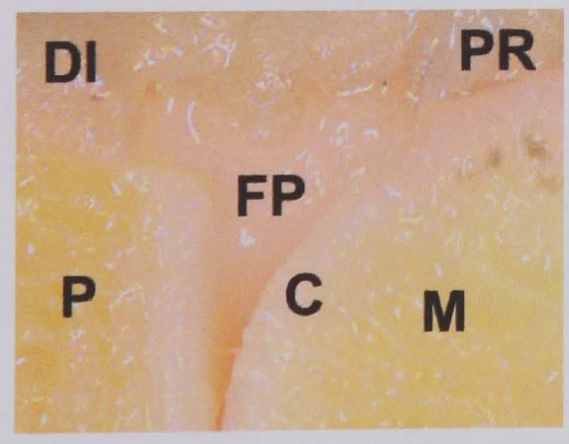

DI: Distal

PR: Proximal

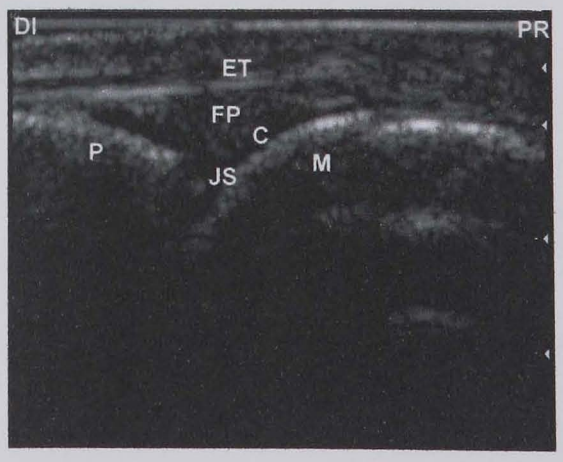

Standardized anterior, oblique parasagittal plane through the anterior hip recess Figure 2.24. Transducer position. Clinical photo.

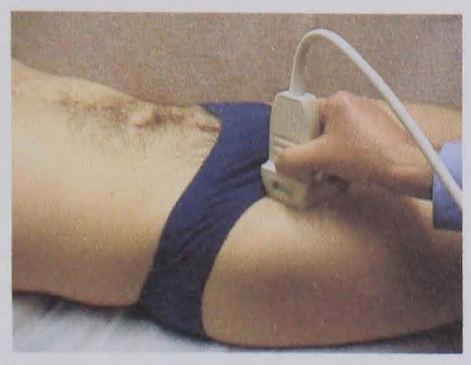

Transducer position

Anterior aspect, oblique sagittal plane through the axis of the femoral head and neck.

Body position

Supine position, straight legs, in a neutral rotation or in slight external rotation with heels in contact with each other.

Normal anatomical reference landmarks

(H)	Head of the femur	(N)	Neck of the femur and femoral shaft
(I)	Iliopsoas muscle	(L)	Iliofemoral ligament and joint capsule
(A)	Acetabulum		

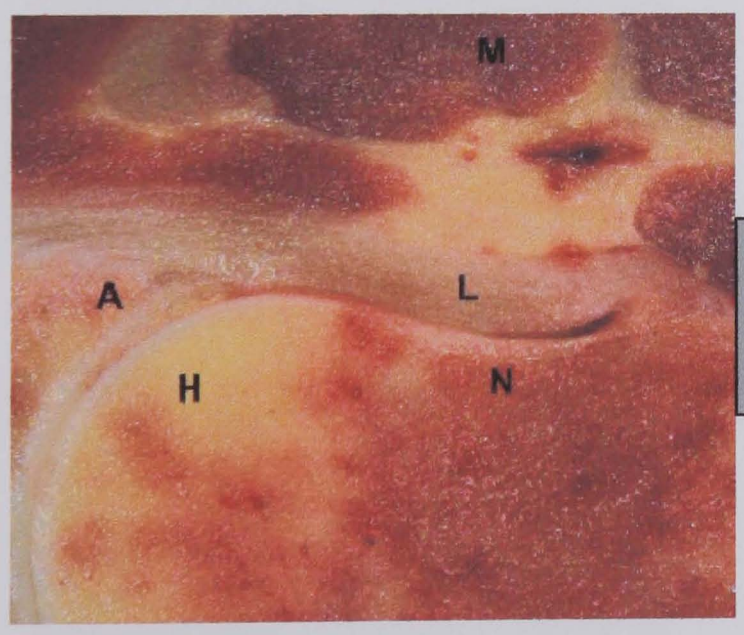

PR: Proximal

DI: Distal

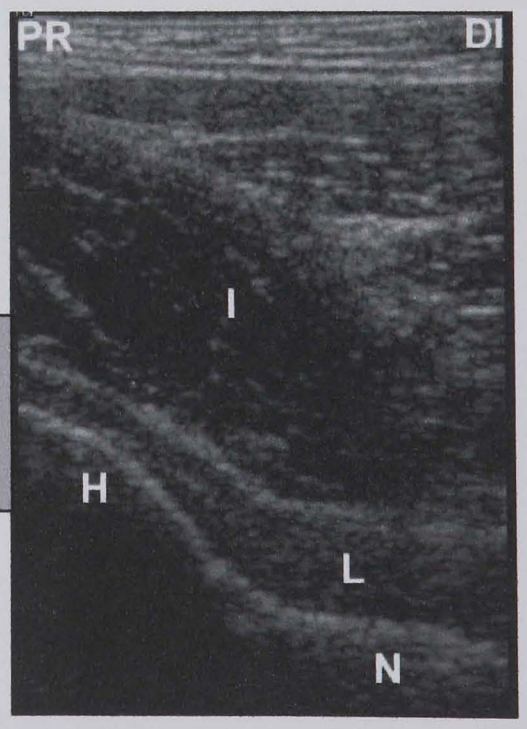

Standardized anterior sagittal plane through the superior pole of the patella

Figure 2.25. Transducer position. Clinical photo.

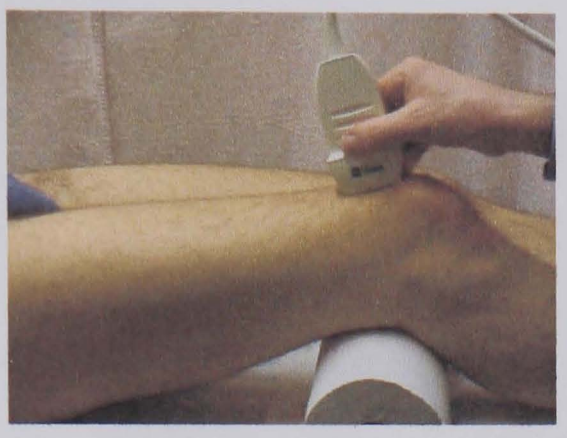

Transducer position

Anterior aspect, sagittal plane through the quadriceps tendon.

Body position

Supine position, with slightly flexed knee.

Normal anatomical reference landmarks

(Q)	Tendon of quadriceps femoris muscle	(B)	Suprapatellar bursa
(SP)	Superior pole of the patella	(PF)	Peribursal fat pad
(F)	Femoral shaft		

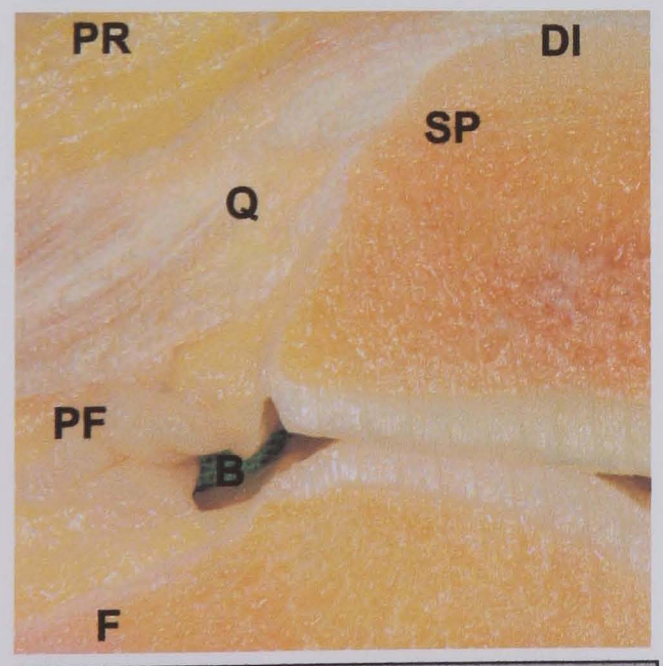

PR: Proximal

DI: Distal

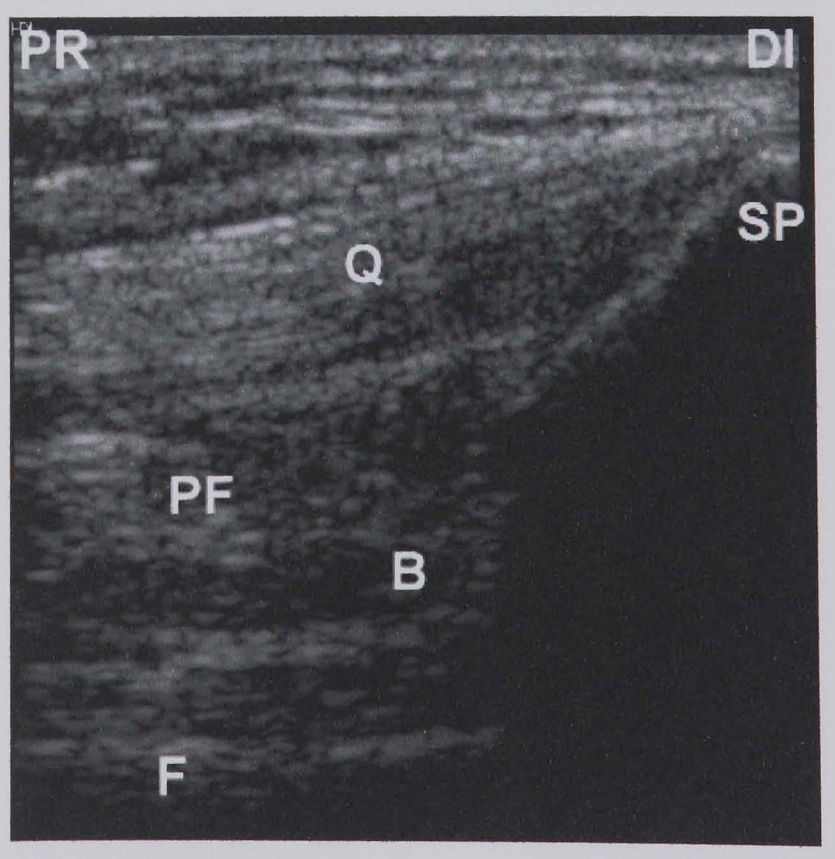

Standardized anterior, sagittal plane through the inferior pole of the patella.

Figure 2.26. Transducer position. Clinical photo.

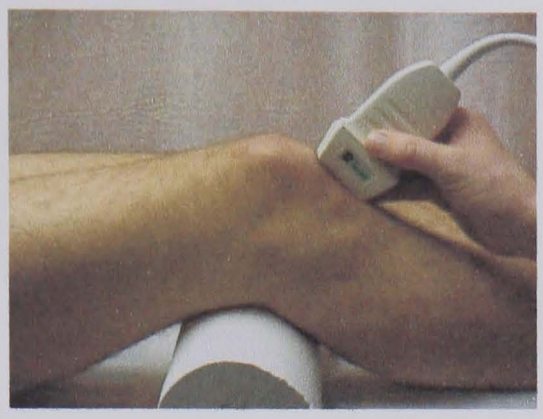

Transducer position

Anterior aspect, sagittal plane through the proximal end of the patellar ligament.

Body position

Supine position, with slightly flexed knee.

Normal anatomical reference landmarks

(L)	Patellar ligament	(P)	Lower pole of the patella
(HF)	Hoffa fat pad (Infrapatellar fat pad)		

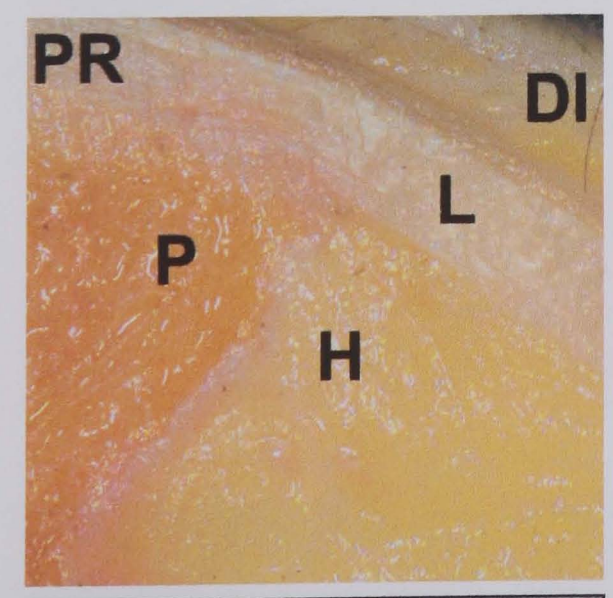

PR: Proximal

DI: Distal

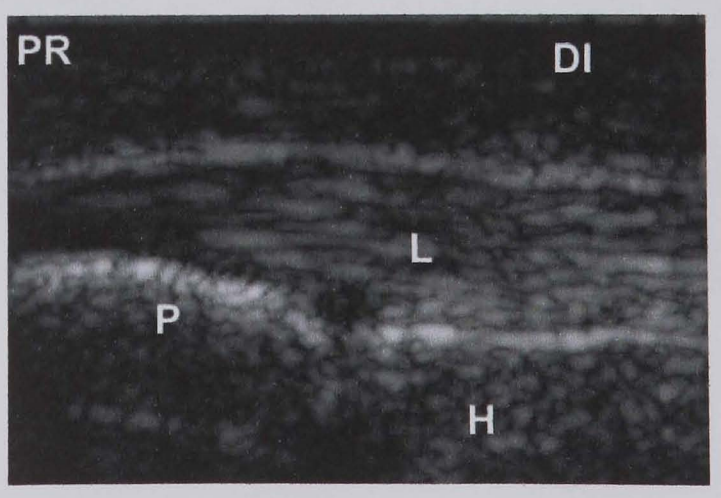

Standardized anterior, sagittal plane through the tibial tuberosity.

Figure 2.27. Transducer position. Clinical photo.

Transducer position

Anterior aspect, sagittal plane through the distal end of the patellar ligament.

Body position

Supine position, with slightly flexed knee.

Normal anatomical reference landmarks

(L)	Patellar ligament	(T)	Tibia
(H)	Infrapatellar fat pad (Hoffa fat pad)		

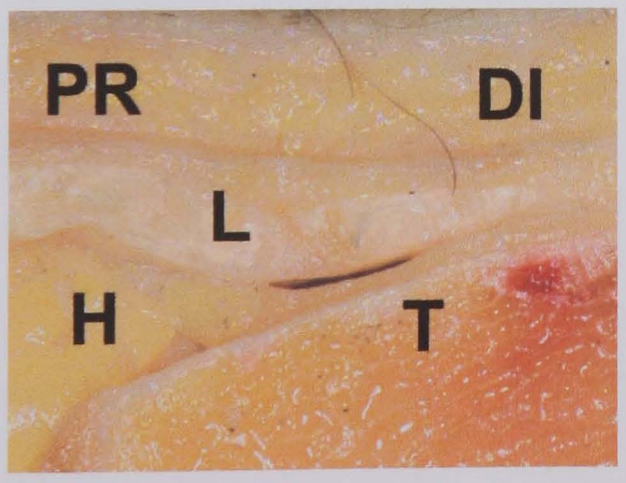

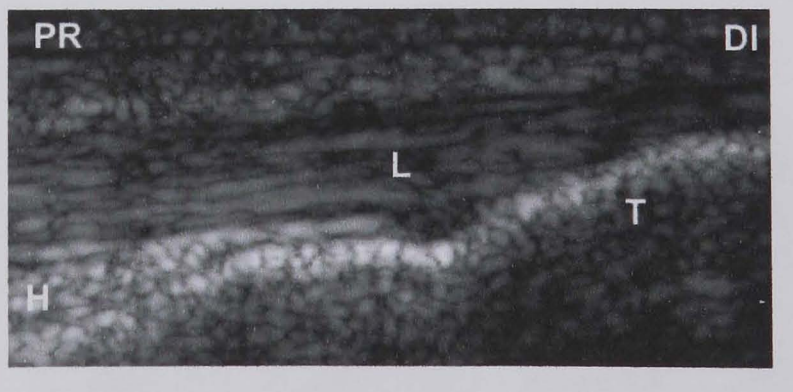

PR: Proximal DI: Distal

Standardized dorsal, sagittal plane through the Achilles tendon.

Figure 2.28. Transducer position. Clinical photo.

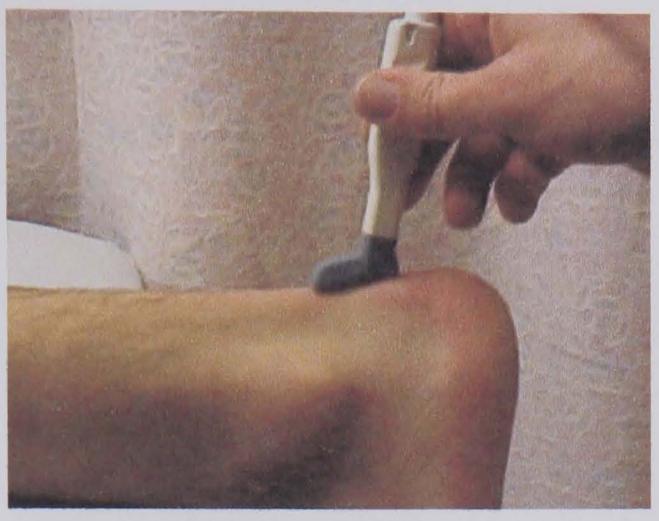

Transducer position

Posterior aspect, sagittal plane through the long axis of the Achilles tendon.

Body position

Prone position with hanging foot over the edge (or end) of the examination table with dorsiflexed foot.

Normal anatomical reference landmarks

(A)	Achilles tendon	(C)	Calcaneus
(B)	Retrocalcaneal bursa	(K)	Kager fat pad

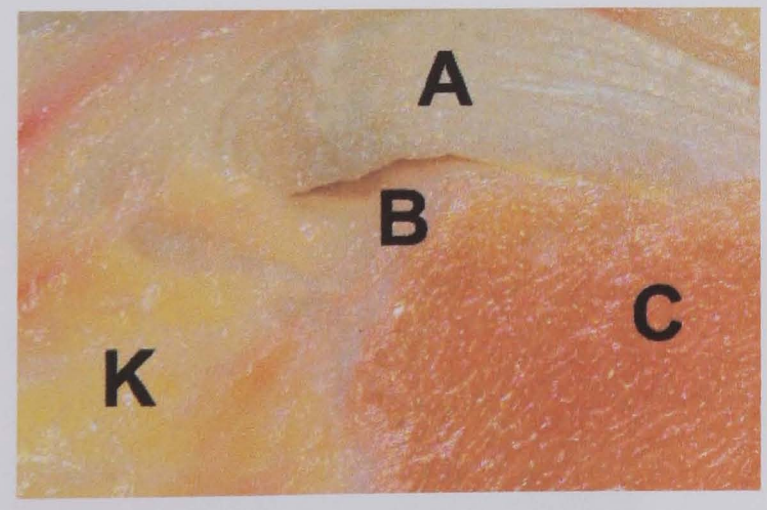

P: Proximal

D: Distal

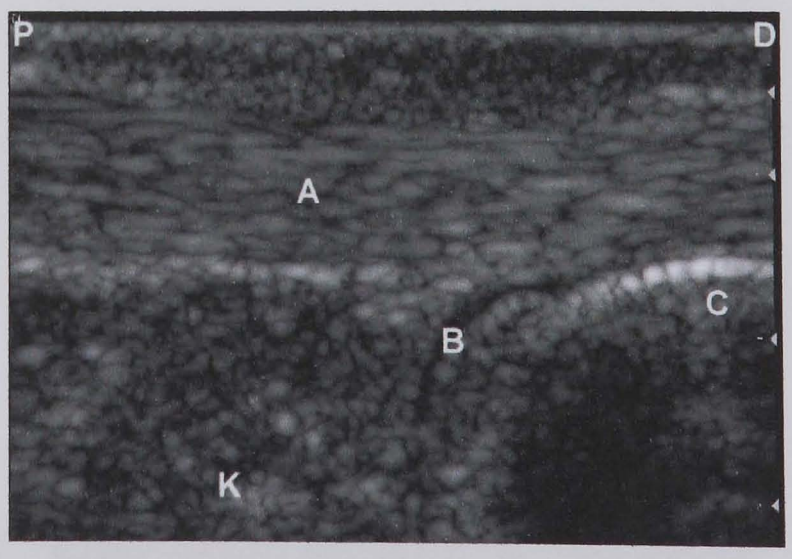

Standardized plantar, medial parasagittal plane through the plantar aponeurosis.

Figure 2.29. Transducer position. Clinical photo.

Transducer position

Plantar aspect, sagittal plane through the calcaneus.

Body position

Prone position with the feet hanging over the edge of the examination table.

Normal anatomical reference landmarks

(CL) Calcaneus	(PF) Plantar fascia
(IPF) Insertion of the plantar fascia on the calcaneus	(HFP)Heel fat pad
(FDB)Flexor digitorum brevis muscle	

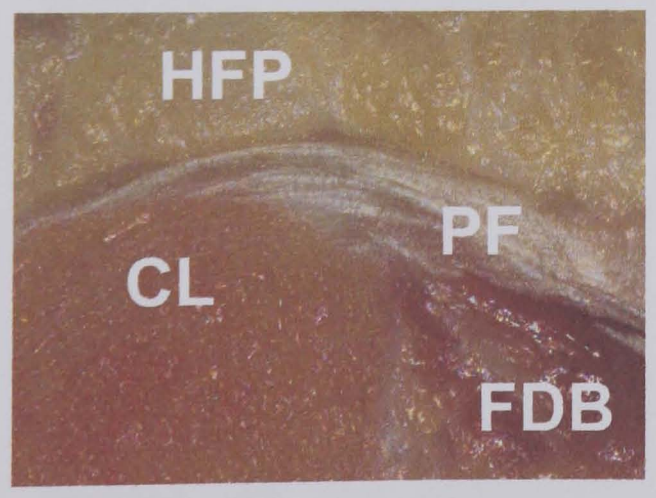

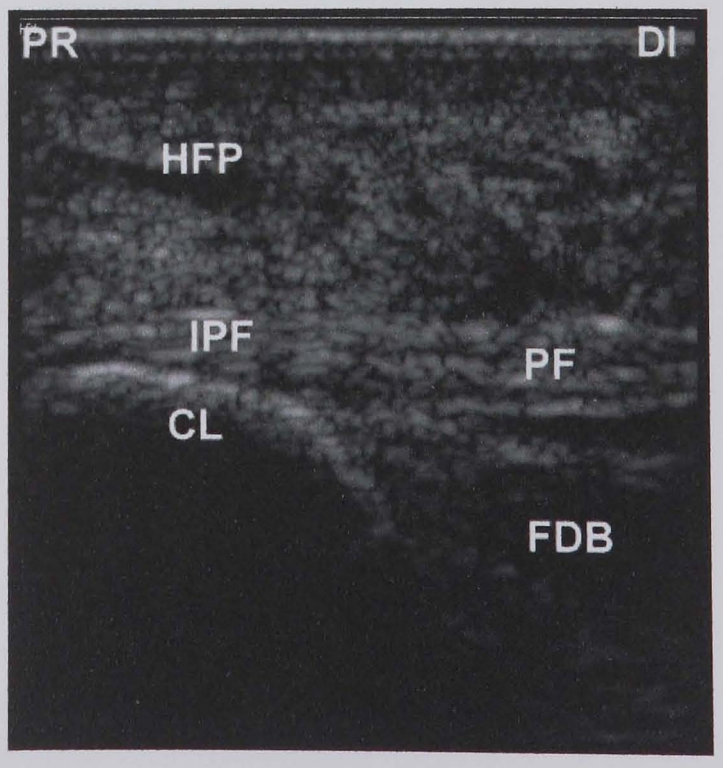

PR: Proximal

DI: Distal

2.4. Discussion

In this study all US images obtained were of acceptable quality. For each well-defined anatomical plane corresponding ultrasound images were obtained. In addition to this a descriptive method was used to characterize ultrasound images. These descriptions form the basis of abnormal tissue and joint structure recognition by ultrasonography. A number of ultrasonographic characteristics of periarticular soft-tissues and articular structures have been described previously but this is the first attempt at direct anatomical correlation. The determination of these characteristics and the description of anatomical landmarks, subject's position, joint position and transducer position allow for reliable standardization and quantification of ultrasound studies of musculoskeletal tissues. Using standard methods also allows for the measurement of intra and interobserver variation. One of the major arguments against the wider application of ultrasound examination as a standard examination in clinical rheumatology, orthopaedics and in sports medicine is the presumed high intra- and interobserver variation. This assumption is based correctly on the fact that there is a close physical contact between the observer and subject during an ultrasound examination and the observer may alter the transducer position thus obtaining different image planes and different quantitative information. However we need to quantify intra- and interobserver variation now that standard image planes can be studied with improved image resolution. In this chapter it is confirmed that normal anatomical structures with an "acoustic window" can be accurately depicted with high resolution. In the future we need to measure intra- and

interobserver variation of pathological tissue using ultrasound and compare with other imaging methods.

Standardization of ultrasound images is not a simple task, but it is an important one. In the musculoskeletal ultrasound literature a number of authors have attempted to use standard planes during their study of a region. A proposed guideline for musculoskeletal ultrasonography in rheumatology has recently been published in the Annals of Rheumatic Diseases (161). This article shows the importance of describing the standardization of the musculoskeletal ultrasonography. Due to the limited space the authors did not publish every image of all described planes nor did they include the standardized ultrasound tissue image of different tissues of the musculoskeletal system with corresponding anatomical images. Clearly, in the future there is a need to publish a detailed, comprehensive ultrasound anatomy book with corresponding ultrasound image and section anatomy using a standardized method for different musculoskeletal tissues and joints.

Part of this chapter was published in the abstract book of the 4th EULAR (European League Against Rheumatism) Sonography Course, Madrid, Spain, 2002

2.5. Future aims

There will be three major tasks after the description of the normal ultrasonographic features of the musculoskeletal system in comparison with cadaver tissues. First the effect of the aging process on the characteristics of different musculoskeletal tissues in comparison with cadaver tissues should be determined. For this purpose a very careful selection of cadavers of different age groups with an accurate medical history to exclude any musculoskeletal diseases will be required. New ultrasound methods such as elastography and tissue harmonic imaging will also be required for this study. During elastography an elastic medium is compressed by a constant uniaxial load (stress or displacement), all points in the medium experience a resulting level of longitudinal strain whose principal components are along the axis of compression. If one or more of the tissue elements has a different stiffness parameter than the others, the level of strain in that element will be higher or lower; a stiffer tissue element will generally experience less strain than one which is less stiff (162). Elastography might be useful to differentiate normal and "ageing" fibrous tissue. During tissue harmonic imaging, the higher harmonic components of the fundamental incident frequency is detected only and results in a better lateral resolution and improved border delineation (65). Tissue harmonic imaging is less dependent on patient tissue characteristics and even in obese patients, reasonable US images can be obtained. Cadaver tissue is not an ideal tissue for conventional ultrasonography but might be well visualised satisfactorily with tissue harmonic imaging.

The second task should be to undertake an ultrasonographic description and pathological comparison of different musculoskeletal lesions such as bone erosion and synovial proliferation, as well as enthesitis etc. Donald Resnick and his team in San Diego have already compared X-ray, CT and MRI with pathological specimens (163). Thirdly, normal ultrasound anatomy for children will also need to be described and standardized.

Chapter 3. Intraobserver repeatability and interobserver reproducibility in musculoskeletal ultrasound imaging measurements

3.1. Introduction

It is a common view that one of the major disadvantages of musculoskeletal ultrasound is operator-dependency (129-136). In musculoskeletal US imaging the images generated are mainly qualitative and agreement has to be reached by different observers as to the presence or absence of pathological signs or disease. If quantitative measurements are required then intra- and interobserver errors become more important. We have therefore determined the magnitude of inter- and intraobserver errors using US imaging for the measurement of the distance between the iliofemoral ligament and the femoral neck in 22 hip joints from an unselected group of normal controls and patients with inflammatory joint disease. Individuals with a history of previous hip surgery were excluded from the study. The hip joint was selected for the following reasons:

1. The hip is a deep joint and not easy to palpate. Hip joint effusions are not easily detected by clinical examination. However the iliofemoral ligament and the neck of the femur are easily identified on US imaging
2. There is an extensive literature describing the US appearances of the anterior hip joint recess in health and disease, but only one non-blind study calculated intra and interobserver errors (99).

In addition, an assessment of intraobserver error was measured using a phantom containing two wires at 4 and 6 cm deep from the surface and measuring the vertical depth between these wires.

3.2. Materials and methods

Two independent investigators studied 22 hips. One investigator (PVB) had previous experience in musculoskeletal ultrasonography (US). The other investigator (RDS) had undergone a short course in hip sonography (only 3 hours). Each hip was studied with an ATL (Advanced Technology Laboratories, Bothell, Washington, USA) HDI (High Definition Imaging) 3000 ultrasound machine with a linear (L) 7-4 MHz 38-mm footprint probe and musculoskeletal software. US imaging was performed in the oblique sagittal plane from an anterior approach with the subject in a supine position with the straight leg in slight external rotation (Figure 3.1.).

Figure 3.1. Standard position of the probe for US imaging of the hip.

Normal anatomical reference landmarks were established (head of the femur, neck of the femur, iliofemoral ligament). The femoral neck-iliofemoral ligament distance was measured in triplicate in quick succession (Figure 3.2). Before each measurement a new image was generated and the measurements taken.

Figure 3.2. Hip ultrasound image.

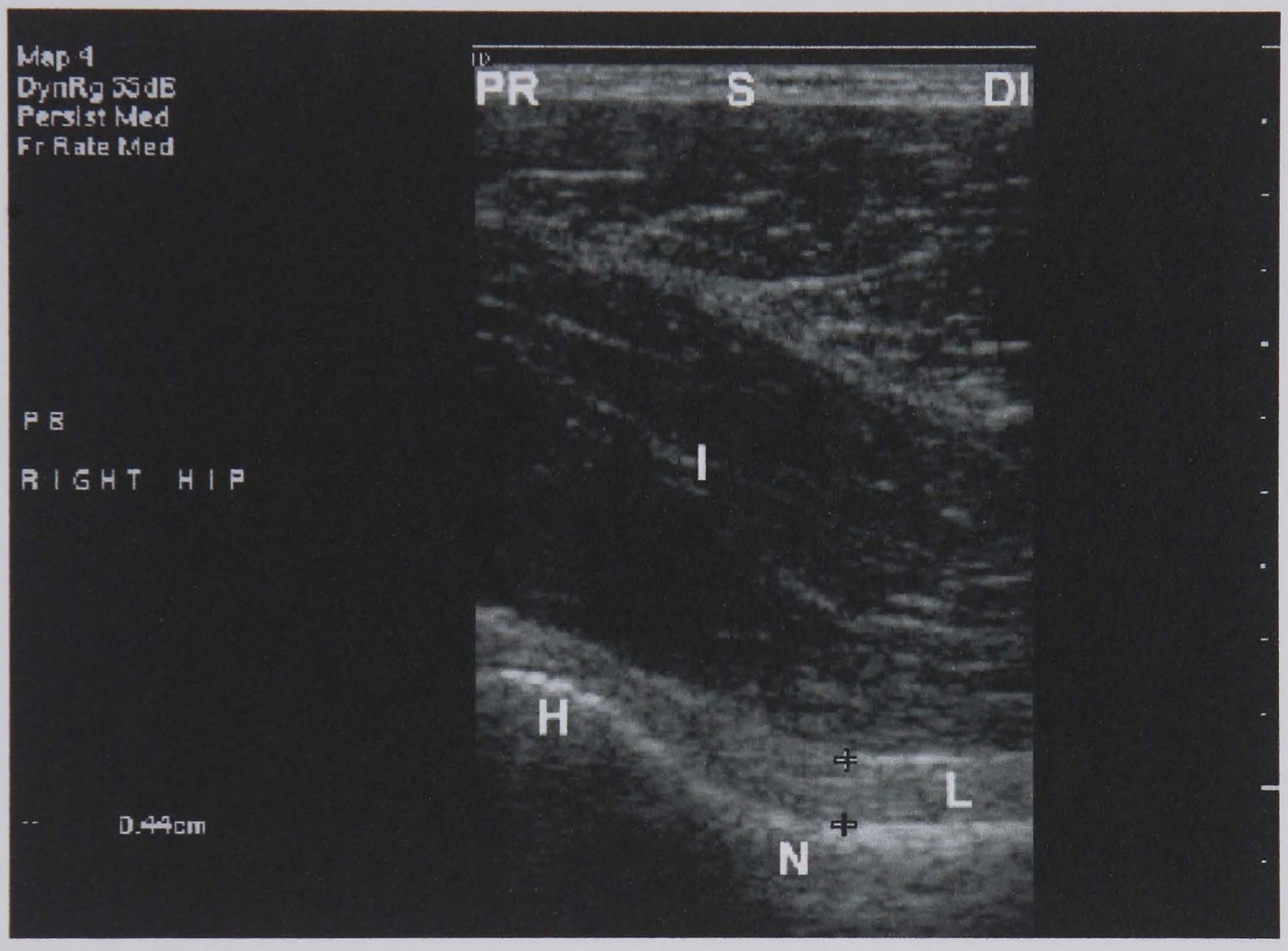

The crosses indicate the position of the iliofemoral ligament and the femoral neck. H: femoral head, N: femoral neck. L: iliofemoral ligament, I: iliopsoas muscle, S: skin, PR: proximal end of probe, DI: distal end of probe.

Using the phantom (Gammex RMI 403GS, Middleton, WI, USA) both observers took 10 vertical measurements at a depth of 6 cm where two wires were placed at 2 cm from each other (Figure 3.3).

Figure 3.3. Phantom US image.

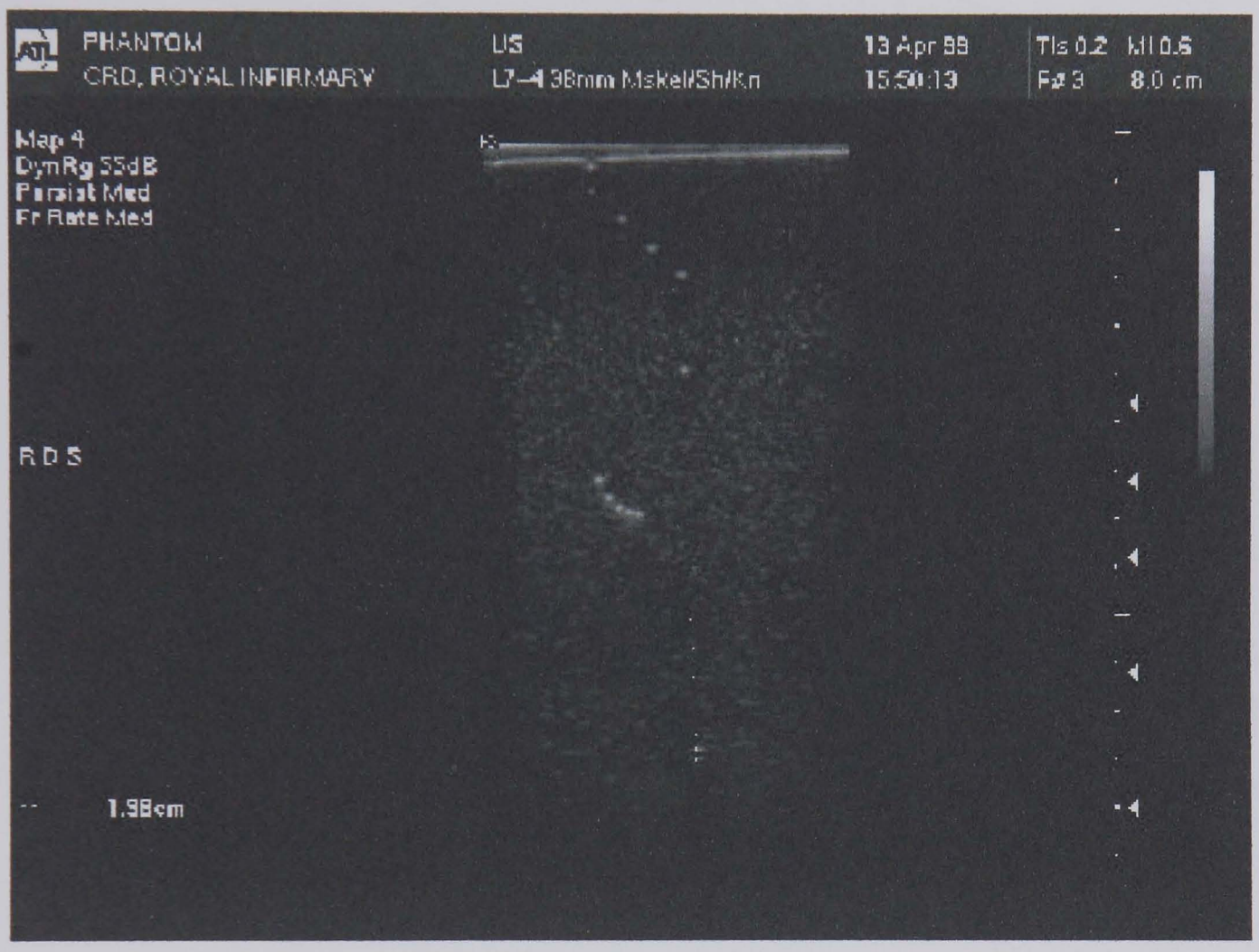

Crosses mark the position of the wire markers and the dotted line is the distance between the two markers.

Again both investigators were blinded to their own and each other's results. Each observer's measurement errors were calculated with within-subject standard deviations. A plot diagram was used to show that the observer's standard deviations were unrelated to the magnitude of the measurement (164). Correlation coefficients were used to assess the linear relation of the two sets of mean measurements between the two observers. We used the Bland-Altman graphic technique to assess the agreement between two observers (165). Phantom measurements were analysed as a percentage of deviation from the known true value (see Appendix A for statistical equations and terminology).

3.3. Results

152 images were recorded and every image was readable.

To obtain the common within-subject standard deviation (s_w) we averaged the variances and the squares of standard deviations. The first investigator's (s_w) was 0.4 mm. A plot diagram was used to prove that the subject's standard deviations are unrelated to the magnitude of the measurement of iliofemoral ligament (Figure 3.4.).

Figure 3.4. **A plot of the standard deviation of the observers measurement of iliofemoral thickness against the mean of the triplicate values for each hip.**

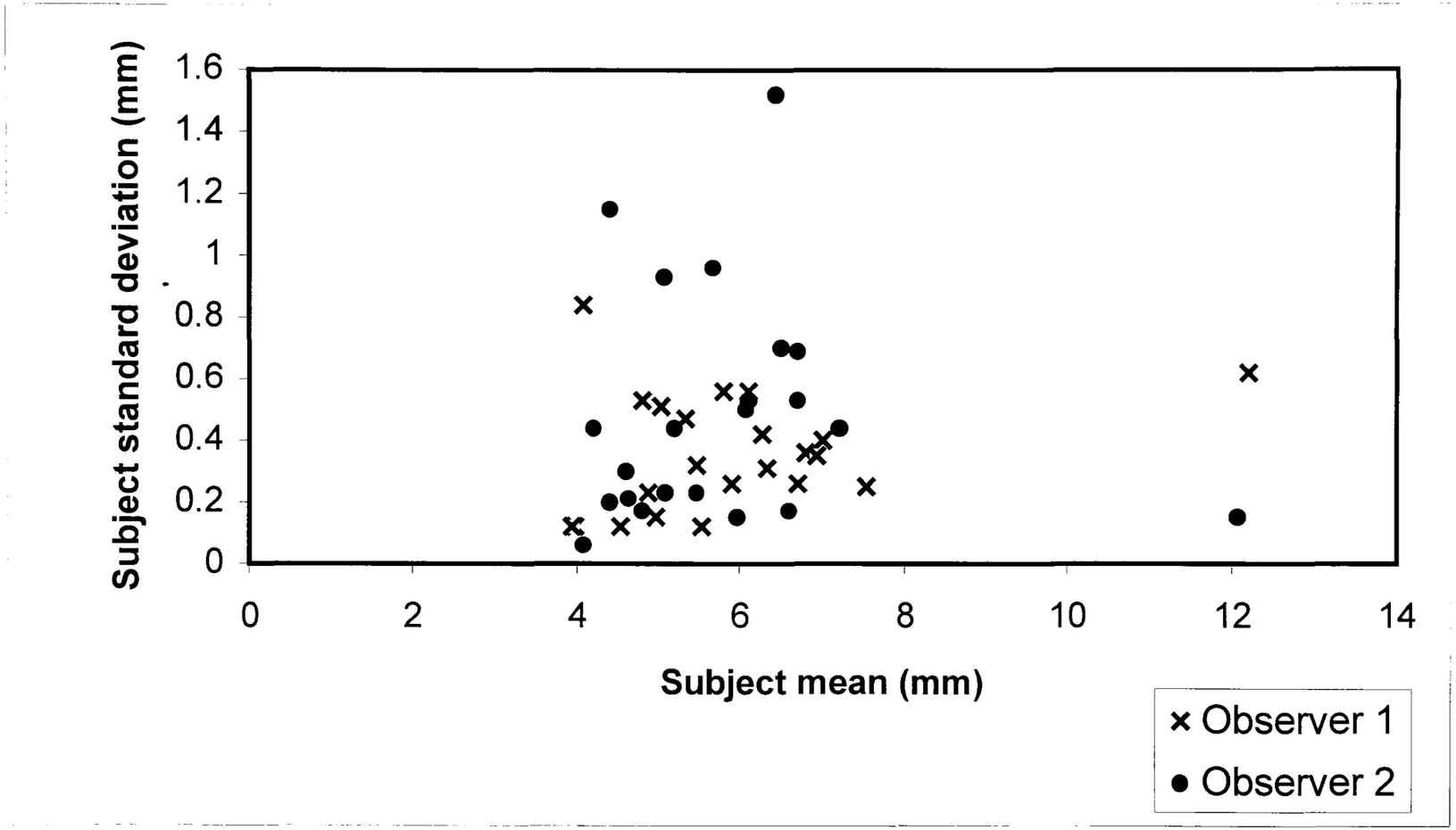

The difference between measurements for the same subject is expected to be less than 2.77 s_w for 95 % of pair measurements. Fig. 3.5. shows the differences against their means. Intraobserver error was also expressed with discrepancies from their means in percentages. The difference of the higher value and the lower value divided by the lower value multiplied by 100 gives the individual percent error. The mean of these individual values over all 22 cases gives the final result. In this case the intraobserver error was 4.75 %.

The second investigator's (s_w) was 0.6 mm. Figure 3.4. shows on a plot diagram that the subject's standard deviations are again unrelated to the magnitude of the measurement.

Figure 3.5. shows the differences against their means. Intraobserver error was also expressed in percentage of deviation from the means. In this case the intraobserver error was 7.00 %. For calculating the interobserver error both investigators' mean values were used. The correlation coefficient was also calculated and there was a relation between the values ($r = 0.89$).

Figure 3. 5. Intraobserver comparisons of the two observers.

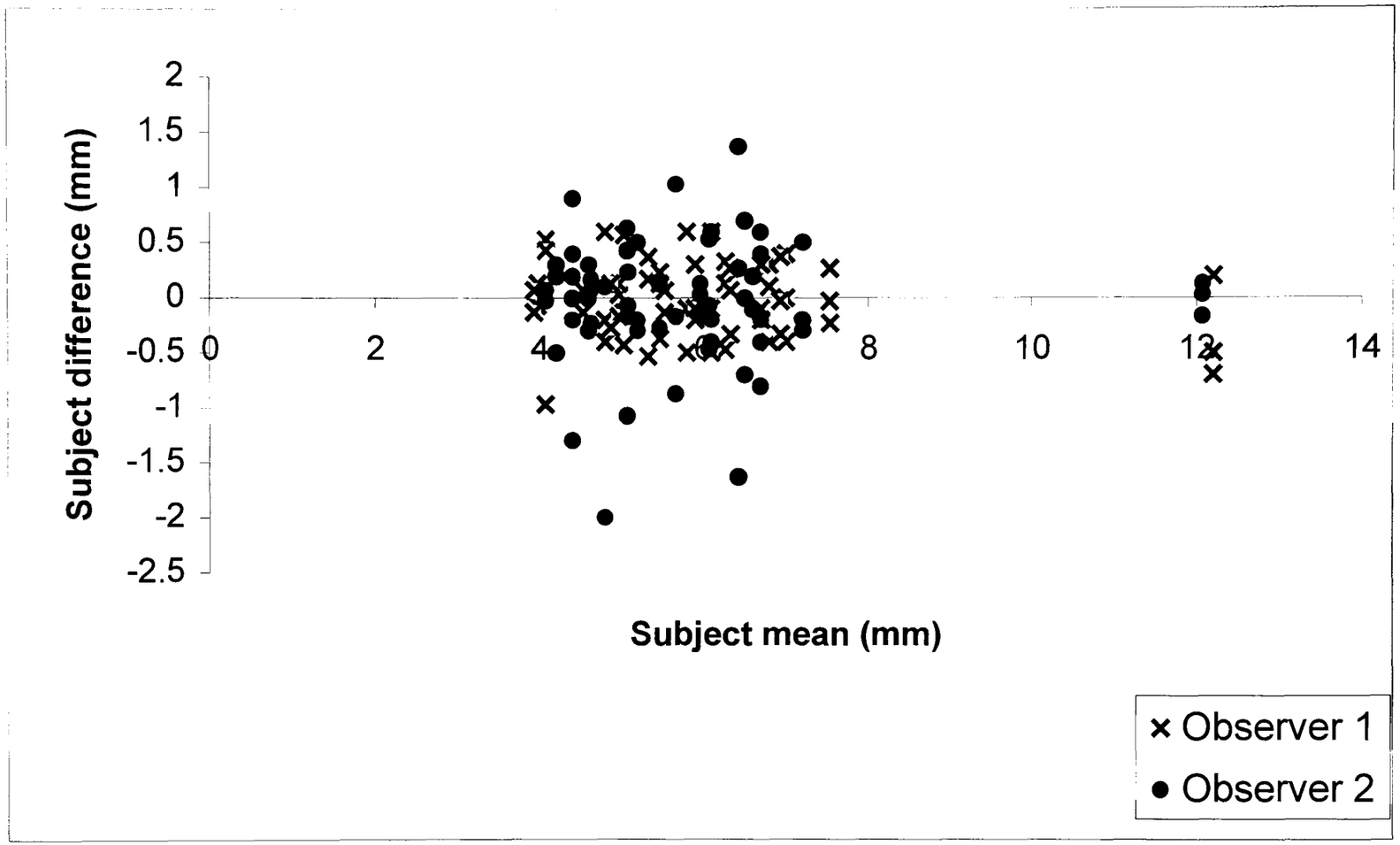

This figure shows the difference between the triplicate measurements of each hip plotted against the mean value obtained at each hip examination for the two observers.

The agreement between the two observers was measured with the Bland-Altman method (Figure 3. 6.).

Fig. 3.6. Bland-Altman plot. Interobserver comparison of iliofemoral thickness.

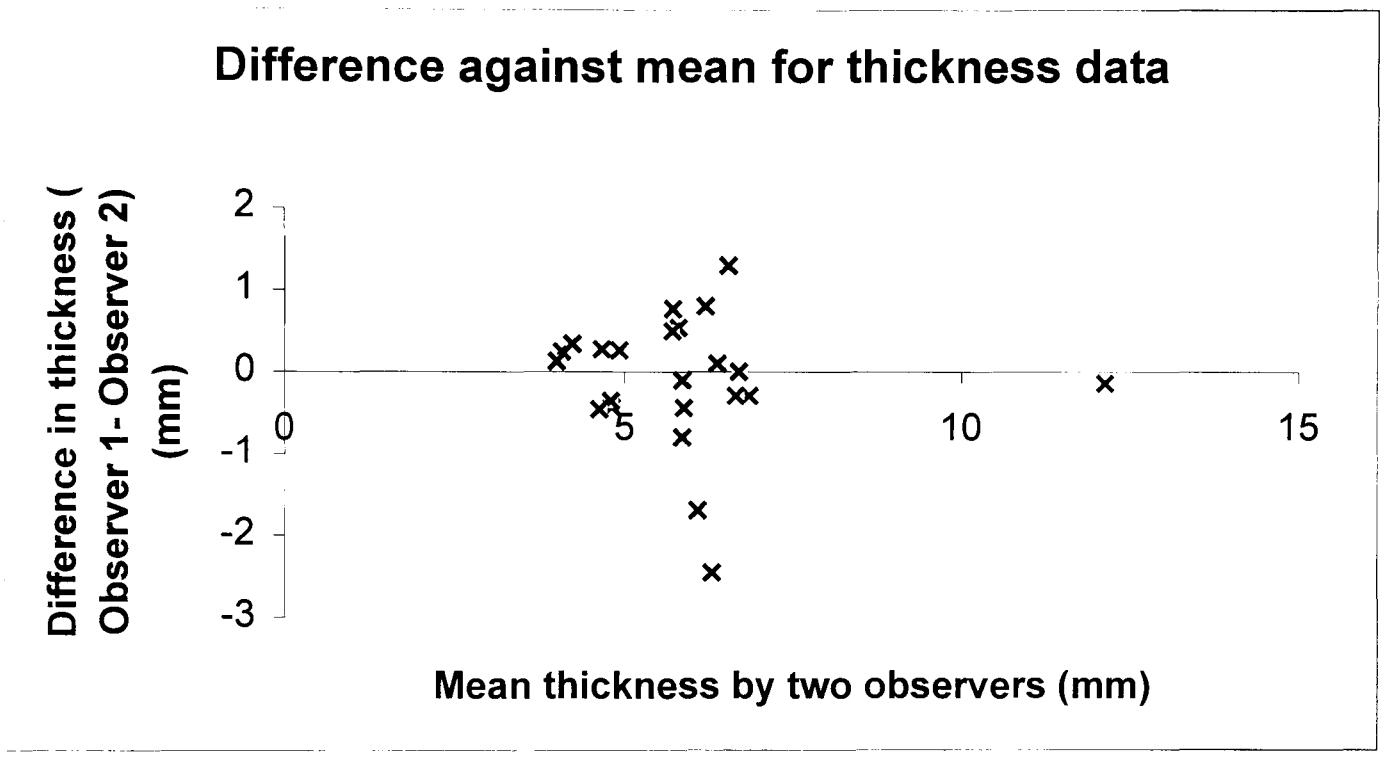

A plot of the difference between the observers mean thickness measurements against the overall mean thickness for the two observers

The interobserver error was 10.91 %. Both investigators were tested blindly on the phantom object and the first investigator's average depth was 19.78 mm, S.D. 0.15 mm. Percent error was 1.11 %. The second investigator's average depth was 19.71 mm, S.D. 0.17 mm. The percent error was 1.47 %.

3.4. Discussion

In this study every US image obtained was of acceptable quality. With well-defined anatomical landmarks and with pre-determined criteria the interobserver variation between the two observers was acceptable. However for US of the hip, measurements were taken in the sagittal plane only as this is the standard approach for hip US. Most US imaging is performed in two different planes, which might lead to greater interobserver errors at the same depth. None of the patients studied weighed more than 90 kg and it is well known that US imaging of the hip is more unreliable in obese subjects and therefore more likely to increase the possibility of interobserver variation. The positioning of US probes is critical in obtaining an interpretable US image and a slight alteration in the angle of the probe in relation to the skin surface or a variation in the amount of gel used can greatly distort the image obtained and increase the occurrence of artefacts. Musculoskeletal US is now becoming a tool increasingly used by rheumatologists (166-169) most of whom have had no formal training in imaging techniques. This study demonstrates that a rheumatologist with experience of US imaging can train a novice within a relatively short space of time to produce acceptable images of the hip and with relatively small interobserver variation. Further studies will be required to assess whether this is possible for more complex joints such as the shoulder.

This chapter was published during my Ph.D.work.

Balint PV, Sturrock RD: Intraobserver repeatability and intraobserver reproducibility in musculoskeletal ultrasound imaging measurements Clin Exp Rheumatol 2001;19: 89-92

3.5. Future aims

After the determination of intra- and interobserver variation of measurements at the hip joint this should be extended to different joints (shoulder, elbow, small hand joints, ankle etc) at different depths (more superficial structures than the hip) and in different tissues (hyaline cartilage, tendon etc). Probably there will not be major differences between these studies but if observer variation occurs this will need further explanation. These studies could also be extended to US images of children with juvenile idiopathic arthritis (JIA), but preliminary data already exist in this field (170). After the determination of intra- and interobserver variation of measurements in gray-scale imaging further study is required for the determination of intra- and interobserver variation of power Doppler imaging in the musculoskeletal field.

Chapter 4. Ultrasonography of lower limb entheseal insertions in spondylarthropathy

4.1. Introduction

Enthesitis – inflammation of the origin and insertion of ligaments, tendons, aponeuroses, annulus fibrosis and joint capsules - is a widely accepted clinical, histopathological and imaging feature of spondylarthropathy (SpA). Inflammation may occur at any enthesis in SpA, though it is most frequent in the entheses of the lower limbs (171, 172). Pathological examination of enthesitis in SpA demonstrates local inflammation, fibrosis, erosion, and ossification (173, 174). Bursitis and synovitis may also occur adjacent to the entheses, and it has been recently postulated that the enthesis may be the initial site of joint inflammation in SpA (175, 176).

The assessment of enthesitis in SpA is predominantly performed by eliciting tenderness at the enthesis (177, 178). An enthesitis index of tenderness assessed at 66 entheseal insertions correlates with pain and stiffness scores in SpA but is time consuming with poor interobserver reliability (177).

Histological examination of the enthesis is the potential "gold standard" for evaluation of enthesitis but is rarely obtained due to ethical and practical constraints. Plain radiography, US and magnetic resonance imaging (MRI) demonstrate soft tissue thickening, cortical bone breakage, new bone proliferation and bone structure alterations at inflamed entheses (138, 179, 180)

and allow quantification of enthesitis. Radiological scoring of the progression of enthesitis in SpA has principally focussed on plain radiography of the spine (181). MRI is useful in the evaluation of enthesitis but is limited by issues of availability and expense (176). The resolution of MRI for superficial structures is not superior to US which achieves 200-450 μm in-plane resolution at 10 MHz insonation frequency (141).

Musculoskeletal US is widely available, inexpensive and readily demonstrates superficial tissue inflammation such as fluid collections, soft-tissue lesions and bone surface lesions with a sensitivity comparable to MRI (127, 128). Three studies of US of the lower extremities in SpA suggest a discrepancy between clinical and sonographic enthesitis. These studies do not provide an exact description of the different imaging features of enthesitis such as erosion, enthesophyte and thickness of tendon, ligament or aponeurosis nor do they report intraobserver variability or specificity and sensitivity of the relative examination techniques (138-140).

The application of US in rheumatology may be limited by a lack of standardized techniques and protocols and the time required to examine multiple sites. In SpA the commonest sites of enthesitis are the knee, heel and ischial tuberosity (182). As the ultrasonographic features of the normal ischial tuberosity have not been described, US examination was limited to the entheses of the knee and heel using a standard midline or long axis, in the case of the plantar aponeurosis (which is not a midline structure), plane for US examination, selecting structures for which a normal definition and thickness had been previously described (125, 183-185).

Ultrasound examination was more sensitive and specific than clinical examination in the detection of enthesitis of the lower limbs in SpA. Ultrasound examination may provide a more objective and reliable index of enthesitis than clinical examination.

4.2. Materials and methods

Patients. Patients satisfying the European Spondylarthropathy Study Group (ESSG) criteria for the diagnosis of SpA (186) were assessed during routine presentation to the rheumatology outpatient clinic. Patients with previous joint surgery of the knee and ankle, corticosteroid injection of the structures examined within the previous 6 weeks or peripheral neuropathy of the lower limbs were excluded from the study.

Clinical examination. The superior pole of the patella (quadriceps tendon insertion), the inferior pole of the patella (patellar ligament origin), the patellar ligament insertion at the tibial tuberosity, the Achilles tendon and the plantar aponeurosis were examined in both lower limbs of each patient. Clinical examination for tenderness and swelling at each site was performed by an experienced rheumatologist.

Ultrasound evaluation. Real-time ultrasonography was performed by an experienced rheumatologist trained in musculoskeletal ultrasonography, using an ATL HDI 3000 machine with L 7-4 MHz and CL 10-5 MHz probes. The clinical examination and ultrasound measurements were performed separately; one immediately after the other, by different investigators who were blinded to each other's results. Examination of the superior pole of the patella (quadriceps tendon insertion), the inferior pole of the patella (patellar ligament origin) and the patellar ligament insertion at the tibial tuberosity was performed with the patient in the supine position with the knee flexed at 30 degrees. The Achilles

tendon and the plantar aponeurosis were examined with the patient lying prone with the feet overhanging the edge of the examination table at 90 degrees of flexion. If the patient was unable to lie prone, the heels were examined with the patient lying supine and the knees and ankles flexed at 90 degrees.

Ultrasonographic assessment of structure thickness and the presence or absence of bony erosion, enthesophyte and bursitis was recorded at each site. Bursitis was defined as a well-circumscribed, localized anechoic or hypoechoic area at the site of an anatomical bursa and which was compressible by the transducer. Bursal dimensions were obtained in long and short axis with a normal bursa being < 2mm in short axis (125). Bony erosion was defined as a cortical breakage with a step-down contour defect and an enthesophyte was defined as a step-up bony prominence at the end of the normal bone contour. Ligament, aponeurosis and tendon thickness were measured at the point of maximal thickness proximal to the bony insertion. The following criteria were used for abnormal structure thickness:- quadriceps tendon thickness ≥ 6.1mm (125), proximal and distal patellar ligament ≥ 4mm (183), Achilles tendon ≥ 5.29mm (184), plantar aponeurosis ≥ 4.4mm (185). In this study only thickened enthesis, fluid collection, erosion and bony spur were accepted as US signs of enthesitis. "hypoechoic oedema" without any thickness change was excluded, as it is a subjective sign of enthesitis. No control group was selected in this study as the normal ultrasound features and dimensions of the structures examined have already described (125, 183-185). In order to further subjectivity, the threshold

of abnormal thickness was set 0.1 mm above the reported standard deviation of each site in the normal population.

An ultrasonographic score of lower limb enthesitis was calculated as follows: one point was scored for each abnormality at each site examined, giving a possible maximum total score of 36 (Table 4.1.).

Table 4.1. Glasgow Ultrasound Enthesitis Scoring System (GUESS)

Superior pole of the patella - Quadriceps tendon enthesis

Quadriceps tendon thickness ≥ 6.1mm	1 point
Suprapatellar bursitis	1 point
Superior pole of patella erosion	1 point
Superior pole of patella enthesophyte	1 point

Inferior pole of the patella - Proximal patellar ligament enthesis

Patellar ligament thickness ≥ 4mm	1 point
Inferior pole of patella erosion	1 point
Inferior pole of patella enthesophyte	1 point

Tibial tuberosity - Distal patellar ligament enthesis

Patellar ligament thickness ≥ 4mm	1 point
Infrapatellar bursitis	1 point
Tibial tuberosity erosion	1 point
Tibial tuberosity enthesophyte	1 point

Superior pole of the calcaneus - Achilles tendon enthesis

Achilles tendon thickness ≥ 5.29mm	1 point
Retrocalcaneal bursitis	1 point
Posterior pole of calcaneus erosion	1 point
Posterior pole of calcaneus enthesophyte	1 point

Inferior pole of the calcaneus - Plantar aponeurosis enthesis

Plantar aponeurosis thickness ≥ 4.4mm	1 point
Inferior pole of calcaneus erosion	1 point
Inferior pole of calcaneus enthesophyte	1 point

Total possible score on both lower limbs is 36

The US score was also calculated separately as a soft-tissue score and as a bone score. The soft tissue score included entheseal thickness and bursitis. The bone score included erosions and enthesophytes. Intraobserver error was not measured in this study however we have already demonstrated a high degree of intraobserver repeatability and interobserver reproducibility of ultrasound measurements of ligament thickness (187). Sonographic images were stored on magneto-optical disks for off-line analysis. After 3 months, the investigator re-scored every patient to calculate intraobserver reliability.

Statistical analysis. All values are given as mean (median) $\pm$ standard deviation. Statistical analysis was performed using Statview software. A p value <0.05 was deemed significant. Intraobserver agreement was calculated using a Kappa test. Sensitivity, specificity, negative and positive predictive value, false negative and false positive rates of clinical examination were also calculated (see in Appendix A for statistical equations and terminology).

4.3. Results

Patient characteristics. 35 patients were examined (ankylosing spondylitis = 27, psoriatic arthritis = 7, reactive arthritis = 1). Twenty-five were male and 10 were female; mean age = 48 (49.3) ± 14. The mean age of disease onset was 20.8 (19) ± 13.1 years with a mean duration of disease of 24.9 (21) ± 10.4 years. The mean ESR was 16.2 (10) ± 18 mm/hr and the mean CRP was 18.0 (6) ± 20.8 g/dL. Six (17%) patients had a family history of spondyloarthropathy, 14 (40%) had previous uveitis, 21 (60%) had peripheral joint disease, 1 (3%) had inflammatory bowel disease, 9 (26%) had psoriasis, and 2 (6%) had joint replacement surgery not involving the lower limbs. Twenty-four (69%) patients were HLA B27 positive, 3 (9%) were negative and the HLA status of 8 (22%) was not known.

Clinical examination. A total of 350 entheseal sites were examined (10 sites x 35 patients) with 71/350 (20.3%) entheseal sites being tender and 13/350 (3.7%) entheseal sites being swollen. The frequencies of clinical findings at individual sites are given in Table 4.2. On clinical examination 61.7 % of entheses were symmetrically involved.

Table 4.2. Ultrasonographic and clinical examination of the entheseal insertions at 5 lower limb enthesis.

	Suprapatellar (n=70)	Infrapatellar (n=69)	Tibial tuberosity (n=69)	Achilles tendon (n=70)	Plantar aponeuroses (n=70)
Clinically tender	15	18	11	14	13
Clinically swollen	8	2	0	3	0
Tendon thickened *	25	39	32	14	35
Bursitis	9	n/a	3	7	n/a
Bone erosion	5	1	1	9	6
Enthesophyte	8	7	2	21	4

* Suprapatellar (Quadriceps tendon) ≥ 6.1mm, Infrapatellar (Proximal patellar ligament) ≥ 4mm, Tibial tuberosity (Distal patellar ligament) ≥ 4mm, Achilles tendon ≥ 5.29mm, Plantar aponeuroses ≥ 4.4mm

Ultrasonographic examination. A total of 350 entheseal sites were examined. Two sites were obscured by overlying psoriatic plaques (one over the inferior pole of the patella and one over the tibial tuberosity in 2 separate patients) and are not included in the analysis. The ultrasound findings at individual sites are given in Table 2. 195/348 (56%) enthesis were abnormal on US examination and 53.9% of entheses were symmetrically involved. Figure 4.1. shows the ultrasonographic features of the five normal entheseal site and Figure 4.2. shows the ultrasonographic features of enthesitis.

Figure 4.1. Normal ultrasonographic appearance on lower limb entheseal insertions.

A.

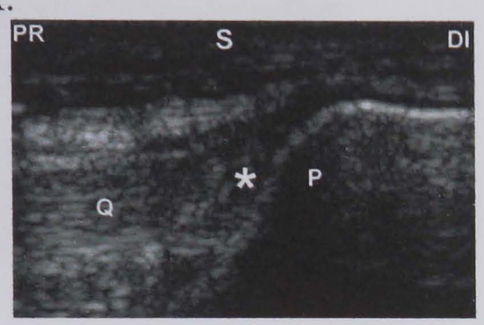

B.

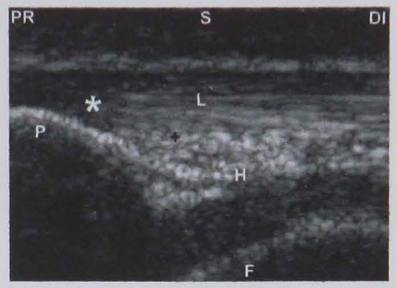

C.

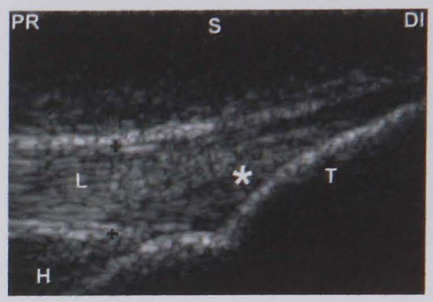

D.

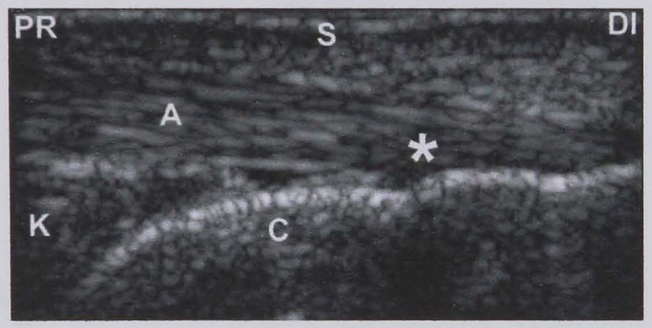

E.

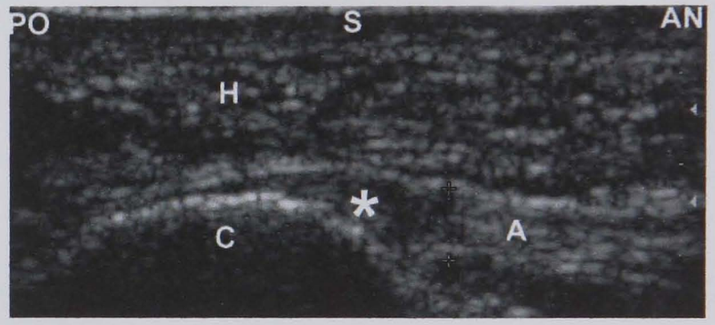

A. Quadriceps tendon enthesis: PR = proximal, DI = distal, S = skin, Q = quadriceps tendon, P = patella, * = tendon attachment
B. Proximal patellar ligament enthesis: PR = proximal, DI =distal, S = skin, L = patellar ligament, P = patella, H = Hoffa fat pad, F = femur, * = ligament attachment
C. Distal patellar ligament enthesis: PR = proximal, DI =distal, S = skin, L = patellar ligament, H = Hoffa fat pad, T = tibia, * = ligament attachment
D. Achilles enthesis: PR = proximal, DI =distal, S = skin, A = Achilles tendon, C = calcaneus, K = Kager fat pad, * = tendon attachment
E. Plantar aponeurosis enthesis: PO = posterior, AN = anterior, S = skin, A = plantar aponeurosis, C = calcaneus, H = heel fat pad, * = aponeurosis attachment

Figure 4.2. Ultrasonographic appearances of lower limb enthesitis.

A.

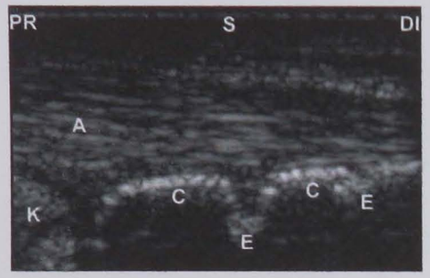

B.

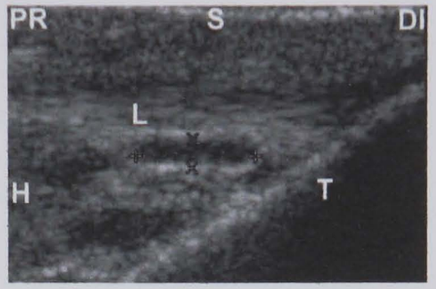

C.

I

D.

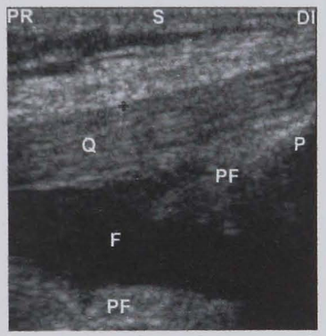

E.

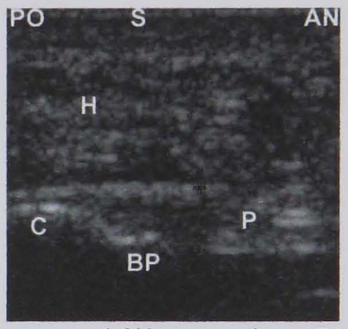

A. Posterior calcaneal erosions: PR = proximal, DI =distal, S = skin, A = Achilles tendon, K = Kager fat pad, C = calcaneus, E = erosion. For comparison with the normal image see figure 1 D.

B. Infrapatellar bursitis: PR = proximal, DI = distal, S = skin, L = patellar ligament, T = tibia, H = Hoffa fat pad, the crosses mark infrapatellar bursa. For comparison with the normal image see figure 1 C.

C. Inferior patella enthesophyte: PR = proximal, DI =distal, S = skin, L = patellar ligament, P = patella, H = Hoffa fat pad, E = enthesophyte. For comparison with the normal image see figure 1 B.

D. Suprapatellar bursitis: PR = proximal, DI = distal, S = skin, Q = quadriceps tendon, F = fluid collection in the suprapatellar bursa, P = patella, PF = perifemoral fat. For comparison with the normal image see figure 1 A.

E. Inferior calcaneal spur: PO = posterior, AN = anterior, S = skin, P = plantar aponeurosis, C = calcaneus, H = heel fat pad, BP = bony spur. For comparison with the normal image see figure 1 E.

The intra-observer kappa value for analysis of all sites was 0.9. Kappa values for analysis of the separate lesions were (bony erosion kappa = 0.97, bursitis kappa = 1.00, enthesophyte kappa = 0.83) and for analysis of separated locations were (superior pole of the patella = 0.92, inferior pole of the patella = 0.7, tibial tuberosity = 0.82, superior pole of the calcaneus = 0.97, inferior pole of the calcaneus = 0.8).

Relationship of clinical and ultrasonographic findings in the lower limb entheses. Ultrasound detected entheseal abnormality in 195/348 (56%) entheseal sites while clinical examination detected entheseal abnormality in 75/348 (22%) sites. The relationship between clinical and ultrasonographic findings at individual sites are given in Figure 4.3.

Figure 4.3. Correlation of clinical abnormality (either swollen or tender) with any US abnormality at entheseal sites in lower limbs.

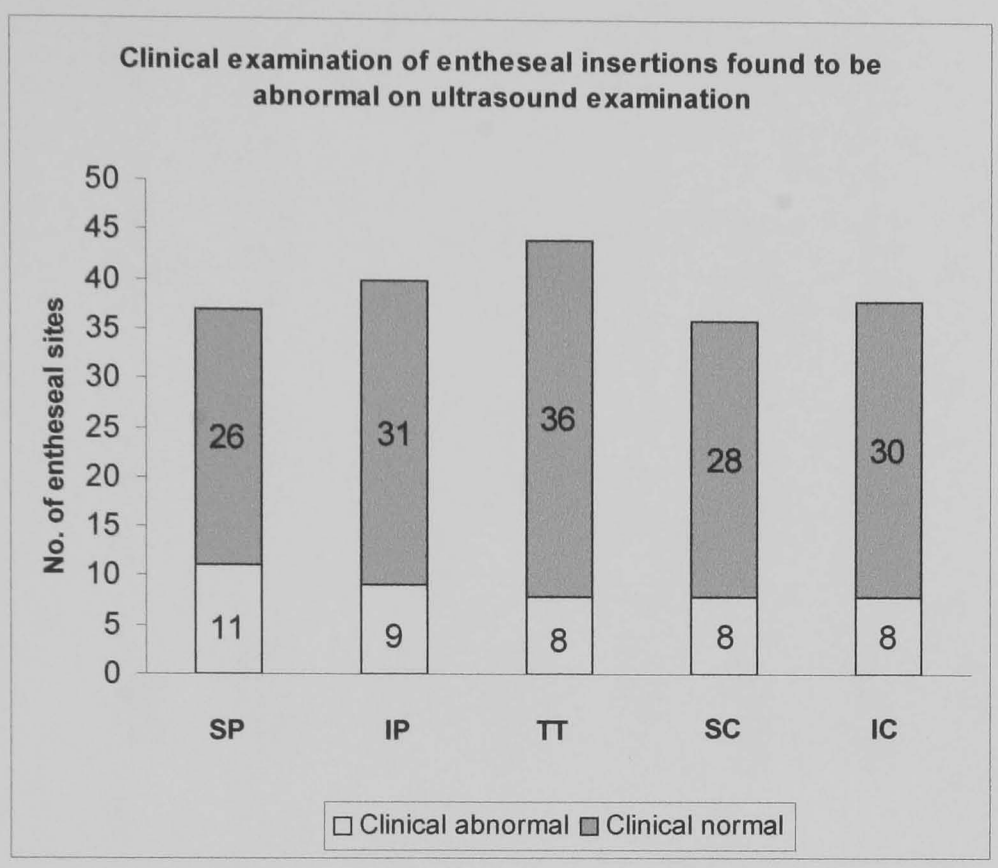

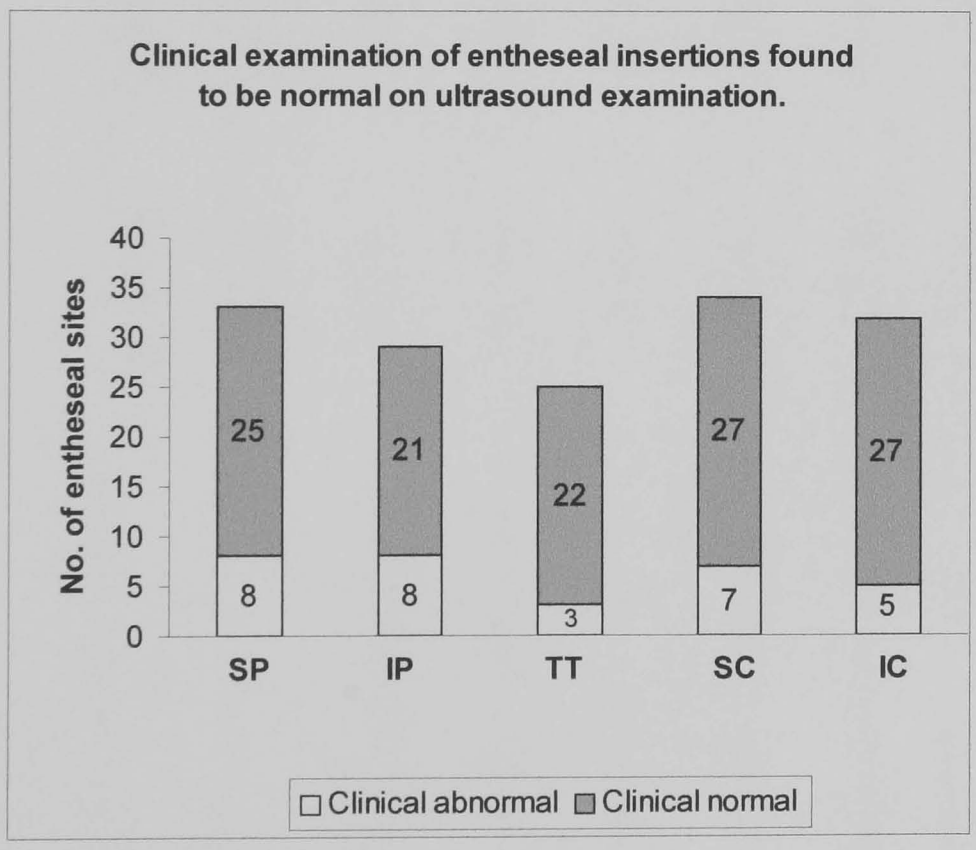

SP = Superior pole of the patella, IP = Inferior pole of the patella, TT = Tibial tuberosity, SC= Superior pole of the calcaneus, IC = Inferior pole of the calcaneus.

Table 4.3. Clinical examination versus US as a gold standard. Data showing sensitivity, specificity, false positive (FPR) and negative rate (FNR), positive (PPV) and negative predictive value (NPR).

	Sensitivity	Specificity	FPR	FNR	PPV	NPR
Total	22.6 %	79.7 %	20.3 %	77.4 %	58.7 %	44.7 %
Superior pole of the patella	29.7 %	75.8 %	24.2 %	70.3 %	57.9 %	49.0 %
Inferior pole of the patella	22.5 %	72.4 %	27.6 %	77.5 %	52.9 %	40.4 %
Tibial tuberosity	18.2 %	88.0 %	12.0 %	81.8 %	72.7 %	37.9 %
Superior pole of the calcaneus	22.2 %	79.4 %	20.6 %	77.8 %	53.3 %	49.1 %
Inferior pole of the calcaneus	26.7 %	84.4 %	15.6 %	79.0 %	61.5 %	47.4 %

Ultrasonographic score of enthesitis. In order to quantify lower limb enthesitis an ultrasonographic (US) score of enthesitis was formulated. A maximum of 36 was possible in each patient. The mean score was 6.9 (6) $\pm$ 4.3 with a soft tissue US abnormality score of 5 (4) $\pm$ 2.8 and a bone (erosion or/and enthesophyte) US score of 1.9 (2) $\pm$ 1.8. There was no significant correlation between the US score of enthesitis and the ESR or CRP.

Clinically detected and undetected bursitis. There was no correlation between the sizes of the bursae on ultrasound and clinical findings and only 5/19 bursa were clinically detected. Two large bursae were detected clinically but two equally large bursae were not detected on clinical examination. No bursa under 13.8 mm x 4.7mm was detected on clinical examination.

4.4. Discussion

On clinical examination, 75/348 (22%) of entheseal insertions were determined to be inflamed which is similar to a previous study of calcaneal entheses (188). Lehtinen noted less clinical enthesitis in lower limbs in SpA (56/372=15.05%) (138) which may reflect differences between the two patient groups. The presence of tenderness was more sensitive than swelling in the detection of enthesitis, being present at 14-28% of entheseal sites while swelling was present at 0-14% of entheseal sites. Ultrasound detected enthesitis at 51.4-63.8% of entheseal sites and was more sensitive than clinical examination for tenderness and swelling taken together or separately. Taking ultrasound as the gold standard, neither tenderness nor swelling was specific in the detection of enthesitis with just 44/75 clinically inflamed entheses confirmed on ultrasound. Some of these sites may have had minor degrees of inflammation not amenable to detection on US. It is possible that certain features of enthesopathy such as plantar spur were overestimated as they may be found in normal subjects, though the presence of erosion and bursitis is relatively specific. In this study, swelling was not a useful sign in detecting enthesitis at the tibial tuberosity or plantar aponeurosis.

Two principal features of soft tissue inflammation –tendon thickening and bursitis- were examined on ultrasonography. In order to reduce the subjectivity of previous studies of enthesitis in SpA, tendon thickness was determined using standardised US views according to previously published protocols. In addition, the threshold of normal tendon thickness was set at 0.1 mm above the reported standard deviation above the mean as measured in normal populations. We have

already demonstrated a high degree of intraobserver repeatability and interobserver reproducibility of ultrasound measurements of ligament thickness (187). Increased tendon or ligament thickness was the most frequent feature of soft tissue inflammation being present at 20-57% of entheses examined. This may underestimate enthesitis as it did not include hypoechoic changes in tendons or ligaments, which is an important but subjective feature of enthesitis and may be influenced by transducer position (189) particularly when parallel fibrils change their directions as is the case at the entheses. Tendon thickening may be due to either oedema or fibrosis and longitudinal studies are required to assess it's reversibility. Significant qualitative and quantitative ultrasonographic changes were demonstrated in a case study of Achilles tendonitis and retrocalcaneal bursitis followed for 1 year (190) while Lehtinen and at al. (139) did not find a reduction in the frequency of ultrasonographic enthesitis in a 6 month follow-up of 23 patients. Bursitis was present at 4-13% of sites examined, being most frequent at the suprapatellar and retrocalcaneal sites.

Enthesophyte formation was the most frequent US bony abnormality being present at 3-30% of entheseal sites while bony erosion was present at 1-13% of sites. This is in keeping with previous radiological studies of SpA where entheseal ossification is a common feature. In addition to entheseal ossification, US also demonstrated intratendineous and interligamentous calcifications adjacent to the point of entheseal insertion. These may represent the end stage of inflammation or may relate to other pathology such as trauma or degenerative changes which are frequent in the general population. Erosive changes at the enthesis may have been underestimated due to the presence of an enthesophyte

which obscures adjacent erosions on US. Clinical examination is not useful in determining the presence of these bony lesions and does not provide this potentially diagnostic information.

This study confirms that there is considerable sub-clinical enthesitis in SpA, which can be objectively measured by US using standardised protocols. At present, only clinical evidence of enthesitis of the heels is included in the European Spondylarthropathy Study Group preliminary classification criteria for the diagnosis of SpA (186) and clinical enthesitis is included in the preliminary core sets to be used as endpoints in clinical trials in ankylosing spondylitis (AS) (191). Ultrasound detection of enthesitis is more sensitive and more specific than clinical examination and soft tissue US has a high degree of reproducibility. Ultrasonography is now widely practised by rheumatologists and should be used to define classification criteria and outcome measures in SpA.

While established therapies of SpA are not proven to reduce spinal entheseal manifestations of disease (192) newer therapies such as anti-TNF have been demonstrated to reduce spinal entheseal inflammation (193, 194). Studies of therapies specifically targeting entheseal inflammation will need objective measures of peripheral enthesitis in order to confirm efficacy. Plain radiography is limited in that established scores (181) provide little information about soft tissue inflammation, which is most amenable to therapy. MRI and US have similar sensitivity in demonstrating superficial soft tissue and bony abnormality (127, 128). While US does not detect insertional bone oedema seen in enthesitis

on MRI (176) the significance of this lesion is not yet determined and bone oedema may also co-exist in overuse syndrome with enthesopathy (195).

By using a limited series of easily reproducible, fixed reference points and established normal parameters we devised an enthesitis score of the lower limbs: Glasgow Ultrasound Enthesitis Scoring System (GUESS), which can be applied to the evaluation of therapies in SpA. Unlike rheumatoid arthritis (196) US did not correlate with systemic parameters of disease activity in SpA though these are less sensitive markers of disease activity in SpA (197). Ultrasonographic assessment is more time-consuming than clinical examination but can be reliably performed in 15 minutes by an experienced musculoskeletal ultrasonographer. Further multicenter studies of GUESS in the assessment of enthesitis are required.

This chapter was accepted as an extended report for publishing during my Ph.D.work.

Balint PV, Kane D, Wilson H, McInnes IB, Sturrock RD: Ultrasonography of lower limb entheseal insertions in spondylarthropathy. Ann Rheum Dis (in press)

4.5. Future aims

These studies should be extended to include less frequently involved entheses such as elbow, shoulder and pelvic enthesis. There is also a need for comparative US, MRI and X-ray studies measuring the effects of new biological treatments to show how can we use US in longitudinal studies in SpA. There are only two single case reports, which described blood flow changes during the follow up after the treatment of Achilles enthesitis (190, 198). Randomised power Doppler and laser Doppler studies are required to show significant flow changes during the treatment of enthesitis. Tissue specific contrast agents are not available currently to study enthesitis but in the future this will be possible.

Chapter 5. Power Doppler and gray-scale imaging of inflammatory hyperaemia in MCP joints

5.1. Introduction

Accurate detection of the early stages of synovitis in rheumatoid arthritis (RA) and other destructive inflammatory joint diseases is important to establish the most appropriate treatment and indicate prognosis. Inflammatory synovitis is the earliest change to occur in RA (199) and thus, its detection is important for both diagnosis and monitoring disease progression. It is becoming increasingly accepted that delaying the onset of destructive changes to the affected joints in RA is best achieved by means of early and aggressive therapy in appropriately selected patients (200). Identification of such patients requires methods for detecting inflammatory synovitis that are both sensitive and specific. Radiographic examination of affected joints depicts only damage such as erosions and loss of joint space, which are associated with longer term disease. Magnetic resonance imaging has proved to be much more sensitive for depiction of soft-tissue changes (201), particularly in the early stages (202, 203) but it has substantial resource implications.

Ultrasonography (US) can depict joint effusion, synovial tissue proliferation and erosions in the metacarpophalangeal (MCP) joint (127,137). However, the lower limit of its accuracy for depicting these abnormalities is not known. Other abnormalities associated with the MCP joint in rheumatoid arthritis such as pannus and effusion around tendons, tendon rupture and rheumatoid nodules can

be detected by US (94, 204). The power Doppler technique creates a colour flow map through a sample volume on the basis of the total integrated power of the Doppler spectrum. The movement of blood cells within vessels generates power signals and power Doppler ultrasonography relates to the volume of blood flowing within the imaging field (205).

Laser Doppler perfusion imaging (LDI) is a recently-developed technique for non-invasive assessment of blood flow through vascular beds, on the basis of the well–known Doppler shift principle, that yields a spatial map of tissue perfusion (206). The red (635nm) wavelength used in conventional laser Doppler imagers limits penetration to the skin but the optical properties of skin are such that longer wavelengths have greater tissue penetration power (207) and thus imaging of perfusion in deeper tissues is possible. Previous work has demonstrated that elevated perfusion associated with the PIP joints is detectable in patients with RA with use of a near infra-red laser (209). However, the MCP joints of RA patients are commonly affected early in the disease process. At present, there are no simple and non-invasive but objective measures of inflammatory activity associated with these joints.

The purpose of this cross-sectional study was to perform LDI and ultrasonography of the hands of patients with known RA who were judged on clinical grounds to have pain and tenderness of the MCP joints and to establish whether elevated perfusion associated with MCP joints 2 and 3 was detectable. Elevated perfusion of MCP joints is a cardinal sign of synovitis and thus its detection provides a surrogate marker of joint inflammation.

5.2. Materials and methods

Study participants. Thirteen consecutive patients (10 women and three men; mean age, 48.8 years ± 14.1 [SD]; age range, 23-62 years) with known RA, on the basis of American Rheumatism Association (ARA) criteria (209), were recruited to the study from the Rheumatology outpatient clinic at the Royal Infirmary. Inclusion criteria were involvement of the hand with pain and tenderness of the MCP joints. Exclusion criteria were age younger than 18 years, hand surgery including joint replacement, local steroid injection in previous 3 months and local use of ointments. Disease duration ranged from 6 months to 24 years. These patients had pain and tenderness of the metacarpophalangeal (MCP) joints at clinical examination. A visual analogue scoring (VAS) system (0-10, with 0 corresponding to no pain and 10 corresponding to worst pain possible) was used to record pain perceptions associated with each hand. Hand dominance was noted for each patient.

A separate group of 13 healthy control subjects (10 women and 3 men; mean age, 41.2 years ± 12.8; age range 27 - 63 years), who were not age matched to the patient group, were recruited consecutively. None of the control subjects had a history of any hand injury or disease; at the time of examination their hands were clinically normal and asymptomatic. The MCP joints 2 and 3 of both hands were examined with LDI.

All study participants were asked to avoid physical activity before the examination, and none had applied any cream to the hand or recently undergone

physical therapy. For the patient group, the joints were also examined with both gray-scale and power Doppler US. The room temperature was monitored, as was the skin temperature over the dorsum of the 4th finger to ensure that the differences between groups were not the result of variations in environmental and, consequently, skin temperature. This study was approved by the institutional ethics committee and informed consent obtained from each participant.

Laser Doppler Imaging. A laser Doppler imager (Moor Instruments, Axminster, UK) was especially modified to incorporate a near- infrared (NIR) (835nm) laser, to increase tissue penetration, in addition to the standard red (635nm) laser. The imager was positioned 60cm above the surface of the hand for all participants. The laser beam (~1mm diameter) was scanned in a raster fashion across the dorsum of the hands. From the backscattered light, a spatial image of tissue perfusion generated that depended on the extent of the Doppler shift of this light (206). An array of as many as 256 × 256 measurement points was obtained, and the typical scan time was about 3 minutes. A perfusion measurement was obtained for each point by calculating the product of erythrocyte velocity and concentration to yield a flux value in arbitrary perfusion units (PU). Red and NIR scans were obtained sequentially, the sequence was randomly varied. Subsequent image analysis was performed (WRF) with the manufacturer's dedicated software, which displayed a colour-coded image of tissue perfusion on a monitor.

All values were stored on a computer disk. On the light intensity (photo) image (Figure 5.1. left hand panel) an area over the MCP joint was designated as the region of interest (ROI). A rheumatologist (RDS) initially defined the region of interest on the basis of the surface anatomy. The region was an ovoid area (size range, 1.8 – 2.6cm$^{2)}$, in which the median flux value was computed. The same ROI placement technique was used for both patients and healthy subjects, and the same person performed the measurements. The LDI method was essentially similar to that previously described for examination of the PIP joints (208).

Ultrasound. Sagittal two-dimensional gray-scale and power Doppler images of the dorsal region of the MCP joint were obtained with US machine ATL HDI 3000 (High Definition Imaging 3000; Advanced Technology Laboratories, Bothell, Washington) with a compact linear (CL) 10-5 MHz, 26 mm probe. At gray-scale US, anechoic metacarpal hyaline cartilage and the hyperechoic triangular central slip were considered to be normal features. Other hypoechoic and anechoic regions in the joint space were defined as synovitis without regard to the size of these lesions. Distinguishing between hypoechoic or anechoic synovitis and effusion is not possible without joint aspiration; therefore, they could not be separated in our study. However, the presence of an inflammatory effusion is pathognomic of synovitis in RA.

The power Doppler zero level was established before the study. The power colour gain was always adjusted to such a level that no power Doppler sign (red pixels inside the active green box) appeared in the active state of the probe with air contact or after gel was applied to the surface of the probe. With this setup,

there was no power Doppler sign when healthy MCP joints were imaged. A low wall filter and low flow optimum were chosen from the software. The pulse repetition frequency was varied between 500 and 1,000 Hz. During the study, scans were obtained when stable red pixels were observed with no pixels present under cortical bone. In this way we attempted to exclude the main disadvantages of the power Doppler technique, namely motion sensitivity and common flash artifacts. Quantification of the hyperaemia was not possible with power Doppler imaging; we could observe only the presence or absence of the pixels in the ROI.

We used a dorsal plane approach in this study because it was the plane used at laser Doppler imaging, and we wanted to avoid the relatively large pulsatile digital arteries, which lie laterally along the joints. For gray-scale ultrasonography the ROI was centered across the MCP joint line and its size was strictly dependent on the 26-mm footprint of the transducer. The region of interest at power Doppler was necessarily smaller and was based on pathological features but always included the whole joint. All sonographic images were stored on magneto-optical disks for off-line analysis.

The laser Doppler imaging and US measurements were performed separately, one immediately after the other, by different operators (CGE and PVB, respectively); the order was randomly varied in successive patients. Laser Doppler Imaging and US measurements were analyzed independently by different investigators (WRF and PVB, respectively) so that they were blinded to results of the other tests until the comparison stage of the study. For each imaging modality, the same person sized and placed the ROIs in each case.

Statistical analysis. Before the main study of patients with RA was started, measurements were taken on two occasions for the first seven control subjects recruited, to obtain data for power calculations and between-day and within-day variability assessment. The other six control patients had not yet been recruited.

On the basis of the data obtained in the seven healthy subjects, power calculations indicated that six participants in each group would require 90% power to depict a 30% change in flux, (alpha = 0.05). Data analysis was performed using Minitab software (MINITAB; Minitab, State College, Pa). Linear correlations were calculated with Pearson's product moment correlation coefficient for two sets of interval scale data (e.g. flux, VAS for pain). The point biserial correlation coefficient was used for comparing interval scale (continuous) data (e.g. flux) with nominal scale (dichotomous) data (e.g. presence or absence of power Doppler sign). The chi- squared test was used for comparing two nominal scale data sets.

Perfusion values between groups were compared by calculating the mean value for all four MCP joints to yield a single value per participant. This calculations was necessary because RA characteristically affects multiple finger joints and thus individual joints can not be considered independent of one another. Independent treatment of the MCP joints was appropriate for comparisons between LDI and the power Doppler sign; however, since the latter yields only dichotomous data that cannot be summed. Comparisons were between two methods, which give rise to contradictory results between individual joints. Two

interval scale data sets were compared with a paired or unpaired Student t-test, as appropriate. Interval scale data are expressed as means ± SD (see in Appendix A for statistical equations and terminology).

5.3. Results

LDI measurements. Scans obtained over the dorsum of the hands with the NIR laser revealed areas of elevated perfusion associated with the MCP joints (Figure 5.1. middle panel) in six patients, whereas the red laser was much less effective in depicting such areas (Fig 5.1. right panel).

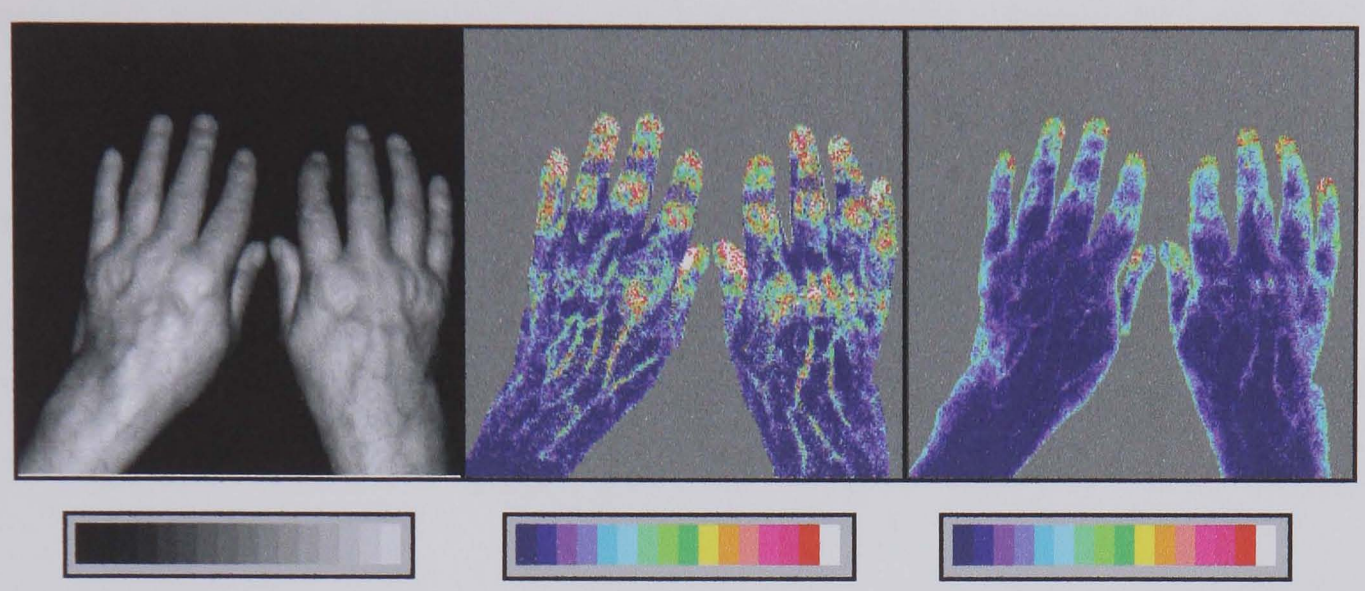

Figure 5.1. Typical LDI appearance for a patient in the high perfusion group. Left: Light intensity (photographic) image of the hands. Middle: Corresponding flux image obtained with a near-infrared laser. Right : Corresponding flux image obtained with a red laser. Elevated perfusion regions associated with the MCP joints are visible with the near-infrared laser but much less so with the red laser. Note that elevated perfusion is also associated with the PIP joints. The visual analog scores for pain in the left and right hand are 8.0 and 6.5, respectively. The light intensity scale ranges from 50 to 175 arbitrary light intensity units. The flux images are colour coded in arbitrary perfusion units according to the same 16-level scale, with lowest perfusion coded dark blue (0-100 perfusion units) and highest perfusion coded white (1,400-1,500 perfusion units).

Because of the greater sensitivity of the NIR laser, all measurements were obtained with this wavelength. At inspection of the near-infrared scans, it was immediately apparent that the patients could be divided into two categories: those who exhibited visually obvious elevated perfusion associated with MCP joints 2 and 3 of either or both hands (high MCP perfusion group, six patients examined) and those who did not (low MCP perfusion group seven patients examined) (Table 5.1.).

Table 5.1. Laser Doppler imaging (LDI) perfusion values (in arbitrary perfusion units, PU) **and Power Doppler sign (PD) in MCP joints of RA patients.** +/– = presence/absence of PD sign; NA = patient unavailable for ultrasound examination.

		RIGHT HAND				**LEFT HAND**				
		MCP 2		**MCP 3**		**MCP 2**		**MCP 3**		
Patient	*Age*	**LDI**	**PD**	**LDI**	**PD**	**LDI**	**PD**	**LDI**	**PD**	
1	30	622	NA	573	NA	395	NA	405	NA	
2	50	283	+	457	–	245	+	182	+	*H*
3	39	524	–	438	+	285	+	390	–	*I*
4	56	301	–	259	–	275	–	417	–	*G*
5	56	562	–	619	–	666	–	438	+	*H*
6	28	387	+	219	+	313	–	237	–	
7	58	92	+	114	+	80	+	100	+	
8	66	198	NA	213	NA	125	NA	115	NA	
9	58	97	+	79	–	68	–	55	–	*L*
10	59	89	+	127	–	144	–	83	–	*O*
11	23	182	+	178	–	146	–	74	–	*W*
12	50	111	–	85	–	106	–	91	–	
13	62	111	+	126	+	129	+	95	+	

The threshold perfusion value for separating the two groups was 200 perfusion units (PU), which lies clearly above the maximum value of 129 PU obtained in healthy subjects in similar environmental conditions. Image analysis strongly confirmed this classification with the high perfusion group showing on average at least a threefold higher perfusion in MCP joints 2 and 3 bilaterally compared with that in the low perfusion group (Figure 5.2.).

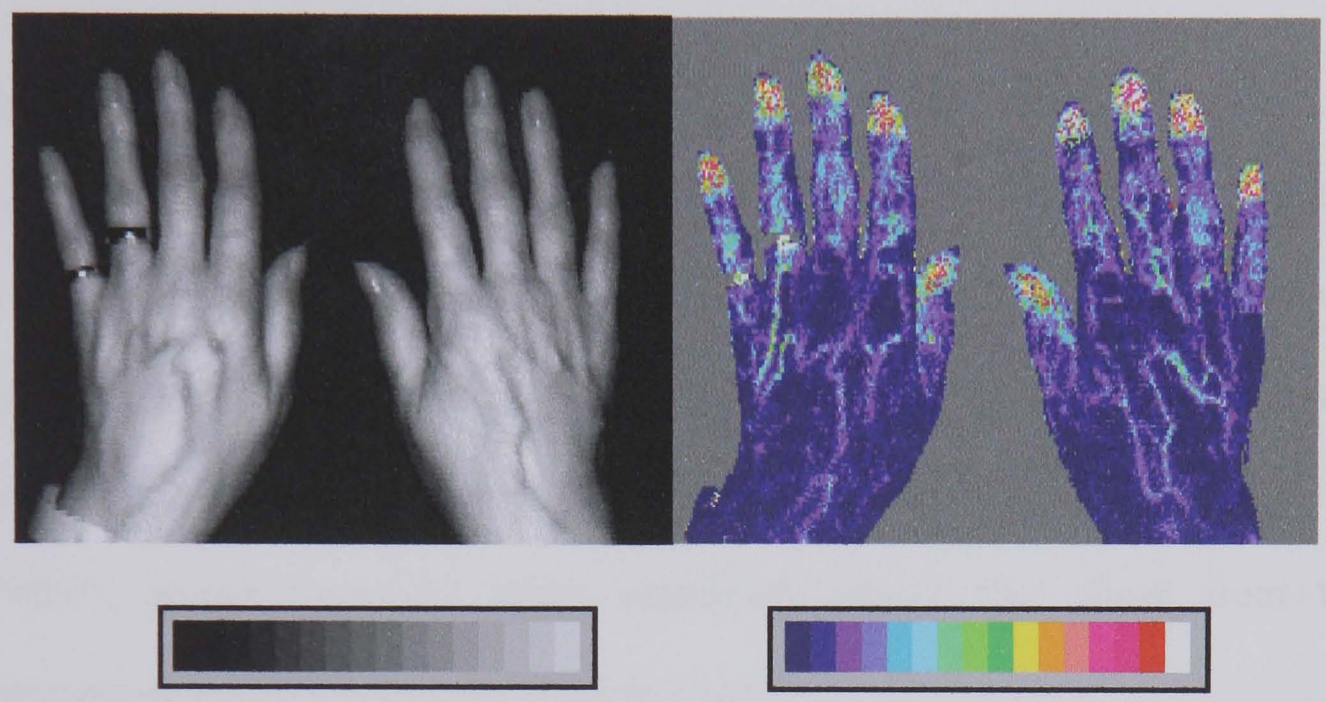

Figure 5.2. Typical LDI appearance for a patient in the low perfusion group.

Left: Light intensity (photographic) image of the hands. Right: Laser Doppler scan obtained with the near-infrared laser of MCP joints that does not show areas of elevated perfusion. The visual analog scores for pain in the left and right hands are 2.5 and 3.5 respectively. The light intensity and perfusion scale values are the same as those used in Fig 5.1.

This was supported by the mean value for the high perfusion group (395.5 ± 118.9 PU), which differed significantly (P=0.002; unpaired t-test) from the value in the low perfusion group (114.8 ± 30.1 PU).

There was very little overlap between high and low groups: measurements in only one of 24 joints in the high perfusion group were below the threshold of 200 PU threshold, and those in only one of 28 joints in the low perfusion group were above the threshold. The perfusion values from MCP joints 2 and 3 of the dominant hand in both the high and low perfusion groups were significantly ($P<0.01$; paired t-test; 52 joints examined) greater than those from the corresponding joints of the non-dominant hand.

Elevated MCP perfusion and hand dominance were significantly correlated (point biserial r = 0.9; $P<0.001$; 52 joints examined). The high perfusion group had a significantly (P = 0.027) lower disease duration (6.1 years ±. 5.5) than the low perfusion group (15.5 years ±. 8.5). Perfusion values from the MCP joints of the 13 healthy subjects ranged from 57 – 129 PU. The mean value (94.3 PU ± 16.6 PU; 13 subjects examined) differed significantly from that in the high perfusion group (P = 0.002) but not from that in the low perfusion groups (P=0.135). Differences between the high and low perfusion groups could not be explained on the basis of temperature variations, because there was no significant difference in room temperature (24.2 °C ±0.82 and 24.6 °C ± 0.34, respectively; P=0.22) or skin temperature (33.6 °C ± 0.43 and 32.2 °C ± 0.34, respectively; P=0.48) between the groups.

Within-day and between-day variability measured at the second MCP joint in seven of the 13 healthy subjects on two occasions were 3.1% ± 3.4 and 3.9% ± 4.1, respectively. The cross-sectional nature of the present investigation precluded such assessment for the patients.

Comparison of Power Doppler and LDI. The power Doppler sign was present in some MCP joints (Figure 5.3.) but the correlation between power Doppler sign and LDI perfusion was weak (point biserial r = 0.244) and non-significant (P = 0.1, 44 joints examined). Comparison of the power Doppler sign (present or absent) and LDI flux signal (high or low), both as nominal scale data, showed that there was agreement in 20 of 44 joints (i.e. the power Doppler sign was present in a high perfusion joint or vice versa). The Chi-squared test indicated that this result did not differ significantly (P = 0.72; 44 joints examined) from that which occurred by chance alone.

Figure 5.3. Sagittal power Doppler ultrasound image of the MCP joint

A. With power Doppler sign

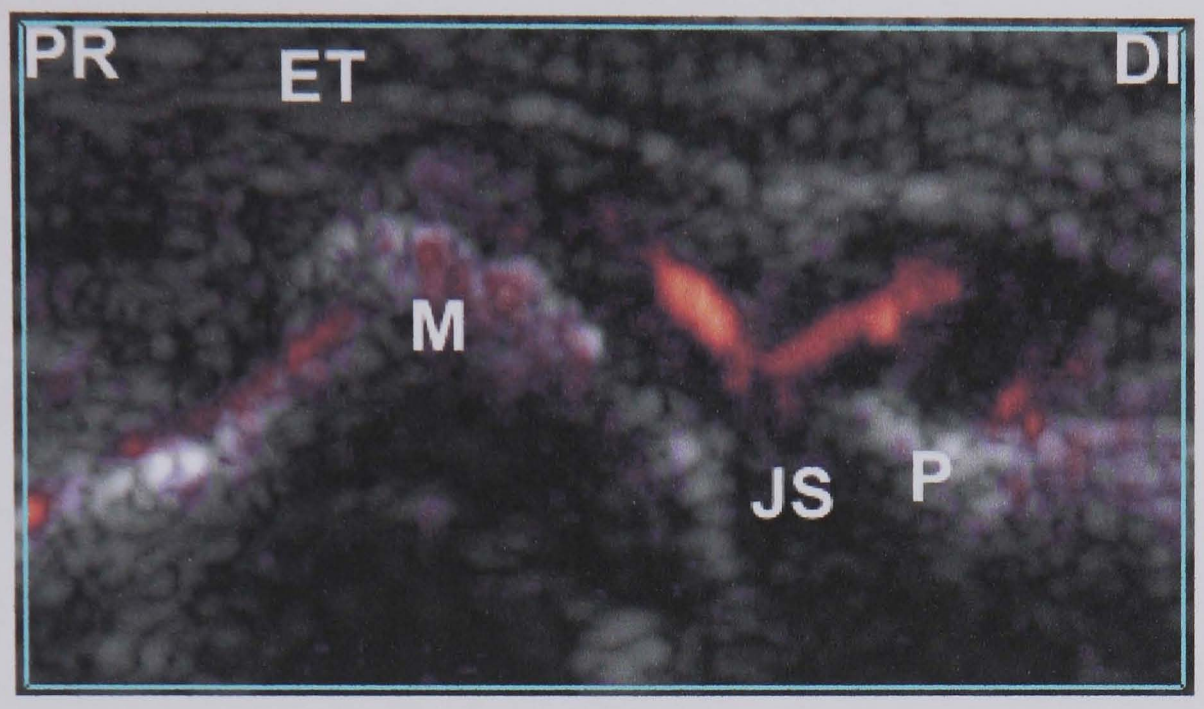

PR = Proximal, DI = Distal, ET = Extensor tendon, M = Metacarpus, JS = joint space, P = Phalanx. The green frame signifies the area of a power Doppler scan and the red colour indicate increased blood flow.

B. Without power Doppler sign

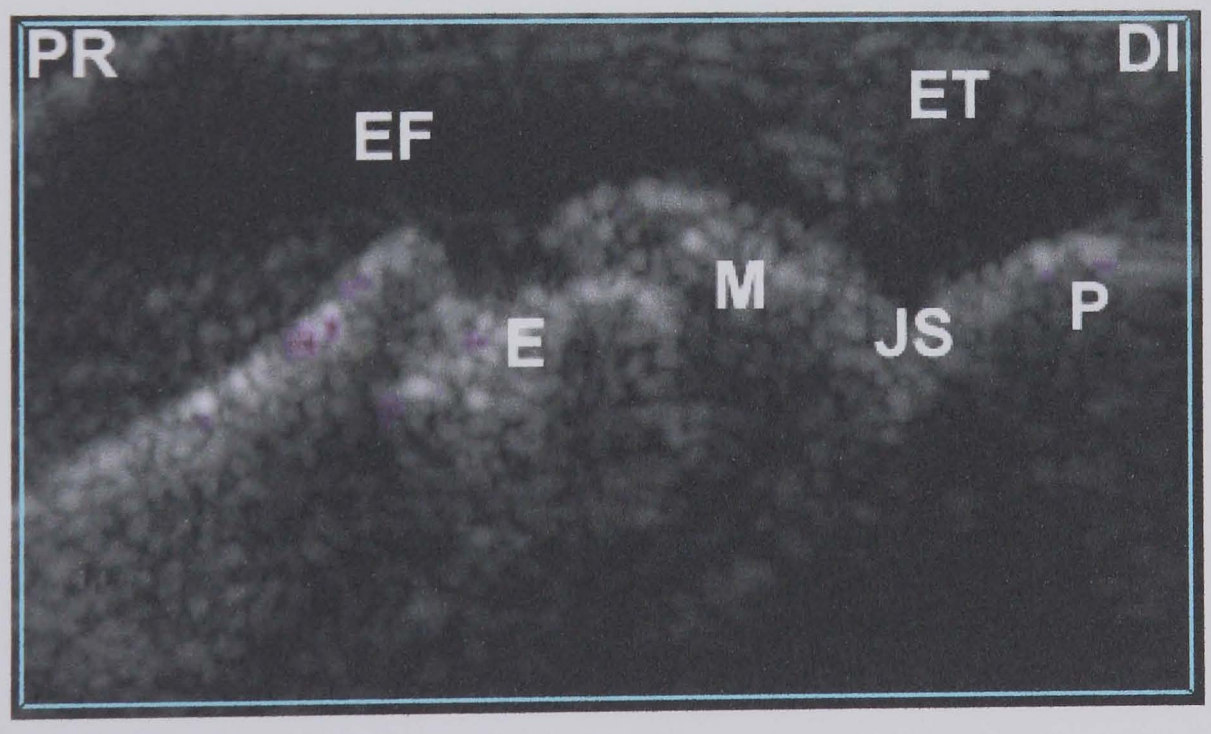

PR = Proximal, DI = Distal, ET = Extensor tendon, M = Metacarpus, JS = joint space, P = Phalanx, EF = Effusion, E = Erosion. The green frame signifies the area of a power Doppler scan.

Correlation with VAS. Patients in both the high and low perfusion groups experienced pains associated with their finger joints but there was a noticeable difference between the groups. Patients in the high perfusion group showed a significantly positive linear correlation ($r = 0.55$) between the MCP perfusion values and the pain score ($P<0.005$, 24 joints examined), which strongly suggests this pain had inflammatory origin (Figure 5. 4.). Analysed separately, the low perfusion group showed an inverse but non-significant correlation ($r = -0.34$; 28 joints examined) between LDI perfusion and the VAS for pain, which suggests that for this patient group, joint pains are unlikely to be of inflammatory origin but are rather of mechanical origin. In contrast, the power Doppler sign was not correlated with the VAS for pain (point biserial $r = -0.001$; 44 joints examined).

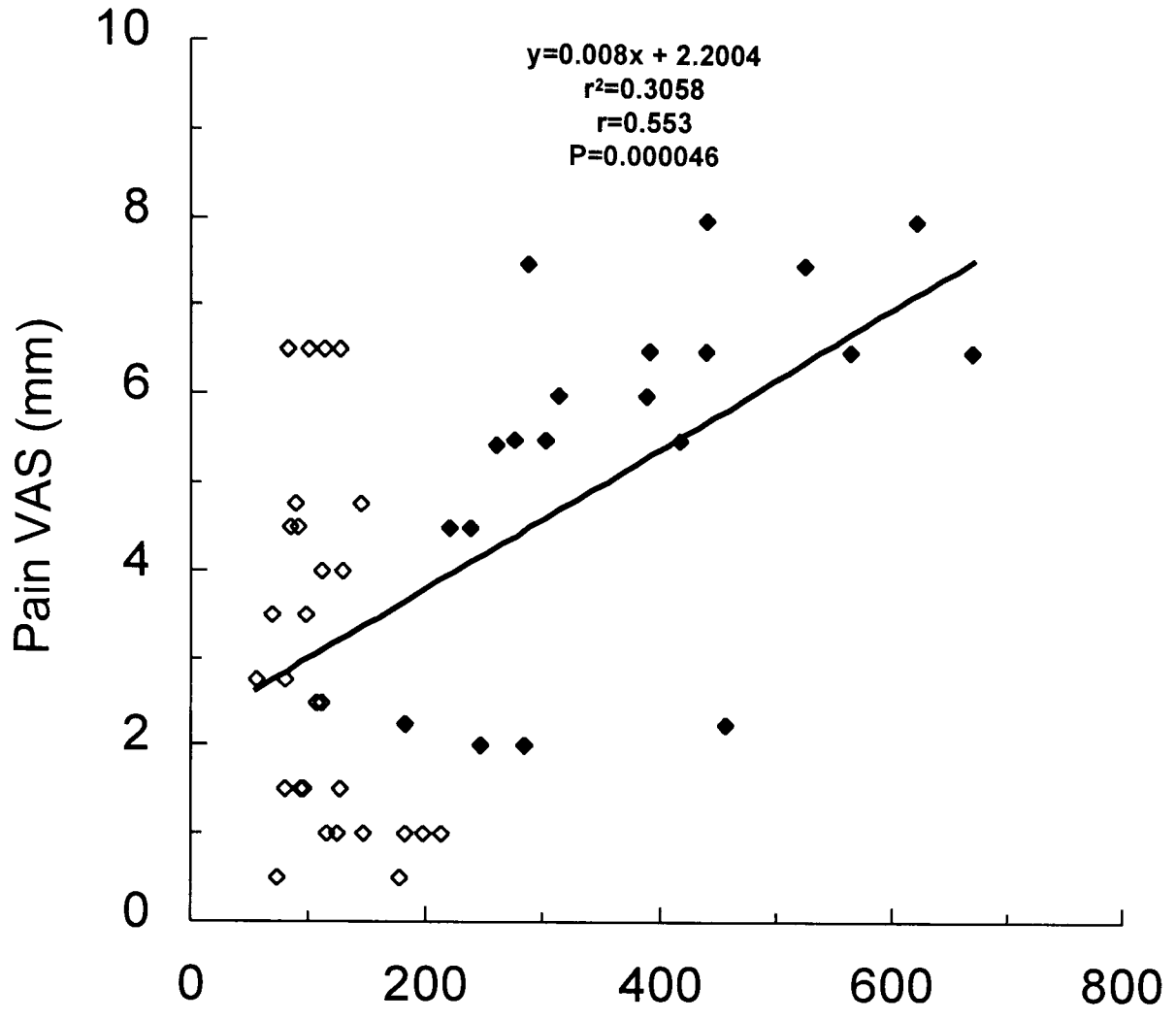

Fig 5.4 **Scatterplot depicts the visual analog score (VAS) for pain in the MCP joints (◆ = high perfusion group, ♫ = low perfusion group) compared with flux determined with laser Doppler imaging.** Note that all but one of the MCP perfusion values in the Low group lie below 200 PU and all except one in the High group lie above that value.

Correlation with ultrasonic assessment of synovitis. Gray-scale ultrasonography revealed anechoic or hypoechoic areas, suggestive of synovitis, associated with the MCP joints with greater frequency in the high perfusion group than in the low perfusion group. There was agreement in 36 of 40 joints (i.e. anechoic region in a high perfusion joint or echoic region in a low perfusion joint) ($P<0.005$ Chi-squared test). Elevated LDI perfusion values were significantly ($P = 0.001$) correlated with anechoic or hypoechoic regions (point biserial $r = 0.76$; 40 joints examined). In contrast, comparisons with the power Doppler sign revealed no close agreement. There was agreement in 18 of 40 joints (i.e. anechoic region in a joint with a power Doppler sign or vice versa) ($P = 0.32$, Chi-squared test).

5.4. Discussion

Findings in this investigation demonstrated that elevated perfusion associated with the MCP joints is detectable in patients with RA. It was possible to distinguish between patients on the basis of high LDI perfusion values associated with the MCP joints. It is unlikely that these areas of elevated perfusion are due to hyperaemia of the skin that overlies the inflamed joint, since scans obtained with the less penetrating red laser failed to show increased perfusion over MCP joints (Figure 5.1.). LDI proved to be more reliable than clinical judgement in the detection of synovitis, since all patients with RA were considered to have inflammation of the finger joints, as judged primarily on the basis of arthralgia. The finding that the highest perfusion values for MCP joints 2 and 3 were associated with the dominant hand agrees with the clinical observation that synovitis in RA is often worse in the joints of the dominant hand (210). However, this finding could be related to differences in hand usage as a consequence of dominance. The lack of correspondence between power Doppler sign and LDI may be related to differences in the parameters measured with the two techniques. Power Doppler imaging can depict the amount of blood flowing in the tissue rather than the velocity of blood flow (205), whereas laser Doppler flux is the product of red blood cell velocity and the concentration of these cells. Thus, these two techniques measure rather different aspects of blood flow, and LDI appears to be more sensitive. Gray- scale ultrasound can be used to detect synovitis associated with inflamed joints in patients with RA (137).

Areas of synovitis are associated with anechoic or hypoechoic signals and there was a strong association between the occurrence of such areas in joints that also showed high perfusion measured with LDI. There was no significant correlation with the power Doppler sign, however, which again suggests that at present this method is less sensitive than LDI. The lack of correspondence between power Doppler sign and synovitis with gray-scale US observed in the present study contrasts with previous findings (137). This may be because of the greater scope for variation between technicians or machines. With LDI, however, there is no contact with the patient, which reduces variation between operators, and laser Doppler imagers automatically compensate for variations in laser power. Within-day and between-day variability of LDI measurements at the MCP joints were similar to values we previously reported for the PIP joints (208).

The observation that the high perfusion group showed a significant positive correlation between perfusion and the pain score suggests that, for this group, the pain was likely to be related to the inflammatory process. In the low perfusion group, there was no correlation between perfusion and the pain score, which suggests that for this group their pain was not inflammatory in origin but may have been related to other factors such as bone and cartilage damage. This information may be useful for determining the most effective drug therapy as anti-inflammatory drugs would be most appropriate for the high perfusion group. In the low perfusion group, however, such drugs would not confer any benefit unless inflammation was present in joints elsewhere.

Joint pain is the most common presenting symptom in patients with RA but as findings in this study indicate, it does not help discriminate between pain of

inflammatory origin and pain of mechanical origin. Such distinction is important as inflammatory pain is likely to arise from hypervascularized pannus formation which is associated with the invasive and destructive phase of RA (211). Clinical assessment of inflammatory status is more difficult at the MCP compared with at the PIP joints, since diameter is difficult to measure at the MCP joints, and joint tenderness does not help discriminate between articular pains of differing origins.

The principal limitation of the LDI methodology is that measurement depth is difficult to establish and is likely to vary depending on the skin properties of the individual patient. However, penetration depth increases with increasing wavelength (207) and thus use of laser sources that operate further into the infra-red wavelength should improve detection of elevated perfusion associated with inflammation. The NIR laser used (835nm) can penetrate skin to a depth of approximately 1,300 μm before the incident optical energy density diminishes to one-third of its original value (207).Altough skin hinders light penetration, only a small fraction of backscattered light is normalized and corrections are made for variations in laser power. Consequently, measurements can be obtained from vascular beds deeper than 1,300 μm, although inflammatory lesions may not be detectable in deeper, more proximal joints such as the shoulder.

Another limitation of laser Doppler imaging is that an external standard of reference is not available for comparison. In animal experiments, however we found that LDI correlates well with absolute measurement of blood flow with radiolabelled microspheres (212). Although this can not be tested in human

subjects, it is likely that tissue perfusion measured with LDI provides an accurate indication of changes in underlying blood flow.

These findings suggest that LDI has the potential to provide an objective assessment of inflammatory hyperaemia in finger joints with RA and possibly in other soft tissues. This could prove to be a useful research tool when investigating efficacy of new treatments and providing further insight into the mechanisms of the disease process. It is possible that future development of this non-invasive and intrinsically safe technique could allow it to be used routinely as an initial assessment of inflammatory status.

This chapter was published during my Ph.D.work.

Ferrell WR, Balint PV, Egan CG, Lockhart JC, Sturrock RD: Metacarpophalangeal joints in rheumatoid arthritis: Laser Doppler Imaging-initial experience Radiology 2001;220: 257-62

5.5. Future aims

Since I completed the work on Power Doppler scanning more published work has appeared concerning power Doppler in MCP, PIP joints, wrist (213 - 217) knee (216, 218 -222) and other joints (216). These studies have found a correlation between power Doppler and histology (218,222) and MRI (214, 216). However synovial tissue histology and MRI have not given direct information about increased blood flow as they only demonstrate the presence of synovitis. Obviously it will be important to plan comparative studies between laser Doppler and histology and MRI. Also it is necessary to further compare laser Doppler, power Doppler and isotope scanning with 99m Tc human immunoglobulin (HIG-scan) in the detection of synovitis. In the last few years' power Doppler methods have improved and for this reason a new comparative study between laser Doppler and power Doppler scanning would be useful. Testing laser Doppler and power Doppler in a musculoskeletal tissue-mimicking phantom could determine the lower limit of detection of blood flow at the same tissue depth with these two modalities. Unfortunately in vivo velocity data does not exist regarding normal and inflamed synovial perfusion. Probably during arthroscopy in vivo videoscope measurement data may be obtained from normal and inflamed joints. Tissue specific contrast agents are not available currently to study synovitis but in the future it will be possible to use such agents.

Chapter 6. Air-coupled ultrasonography of the skeleton of the human hand

6.1. Introduction

On a historic day – 22nd December 1895, Wilhelm Konrad Röntgen performed the first X-ray film on his wife's hand and subsequently the hand X-ray became a symbol of clinical imaging (223). The development of imaging modalities such as radioisotope scanning, thermography, ultrasonography, computer-assisted tomography, and magnetic resonance imaging (MRI) required the hand to be satisfactorily depicted as a "gold standard" for the particular imaging technique. However radioisotope imaging does not display an adequate morphological image of the hand and neither does thermography (224,225). Computed tomography (CT) was a big step forward for detailed morphology, but it also uses X-rays with a rather high radiation dose. Studying different cross-section layers of the hand is the real advantage of CT scans (226) but its use to image the entire hand is not a routine procedure. MRI is an excellent method providing good images both for bony and soft-tissues (227) but it is expensive thus limiting its use for frequent follow-up examinations.

Ultrasound (US) -on the contrary- is a cheap, transportable technique, suitable for bedside use, and good for examining both soft tissues and bony surfaces on backscattered images (228) but larger surfaces such as an entire hand (142) cannot be obtained using routine methods. In order to obtain an image of the entire hand, direct contact with the surface of the hand or immersion in water is

required. The advantage of US is that it is real-time and one can obtain images from different angles. At present US is mainly used for soft-tissue evaluation, but it can detect bony erosions (128) and bone fractures (229). However, commercial US equipment cannot currently visualise the entire morphology and structure of bone.

US has long been used in the aerospace industry to detect small defects in aircraft wings and the use of airborne non-contact ultrasound imaging has recently been used for this purpose (15,230,231). Currently medical US cannot detect small defects in large objects such as the skeletal bones of the whole hand and requirement for gel contact is subject to operator variation. Our hypothesis is that the airborne non-contact imaging apparatus could provide a satisfactory image of a large structure such as the skeleton of the human hand. To test this hypothesis we scanned non-biological test specimen to establish the possible resolution of the system prior to scanning a detached human skeletal hand.

6.2. Materials and methods

In order to investigate air-coupled ultrasonic analysis of the skeletal hand, an existing system was employed that was initially designed to perform air-coupled non-destructive evaluation (NDE) of complex aircraft materials in the aerospace industry (15). This test system was modified to suit the current application and a basic schematic diagram is provided in Figure 6.1. where the transmitter has a 30mm by 30mm active area. The original system comprised eight receiver elements aligned linearly (each with an active area 30mm by 2mm) with the aim of increasing successful scan rates. Only one of these elements is used in the current system.

Figure 6.1. Schematic outline of the air-coupled scanning system.

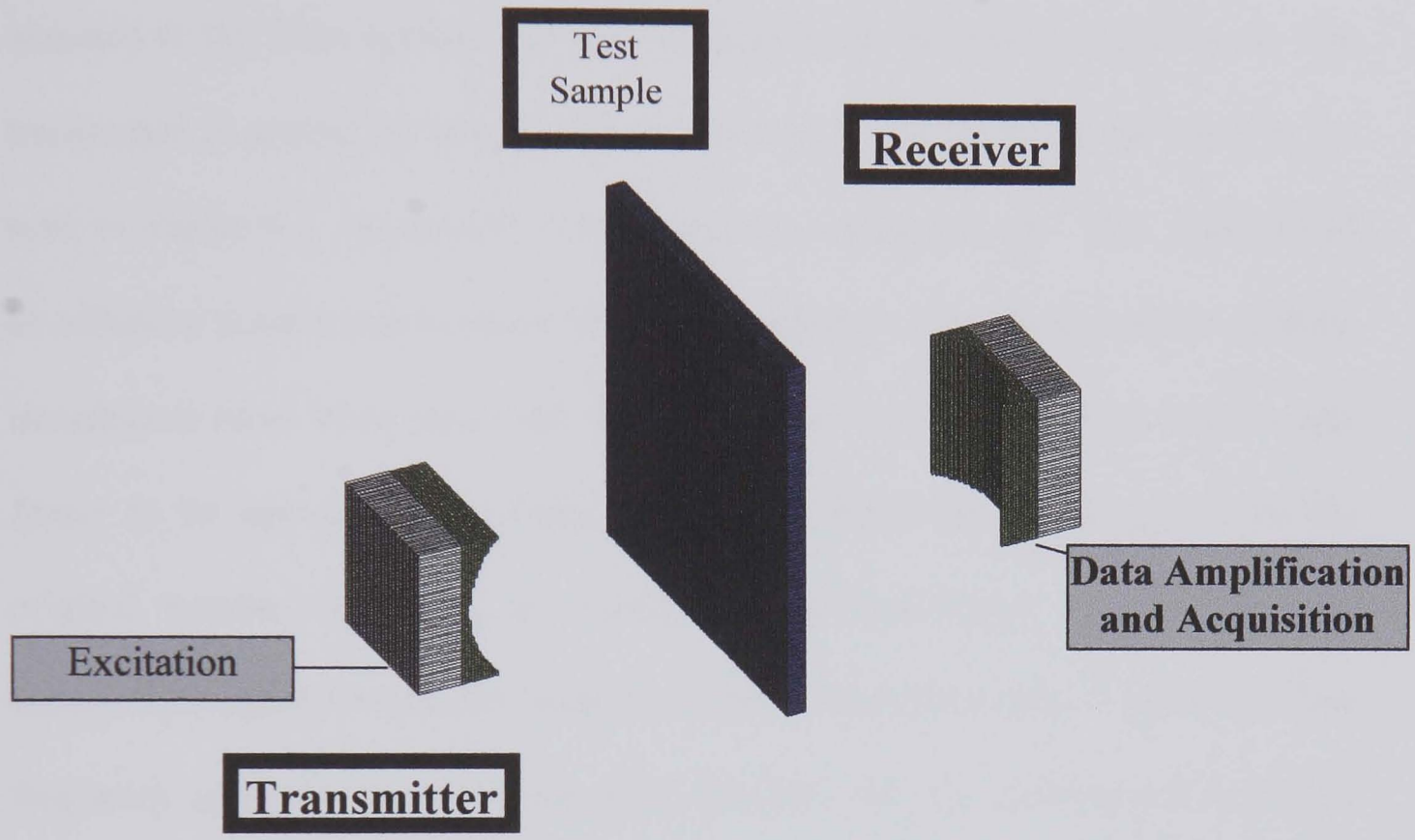

The system is a through transmission arrangement where the transmitting transducer generates an ultrasonic signal in air. This signal passes through the test sample and is monitored with a receiver transducer on the other side. The distance between each transducer and the test sample is 40mm. Linearly focused Perspex (polymethyl methacrylate) lenses with 40mm radius of curvature are attached to the front surfaces of both transducers to enhance the resolution. The transmitter is rotated by ninety degrees relative to the angle of the receiver, as seen in Figure 6.1. to provide further resolution enhancement. This achieves of an effective point focus between the two transducers. The beam profiles of these transducers have been measured and the beam width at the focal region was found to be approximately 1mm at the 3dB signal magnitude (232). In the original system, there was no rotation of the transmitter in order that the transmitted signal was in line with all eight-receiver elements. A relatively low frequency approach has been adopted (600kHz) and the excitation is a narrow band tone burst in order to facilitate simple real time processing to improve signal to noise ratio. The test sample is situated at the focal region between the transducers. In this system, an arbitrary function generator and a power amplifier are used to achieve transmitter excitation and a high gain, ultra-low noise pre-amplifier is used to amplify the detected signal in reception (230).

Both of the transducers were thickness mode piezoelectric composite devices that were designed specifically for use in air (233, 234). This transducer technology provides improved sensitivity in comparison with monolithic ceramic methods and also demonstrates lower acoustic impedance that is better matched to the air load by around 30% and 70% for either the transmitter or receiver

respectively. There is, however, still a massive impedance mismatch between the transducers and the air load. This may be appreciated when it is noted that impedance of air is $0.0004 kgm^{-2}s^{-1}$ and that of the transducer is $22 kgm^{-2}s^{-1}$. Acoustic matching layers have been designed and attached to the front surfaces of the two lenses in an attempt to overcome this and a 30dB increase in the received signal magnitude has been achieved when these are in place on both transducers (235).

Test sample inspection is achieved by scanning both transducers over the sample at a fixed distance of 40mm. Movement is in a raster pattern and stepper motors are used to achieve this in the horizontal and vertical axes. The scan step size is selected to be 0.5mm and after each step the amplitude of the received signal is measured and stored. A plot of this data then forms a two-dimensional picture of the internal structure of the sample. In each case, a grey scale is employed where the shade depicts the magnitude of the received signal. Light shade represents high magnitude received signal, whereas dark shade represents low magnitude.

Before scanning biological samples, attempts were made to test non-biological samples with the new air-coupled system arrangement. The intention of this was to establish sensitivity and defect detection resolution. Several aircraft test specimens were investigated including solid carbon fibre and honeycomb samples. One such scan is provided in Figure 6.2. and this is a 3.7mm thick solid carbon fibre plate that has nine inclusions of various shapes and sizes.

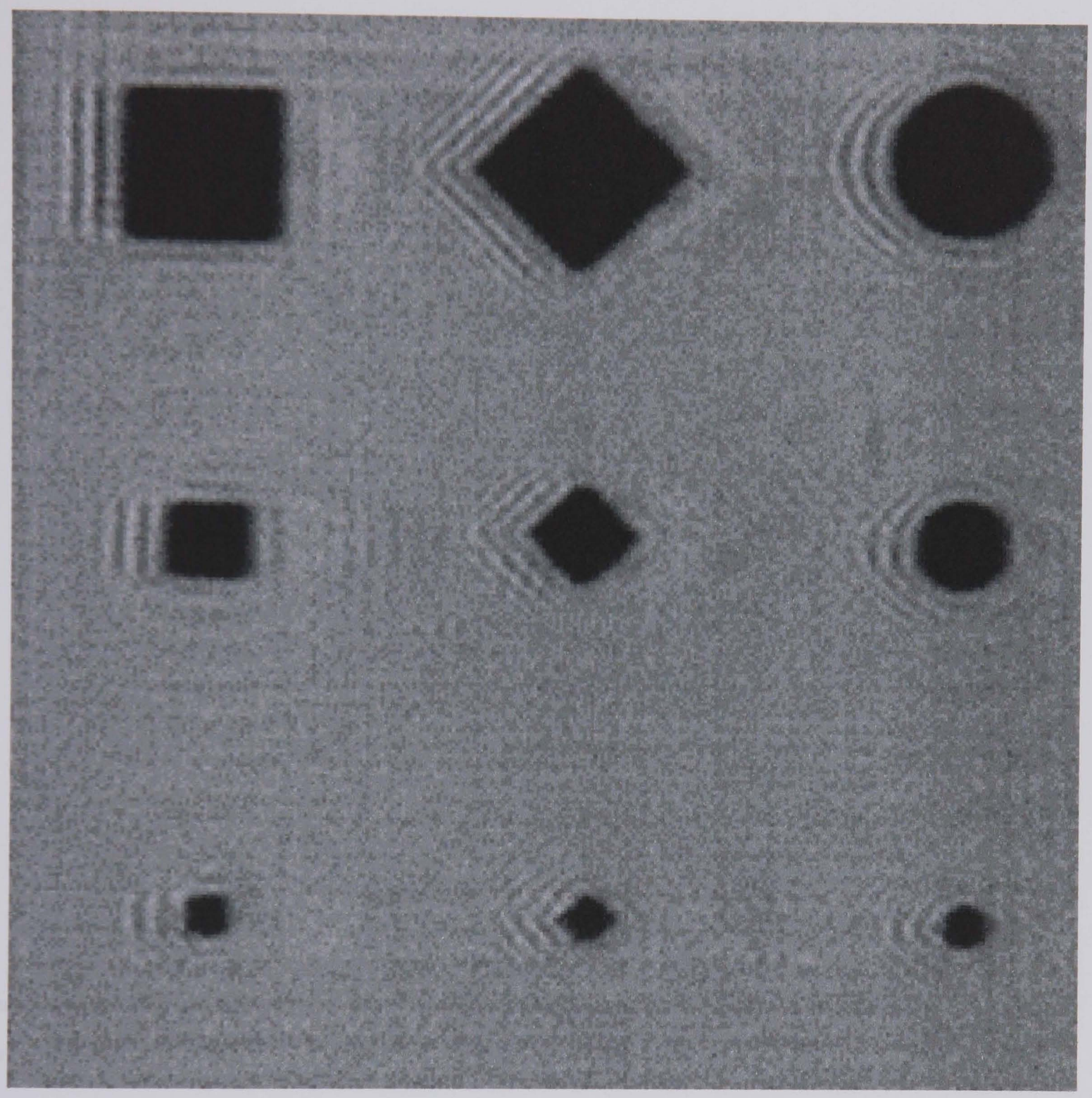

Figure 6.2. **Scan of the carbon fibre sample with 9 artificial inclusions. The scan clearly shows these inclusions as the black areas.**

The scan area here is 170mm by 170mm, the scan time was 2.75 hours and the inclusion sizes were 6mm, 12mm and 24mm. The inclusions were made from PTFE (Polytetrafluoroethylene) of various shapes that have been folded in two and so trap air within the sample. The presence of this air again results in signal reflection and effectively means that no detectable signal is received when the transducers pass over an inclusion. In the case of biological sample inspection, the specimen used was an articulated bony hand detached from a standard skeleton supplied for anatomical teaching.

6.3. Results

Signal transmission through the carbon fibre plate was achievable and adequate signal amplitude was received through the sample areas where no defect was present. Where a defect was encountered, resulting in reduced signal amplitude, the clarity and resolution of the defect edge detection was encouraging. When the accuracy of detection of the corners of the square defects is considered, it is proposed that a resolution of approximately 1mm has been achieved. This is in keeping with the previously measured beam width at 3dB reduction in signal magnitude. In addition to this, it is noted that some evidence of the carbon fibre structure is apparent with the faint horizontal and vertical lines in the sections with no defect present. Note also that there are band patterns round each of the inclusions and these are believed to be due to signal diffraction from the sharp edges at the defect boundaries. Importantly, scan repeatability and reproducibility has also been found to be adequate with the wide range of testing that has been performed and repeated on various different samples. It was concluded from these results that further investigation using this air-coupled ultrasonic system to investigate biological samples would be merited.

The selected biological sample for the continuation of this air-coupled work was a detached articulated hand from a human skeleton. A photograph and an X-ray scan of this skeleton are provided in Figure 6.3. and Figure 6.4. respectively.

Figure 6. 3. Clinical photo of human skeletal hand.

Figure 6.4. X-ray of a human skeletal hand.

Air-coupled scanning of this sample proceeded in the same way as with the carbon fibre plate scan, with transducer separation from the skeleton of 40mm and a scan step size of 0.5mm. The scanned area was 220mm by 140mm, the scan time was approximately 3 hours and the result is shown in Figure 6.5.

Figure 6.5. Air-coupled scan of a human skeletal hand.

In this case, the outline of the bones in the hand was resolved by detecting the sections within the scanned area where no signal was received. The detection of the bone and joint outline is apparent with this scan (Figure 6.5.) although resolution is obviously reduced when compared with the photograph and X-ray in Figure 6.3. and 6.4. The edges round each bone and joint are clearly less well defined than the X-ray and there is also no internal detail of the joining wires since the signal does not pass through the bone at any point. The faint dark lines on the top right corner of the air-coupled scan in Figure 6.5. are believed to have been as a result electrical interference during the scan at that time.

6. 4. Discussion

We were able to depict the skeleton of a human hand using a non-contact air-coupled transducer configuration. Unfortunately we could not obtain a real-tomographic view of the hand bones. An X-ray clearly demonstrates the metal wires in the bones (Figure 6.4.). On the US image we cannot see these wires. The US picture shows only a negative relief of the skeleton of a human hand so that the inner bone structure cannot be visualised. However surface pathology can be investigated even on a negative relief image. Rheumatoid arthritis causes small bone erosions of the hand. Hand involvement is an early manifestation of the disease (less than 6months) and one of the classification criteria of the disease (209). Conventional X-rays are used as a standard technique to measure the progression of the disease, but frequent examinations are limited due to radiation hazards. Routine X-rays have a low sensitivity for detecting bone erosion especially in the first 6 months of disease. MRI can be used for following disease progression but its use is limited by cost and by long waiting lists for examination.

It is understood that although the resolution of the scan in Figure 6.5. would be adequate for the purpose of bone erosion monitoring, the more realistic situation when soft-tissues are included poses a very different problem. This could therefore be overcome if higher frequency (3MHz) transducers were to be used although this would also introduce additional difficulty as a result of the square relationship between frequency and signal attenuation in an air load. This means that if the operational frequency was increased by a factor of five, the attenuation

experienced by the signal in air would be increased by a factor of twenty-five. Although this is not a straightforward problem, it is believed to be achievable through continued development of transducer technology.

Non-contact US has potential for providing a better perspective of the morphology of the musculoskeletal system but clearly requires more development. Non-contact US has a major advantage over contact US in respect of operator variation. Roentgen's invention was one of the fastest methods to spread and be accepted around the world. In 1896 X-ray films were used for the first time as evidence in a court of law (236). Early X-ray technology required an exposure lasting 45 minutes to obtain suitable films for interpretation. In a similar way, non-contact US technology will hopefully improve to enable high quality images of the morphology of the bones, joints and soft tissues of the musculoskeletal system to be usefully applied in clinical practice.

6.6. Future aims

Further work will be required in developing air-coupled US for musculoskeletal imaging. The next step will be to examine thin, fresh animal soft-tissue and bone slices with air-coupled US to establish the maximum penetration ability and the optimum frequency for tomographic and backscattered images. If it is possible to obtain an image of adequate quality with a thickness of animal tissue comparable to human hand dimensions then imaging of fresh human cadaver hands will be performed. When the acquisition time is reduced to approx. less than 30 minutes then the normal living human hand can be examined. The minimum achievement here will be to obtain full-thickness soft-tissue tomography and back-scattered images from bone surfaces showing the outline of the bones with an embedded image.

In parallel with the air-coupled experiments, a water-bath backscattered, tomographic and 3D hand scanner will need to developed and tested on the normal and rheumatoid hand. After optimising the US frequency and image quality, US images need to be compared with tomographic and 3D MRI images. Even after modification this hand scanner is unlikely to be used in axial or girdle joints but might be used for examination of peripheral joints and extremities. Other specialities of medicine e.g. pathology may be use this full tomographic US scan for studying internal organs such as brains, livers and kidneys to obtain high resolution post-mortem images surveying different minimal lesions thus enabling targeted dissection of pathological lesions.

Chapter 7. Conclusion

A comparison of living adult human ultrasound images with the image of periarticular and articular anatomical specimens in different planes was previously lacking and musculoskeletal ultrasound examination has not been previously standardized.

My work has shown that using standardized ultrasound examination techniques, articular and periarticular tissues can be depicted well and provided virtually identical images, with those of similar anatomical preparations. Standardization of the position of the subject, the position of his/her examined joints and the position of the probe in different planes during ultrasound examination are essential to obtain images, which are reproducible. Determination and use of anatomical landmarks for proper orientation and a clear description of ultrasound anatomy of a number of joints and periarticular tissues is now available for further pathological investigations.

A diagnostic method is reliable when its intra- and interobserver reproducibility is acceptable. It was shown by this work that intra – and interobserver variation of US imaging was low and acceptable.

In order to show how this standardized ultrasonography technique can be used in the assessment of inflammatory joint diseases; two trials were performed. In spondylarthopathy it was shown, that sonography is significantly more sensitive and specific than physical examination in detecting enthesitis. Enthesitis is a

hallmark and often the first peripheral manifestation of the disease. Different enthesitis indices have been developed for assessing clinical inflammatory activity of the disease but currently none of them is in regular use. The GUESS index was developed and may fulfil the criteria of a clinically useful enthesitis index. Certainly, further research is needed to evaluate this index.

Unlike SpA, in RA we do have good, reproducible and widely used clinical parameters. The different joints counts used for this purpose are based on joint pain, joint tenderness and joint swelling (237). However, joint swelling of some joints, like the hip cannot be detected and in others moderate or minor swelling cannot be recognized with certainty. In our study we compared power Doppler images, gray scale ultrasound images and laser Doppler images of the 2^{nd} and 3^{rd} MCP joints in RA patients. LDI depicts increased circulation due to inflammation. Although all 2^{nd} and 3^{rd} MCP joints of the RA patients seemed to be swollen, painful and tender, LDI verified increased circulation in only some of the patients and not in others. Probably in this second group of patients the pain and tenderness of the MCP joint was caused by degenerative changes secondary to inflammation, and swelling –when it was present-, represented thickened synovial membrane and joint capsule without increased blood flow. Power Doppler ultrasound images did not show a correlation with LDI depicting increased blood flow of RA MCP joints. The reason for this should be further investigated. The gray scale ultrasound images of the investigated MCP joints however correlated well with LDI. Anechoic and hypoechoic echoes reflecting inflamed synovial tissue and/or synovial effusion were detected in cases with increased blood flow as shown by LDI. Gray scale ultrasound images of joints

showing anechoic and hypoechoic echoes, can be regarded as joints having active synovitis and can be used for assessing inflammatory activity either in single or in multiple joints.

In order to reduce observer variation in musculoskeletal ultrasound examination we tested air-coupled ultrasonography to avoid any observer variation and to depict human anatomy. An ultrasonic system that was designed originally for testing in the aerospace industry was modified and used to depict the skeleton of the human hand. Airborne ultrasound was able to depict the surface of the skeleton of a human hand in an experimental study but cannot obtain a real tomographic view of the hand bones. The scan showed the outline of the hand bones but no internal structure.

In summary several final conclusions were deduced from the experiments:

i) Ultrasound can depict normal musculoskeletal tissues which correlate with the anatomical structures.

ii) Where an acoustic window allows the use of ultrasound it is possible to depict normal peripheral joint structure according to the well-known anatomical structures in standardized anatomical planes.

iii) With well-defined anatomical landmarks and with pre-determined criteria, acceptable intra- and interobserver variation was obtained when musculoskeletal ultrasound was performed by two different observers.

iv) A rheumatologist with experience of US imaging can train a novice within a relatively short space of time to produce acceptable musculoskeletal ultrasound images.

v) Ultrasound detection of enthesitis is more sensitive and more specific than clinical examination and considerable sub-clinical enthesitis can be detected in SpA.

vi) With the present US equipment, laser Doppler imaging is more sensitive in measuring blood flow of MCP joints in RA than power Doppler imaging.

vii) Laser Doppler images correlated with gray-scale ultrasound images of MCP joint synovitis. There was no correlation between gray-scale US and power Doppler ultrasound images in relation to MCP joint synovitis.

viii) Airborne ultrasound is able to depict the surface of the skeleton of a human hand in an experimental study but cannot obtain a real tomographic view of the hand bones.

References

1. Eisenberg RL. Radiology: an illustrated history. St. Louis, Mosby-Year Book, 1992.
2. Griffin DR. Listening in the dark. The acoustic orientation of bats and men. New Haven, Yale University Press, 1958; 57-64.
3. Pierce GW, Griffin DR. Experimental determination of supersonic notes emitted by bats. J Mammal 1938; 19: 454-5.
4. Galambos R, Griffin DR. The supersonic cries of bats. Anat Rec 1940; 78: 95.
5. Griffin DR, Galambos R. Obstacle avoidance by flying bats. Anat Rec 1940; 78:95.
6. Griffin DR, Galambos R. The sensory basis of obstacle avoidance by flying bats. J Exp Zool 1941; 86: 481-506.
7. Curie J, Curie P. Dèveloppement, par pression, de l'èlectricitè polaire dans les cristaux hèmièdres à faces inclinèes. C. R. Acad Sci Paris 1880; 91: 294-5.
8. Crystal D. ed. The Cambridge Encyclopedia. 2nd ed. Cambridge University Press, 1994; 367-8.
9. Hill CR. Medical ultrasonics: an historical review. Br J Radiol 1973; 46: 899-905.
10. Woo J. A short history of the developments of ultrasound in obstetrics and gynecology. http://www.ob-ultrasound.net/hydrophone.html. 1999.

11. Firestone FA. The supersonic reflectoscope for interior inspection. Met Progr 1945; 48: 505-12.

12. Firestone FA. The supersonic reflectoscope, an instrument for inspecting the interior of solid parts by means of sound waves. J Acoust Soc Am 1946; 17: 287-99.

13. Saijo Y, Chubachi N. Microscopy. Ultrasound Med Biol 2000; 26: Suppl. 1, S30-S32.

14. Wade G. Human uses of ultrasound: ancient and modern. Ultrasonics 2000; 38: 1-5.

15. Kelly SP, Farlow R, Hayward G. Applications of through-air ultrasound for rapid NDE scanning in the aerospace industry. IEEE T Ultrason Ferr 1996; 43: 581-91.

16. Dussik KT. On the possibility of using ultrasound waves as a diagnostic aid. Z Neurol Psychiatr 1942; 174: 153-68.

17. Shampo MA, Kyle RA. Karl Theodore Dussik - pioneer in ultrasound. Mayo Clin Proc 1995; 70:1136.

18. Ludwig GD, Struthers FW. Detecting gallstones with ultrasonic echoes. Electronics 1950; 23:172-8.

19. Ludwig GD, Bolt RH, Heuter TF, Ballantine HT. Factors influencing the use of ultrasound as a diagnostic aid. Trans Am Neurol Assoc 1950; 75: 225-8.

20. Ludwig GD. The velocity of sound through tissues and the acoustic impedance of tissues. J Acoustic Soc Am 1950; 22: 862-6.

21. Wild JJ. The use of ultrasonic pulses for the measurement of biologic tissues and the detection of tissue density changes. Surgery 1950; 27:183-8.

22. Wild JJ, Neal D. Use of high-frequency ultrasonic waves for detecting changes of texture in living tissues. Lancet 1951; 1: 655-7.

23. Wild JJ, Reid JM. Application of echo-ranging techniques to the determination of structure of biological tissues. Science 1952; 115: 226-30.

24. Shampo MA, Kyle RA. John Julian Wild - pioneer in ultrasonography. Mayo Clin Proc 1997; 72: 234.

25. Woo J. A short history of the developments of ultrasound in obstetrics and gynecology. http://www.ob-ultrasound.net/history.html. 1999

26. Reid JM. Development of medical ultrasonics. Ultrasound Med Biol 1983; Suppl 2, 3-7.

27. Howry DH. The ultrasonic visualisation of soft tissue structures and disease processes. J Lab Clin Med 1952; 40: 812-3.

28. Howry DH, Bliss WR. Ultrasonic visualisation of soft tissue structures of the body. J Lab Clin Med 1952; 40: 579-92.

29. Howry DH. Development of an ultrasonic diagnostic instrument. Am J Phys Med 1958; 37: 234.

30. Holmes JH, Howry DH, Posakony GJ, Cushman CR. The ultrasonic visualisation of soft tissue structures in the human body. Trans Am Clin Climatol Assoc 1954; 66: 208-23.

31. Goldberg BB, Gramiak R, Freimanis AK. Early history of diagnostic ultrasound: the role of American radiologists. AJR Am J Roentgenol 1993; 160: 189-94.

32. French LA, Wild JJ, Neal D. Detection of cerebral tumors by ultrasonic pulses. Cancer 1950; 3: 705-8.

33. Fry WJ, Mosberg WH Jr, Barnard JW, Fry FJ. Production of focal destructive lesions in the central nervous system with ultrasound. J Neurosurg 1954; 11: 471-8.

34. Holmes JH. Diagnostic ultrasound during the early years of A.I.U.M. J Clin Ultrasound 1980; 8:299-308.

35. Csanyi AF. The history of neuro-sonology. J Hist Neurosci 1994; 3: 123-30.

36. Leksell L. Echo-encephalography I. Detection of intracranial complications following head injury. Acta Chir Scand 1956; 110: 301-15.

37. Edler I, Hertz CH. The use of ultrasonic reflectoscope for the continuous recording of the movements of heart walls. Kungl Fysiogr Sällsk I Lund Förhandl 1954; 24: 40-58.

38. Edler I, Hertz CH. The early work on ultrasound in medicine at the University of Lund. J Clin Ultrasound 1977; 5: 352-6.

39. Feigenbaum H. A milestone for medical ultrasound. J Am Soc Echocardiogr 1988; 1: 255-6.

40. Feigenbaum H. Evolution of echocardiography. Circulation 1996; 93: 1321-7.

41. Satomura S. Study of the flow patterns in peripheral arteries by ultrasonics. J Acoust Soc Jpn 1959; 15: 151-8.

42. Barber FE, Baker DW, Nation AW, Strandness DE Jr, Reid JM. Ultrasonic duplex echo-Doppler scanner. IEEE Trans Biomed Eng 1974; 21: 109-13.

43. Strandness Jr DE. History of ultrasonic duplex scanning. Cardiovasc Surg 1996; 4: 273-80.

44. Sigel B. A brief history of Doppler ultrasound in the diagnosis of peripheral vascular disease. Ultrasound Med Biol 1998; 24: 169-76.

45. Donald I. Sonar-the story of an experiment. Ultrasound Med Biol 1974; 1: 109-17.

46. Willocks J. Medical ultrasound. A Glasgow development, which swept the world. Avenue, University of Glasgow 1996; 19: 5-7.

47. McNay MB, Fleming JEE. Forty years of obstetric ultrasound 1957-1997 from A-scope to three dimensions. Ultrasound Med Biol 1999; 25: 3-56.

48. Fleming JEE, Spencer IH, Nicolson MA. Forty years of ultrasound. In: Cockburn F, ed. Advances in perinatal medicine. New York, London: The Parthenon Publishing Group, 1996; 92-9.

49. Donald I, MacVicar J, Brown TG. Investigation of abdominal masses by pulsed ultrasound. Lancet 1958; 1: 1188-95.

50. Campbell S. An improved method of fetal cephalometry by ultrasound. J Obstet Gynaecol Br Commonw 1968; 75: 568-76.

51. Kurjak A. Ultrasound scanning- Prof. Ian Donald (1910-1987). Eur J Obstet Gynecol Reprod Biol 2000; 90:187-9.

52. Donald I, Abdulla U. Placentography by sonar. J Obstet Gynaecol Br Commonw 1968; 75: 993-1006.

53. Boyd E, Abdulla U, Donald I, Fleming JEE, Hall AJ, Ferguson-Smith MA. Chromosome breakage and ultrasound. BMJ 1971; 29: 501-2.

54. Kossof G. An historical review of ultrasonic investigations at The National Acoustic Laboratories. J Clin Ultrasound 1975; 3: 39-43.

55. Kossoff G. Diagnostic ultrasound – the view from down under. J Clin Ultrasound 1978; 6: 144-9.

56. Leopold GR. A sound perspective. AJR Am J Roentgenol 2000; 174: 9-15.

57. Wells PNT. Physics and engineering: milestones in medicine. Med Eng Phys 2001; 23: 147-53.

58. Leopold GR. The Radiological Society of North America. Diamond Jubilee lecture. Seeing with sound. Radiology 1990; 175: 23-7.

59. Holm HH, Skljoldbye B. Interventional ultrasound. Ultrasound Med Biol 1996; 22: 773-89.

60. Holm HH. Kristensen JK, Rasmussen SN, Northeved A, Barlebo H. Ultrasound as a guide in percutaneous puncture technique. Ultrasonics 1972; 10: 83-6.

61. Goldberg BB, Pollack HM. Ultrasonic aspiration transducer. Radiology 1972; 102:187-9.

62. Goldberg BB. Obstetric US imaging: the past 40 years. Radiology 2000; 215: 622-9.

63. Staiano S. In Memoriam--Dr. von Micsky. J Clin Ultrasound 1976; 4: 320-1.

64. Levi S. The history of ultrasound in gynecology 1950-1980. Ultrasound Med Biol 1997; 23: 481-552.

65. Burns PN, Simpson DH, Averkiou MA. Nonlinear imaging. Ultrasound Med Biol 2000; 26: Suppl. 1, S19-S22.

66. Campbell S. 4D, or not 4D: that is the question. Ultrasound Obstet Gynecol 2002; 19: 1-4.

67. Newman PG, Rozycki GS. The history of ultrasound. Surg Clin North Am 1998; 78: 179-95.

68. Wood RW, Loomis AL. The physical and biological effects of high-frequency sound waves of great intensity. Phil Mag 1927; 7: 417-36.

69. Harvey EN, Loomis AL. High frequency sound waves of small intensity and their biological effects. Nature 1928; 121: 622-4.

70. Szent-Györgyi A. Chemical and biological effects of ultrasonic radiation. Nature 1933; 131: 278.

71. ter Haar G Intervention and therapy Ultrasound Med Biol 2000; 26; Suppl 1.S51-S54.

72. Erickson KR, Fry FJ, Jones JP. Ultrasound in Medicine- a review. IEEE Transactions on Sonics and Ultrasonics 1974; su-21: 144-70.

73. Barnett SB, Rott HD, ter Haar GR, Ziskin MC, Maeda K. The sensitivity of biological tissue to ultrasound. Ultrasound Med Biol 1997; 23: 805-12.

74. Nyborg WL. Biological effects of ultrasound: development of safety guidelines. Part II: general review. Ultrasound Med Biol 2001; 27: 301-33.

75. Nyborg WL. Biological effects of ultrasound: development of safety guidelines. Part I: personal histories. Ultrasound Med Biol 2000; 26: 911-64.

76. Barnett SB. Biophysical aspects of diagnostic ultrasound. Ultrasound Med Biol 2000; 26: Suppl. 1, S68-S70.

77. Foldes K, Hynynen K, Shortkroff S et al. Magnetic Resonance Imaging-guided focused ultrasound synovectomy. Scand J Rheumatol 1999; 28: 233-7.

78. Hynynen K, Foldes K, Jolesz F, Winalski C, Shortkroff S. Method for the treatment of joint diseases characterized by unwanted pannus. US Patent 6,074,352.

79. Miller MW. Gene transfection and drug delivery. Ultrasound Med Biol 2000; 26: Suppl.1, S59-S62.

80. Weng L, Tirumalai AP, Lowery CM et al. US extended-field-of-view imaging technology. Radiology 1997; 203: 877-80.

81. Delius M. Lithotripsy. Ultrasound Med Biol. 2000; 26: Suppl 1, S55-8.

82. Langton CM, Palmer SB, Porter RW. The measurement of broadband ultrasonic attenuation in cancellous bone. Eng Med 1984; 13: 89-91.

83. American Institute of Ultrasound in Medicine. Medical ultrasound safety. Laurel, 1994.

84. Dussik KT, Fritch DJ, Kyriazidou M, Sear RS. Measurements of articular tissues with ultrasound. Am J Phys Med 1958; 37:160-5.

85. McDonald DG, Leopold GR. Ultrasound B-scanning in the differentiation of Baker's cyst and thrombophlebitis. Br J Radiol 1972; 45:729-32.

86. Seltzer SE, Finberg HJ, Weissman BN Arthrosonography- technique, sonographic anatomy, and pathology. Investigate Radiology 1980; 15: 19-28.

87. Seltzer SE, Finberg HJ, Weismann BN et al. Arthrosonography: gray scale ultrasound evaluation of the shoulder. Radiology 1979; 132: 467.

88. Middleton WD, Edelstein G, Reinus WR, Melson GL, Murphy WA. Ultrasonography of the rotator cuff: technique and normal anatomy. J Ultrasound Med 1984; 3:549-51.

89. Miles KA, Lamont AC. Ultrasonic demonstration of the elbow fat pads. Clin Radiol 1989; 40: 602-4.

90. Koski JM. Ultrasonography of the elbow joint. Rheumatol Int 1990; 10: 91-4.

91. De Flaviis L, Scaglione P, Nessi R, Ventura R, Calori G. Ultrasonography of the hand in rheumatoid arthritis. Acta Radiol 1988; 29: 457-60.

92. Fornage BD, Rifkin MD. Ultrasound examination of the hand and foot. Radiol Clin North Am 1988; 26:109-29.

93. Koski JM. Ultrasonography in detection of effusion in the radiocarpal and midcarpal joints. Scand J Rheumatol 1992; 21: 79-81.

94. Fornage BD. Soft-tissue changes in the hand in rheumatoid arthritis: evaluation with US. Radiology 1989; 173: 735-7.

95. Grassi W, Tittarelli E, Pirani O, Avaltroni D, Cervini C. Ultrasound examination of metacarpophalangeal joints in rheumatoid arthritis. Scand J Rheumatol 1993; 22:243-7.

96. Grassi W, Filippucci E, Farina A, Cervini C. Sonographic imaging of the distal phalanx. Semin Arthritis Rheum 2000; 29:379-84.

97. Baratelli M, Parrini L. Ultrasonography in the study of pathological conditions of the hip. Ital J Orthop Traumatol 1986; 12: 233-7.

98. Koski JM. Ultrasonographic evidence of hip synovitis in patients with rheumatoid arthritis. Scand J Rheumatol 1989; 18: 127-31.

99. Koski JM, Anttila PJ, Isomaki HA. Utrasonography of the adult hip joint. Scand J Rheumatol 1989; 18: 113-7.

100. Ambanelli U, Manganelli P, Nervetti A, Ugolotti U. Demonstration of articular effusions and popliteal cysts with ultrasound. J Rheumatol 1976; 3: 134-9.

101. Carpenter JR, Hattery RR, Hunder GG, Bryan RS, McLeod RA. Ultrasound evaluation of the popliteal space: comparison with artrography and physical examination Mayo Clin Proc 1976; 51: 498-503.

102. Cooperberg PL, Tsang IT, Truelove L, Knickerbocker WJ. Gray scale ultrasound in the evaluation of rheumatoid arthritis of the knee. Radiology 1978; 126: 759-63.

103. Cheung Y, Rosenberg ZS, Magee T, Chinitz L. Normal anatomy and pathologic conditions of ankle tendons: current imaging techniques. Radiographics 1992; 12: 429-44.

104. Koski JM. Ultrasonography of the metatarsophalangeal and talocrural joints. Clin Exp Rheumatol 1990; 8:347-51.

105. Stephenson CA, Seibert JJ, McAndrew MP, Glasier CM, Leithiser RE Jr, Igbal V. Sonographic diagnosis of tenosynovitis of the posterior tibial tendon. J Clin Ultrasound 1990; 18:114-6.

106. Dillehay GL, Deschler T, Rogers LF, Neiman HL, Hendrix RW. The ultrasonographic characterization of tendons. Invest Radiol 1984; 19 : 338-41.

107. Crass JR, van de Vegte GL, Harkavy LA. Tendon echogenicity: ex vivo study. Radiology 1988; 167: 499-501.

108. Fornage BD, Rifkin MD. Ultrasound examination of tendons. Radiol Clin North Am 1988; 26: 87-107.

109. Grassi W, Filipucci E, Farina A, Cervini C. Sonographic imaging of tendons. Arthritis Rheum 2000; 43: 969-76.

110. Martinoli C, Bianchi S, Dahmane M, Pugliese F, Bianchi-Zamorani MP, Valle M. Ultrasound of tendons and nerves. Eur Radiol 2002; 12: 44-55.

111. Aisen AM, McCune WJ, MacGuire A et al. Sonographic evaluation of the cartilage of the knee. Radiology 1984; 153: 781-4.

112. McCune WJ, Dedrick DK, Aisen AM, MacGuire A. Sonographic evaluation of osteoarthritic femoral condylar cartilage. Correlation with operative findings. Clin Orthop 1990; 254 :230-5.

113. Martel W, Adler RS, Chan K, Niklason L, Helvie MA, Jonsson K. Overview: new methods in imaging osteoarthritis. J Rheumatol Suppl. 1991; 27:32-7.

114. Iagnocco A, Coari G, Zoppini A. Sonographic evaluation of femoral condylar cartilage in osteoarthritis and rheumatoid arthritis. Scand J Rheumatol 1992; 21: 201-3.

115. Adler RS, Dedrick DK, Laing TJ et al. Quantitative assessment of cartilage surface roughness in osteoarthritis using high frequency ultrasound. Ultrasound Med Biol 1992; 18: 51-8.

116. Jonsson K, Buckwalter K, Helvie M, Niklason L, Martel W. Precision of hyaline cartilage thickness measurements. Acta Radiol 1992; 33: 234-9.

117. Martino F, Ettore GC, Angelelli G et al. Validity of echographic evaluation of cartilage in gonarthrosis. Preliminary report. Clin Rheumatol 1993; 12: 178-83.

118. Martino F, Ettore GC, Patella V et al. Articular cartilage echography as a criterion of the evolution of osteoarthritis of the knee. Int J Clin Pharmacol Res 1993; 13: Suppl:35-42.

119. Hodler J, Resnick D. Current status of imaging of articular cartilage. Skeletal Radiol 1996; 25: 703-9.

120. Grassi W, Lamana G, Farina A, Cervini C. Sonographic imaging of normal and osteoarthritic cartilage. Semin Arthritis Rheum. 1999; 28: 398-403.

121. Monteforte P, Rovetta G. Sonographic assessment of soft tissue alterations in osteoarthritis of the knee. Int J Tissue React 1999; 21:19-23.

122. Graf R. Classification of hip joint dysplasia by means of sonography. Arch Orthop Trauma Surg 1984; 102: 248-55.

123. Harcke HT, Clarke NMP, Lee MS, Borns PF, MacEwan GD. Examination of the infant hip with real-time ultrasonography. J Ultrasound Med 1984; 3: 131-7.

124. Fornage BD. Musculoskeletal Ultrasound. New York: Churchill Livingstone, 1995.

125. van Holsbeeck M, Introcaso JH. Musculoskeletal Ultrasound. St. Louis: Mosby-Year Book, 1991.

126. Swen WA, Jacobs JW, Algra PR, Manoliu RA, Rijkmans J, Willems WJ, Bijlsma JW. Sonography and magnetic resonance imaging equivalent for

the assessment of full-thickness rotator cuff tears. Arthritis Rheum 1999; 42: 2231-8.

127. Backhaus M, Kamradt T, Sandrock D et al. Arthritis of the finger joints: a comprehensive approach comparing conventional radiography, scintigraphy, ultrasound, and contrast- enhanced magnetic resonance imaging. Arthritis Rheum 1999; 42: 1232-45.

128. Wakefield RJ, Gibbon WW, Conaghan PG et al. The value of sonography in the detection of bone erosions in patients with rheumatoid arthritis: a comparison with conventional radiography. Arthritis Rheum 2000; 43: 2762-70.

129. Middleton WD, Reinus WR, Melson GL, Totty WG, Murphy WA. Pitfalls of rotator cuff sonography. AJR Am J Roentgenol 1986; 146: 555-60.

130. Mack LA, Nyberg DA, Matsen FA III. Sonographic evaluation of the rotator cuff. Radiol Clin North Am 1988; 26:161-77.

131. Hall FM. Sonography of the shoulder. Radiology 1989; 173:310.

132. Brandt TD, Cardone BW, Grant TH, Post M, Weiss CA. Rotator cuff sonography: a reassessment. Radiology 1989; 173: 323-7.

133. Burk DL Jr, Karasick D, Kurtz AB et al. Rotator cuff tears: prospective comparison of MR imaging with arthrography, sonography, and surgery. AJR Am J Roentgenol 1989; 153:87-92.

134. Soble MG, Kaye AD, Guay RC. Rotator cuff tear: clinical experience with sonographic detection. Radiology 1989; 173: 319-21.

135. Hodler J, Terrier B, von Schulthess GK, Fuchs WA. MRI and sonography of the shoulder. Clin Radiol 1991; 43:323-7.

136. Jacobson JA, van Holsbeeck MT. Musculoskeletal ultrasonography. Orthop Clin North Am 1998; 29:135-67.

137. Hau M, Schultz H, Tony H-P et al. Evaluation of pannus and vascularization of the metacarpophalangeal and proximal interphalangeal joints in rheumatoid arthritis by high resolution ultrasound (multidimensional linear array). Arthritis Rheum 1999; 42: 2303-8.

138. Lehtinen A, Taavitsainen M, Leirisalo-Repo M. Sonographic analysis of enthesopathy in the lower extremities of patients with spondylarthropathy. Clin Exp Rheumatol 1994; 12: 143-8.

139. Lehtinen A, Leirisalo-Repo M, Taavitsainen M. Persistence of enthesopathic changes in patients with spondylarthropathy during a 6-month follow-up. Clin Exp Rheumatol 1995; 13: 733-6.

140. Galluzzo E, Lischi DM, Taglione E et al. Sonographic analysis of the ankle in patients with psoriatic arthritis. Scand J Rheumatol 2000; 29: 52-5.

141. Erickson SJ. High-resolution imaging of the musculoskeletal system. Radiology 1997; 205:593-618.

142. Hentz VR, Green PS, Ariditi M. Imaging studies of the cadaver hand using transmission ultrasound. Skeletal Radiol 1987;16:474-80.

143. Sakai F, Sone S, Kiyono K et al. High resolution ultrasound of the chest wall. Rofo Fortschr Geb Rontgenstr Neuen Bildgeb Verfahr 1990;153: 390-4.

144. King AD, Hine AL, McDonald C, Abrahams P. The ultrasound appearance of the normal psoas muscle. Clin Radiol 1993; 48:316-8.

145. Milz P,Milz S, Putz R, Reiser M. 13 MHz high-frequency sonography of the lateral ankle joint ligaments and the tibiofibular syndesmosis in anatomic specimens. J Ultrasound Med 1996;15: 277-84.

146. Buchberger W. Radiologic imaging of the carpal tunnel. Eur J Radiol 1997; 25: 112-7.

147. Starok M, Lenchik L, Trudell D, Resnick D. Normal patellar retinaculum: MR and sonographic imaging with cadaveric correlation. AJR Am J Roentgenol 1997; 168: 1493-9.

148. Bachmann GF, Melzer C, Heinrichs CM, Mohring B, Rominger MB. Diagnosis of rotator cuff lesions: comparison of US and MRI on 38 joint specimens. Eur Radiol 1997; 7:192-7.

149. Jacobson JA, Andersen R, Jaovisidha S et al. Detection of ankle effusions: comparison study in cadavers using radiography, sonography, and MR imaging. AJR Am J Roentgenol 1998; 170:1231-8.

150. De Maeseneer M, Lenchik L, Starok M, Pedowitz R, Trudell D, Resnick D. Normal and abnormal medial meniscocapsular structures: MR imaging and sonography in cadavers. AJR Am J Roentgenol 1998; 171: 969-76.

151. De Maeseneer M, Jacobson JA, Jaovisidha S et al. Elbow effusions: distribution of joint fluid with flexion and extension and imaging implications. Invest Radiol 1998; 33:117-25.

152. Hauger O, Chung CB, Lektrakul N et al. Pulley system in the fingers: normal anatomy and simulated lesions in cadavers at MR imaging, CT, and US with and without contrast material distention of the tendon sheath. Radiology 2000; 217: 201-12.

153. Chleboun GS, France AR, Crill MT, Braddock HK, Howell JN. In vivo measurement of fascicle length and pennation angle of the human biceps femoris muscle. Cells Tissues Organs 2001; 169: 401-9.

154. Kamolz LP, Schrogendorfer KF, Rab M, Girsch W, Gruber H, Frey M. The precision of ultrasound imaging and its relevance for carpal tunnel syndrome. Surg Radiol Anat 2001; 23: 117-21.

155. Sattler H, Harland U. Arthrosonography. Berlin: Springer-Verlag, 1990.

156. Dondelinger RF. Peripheral Musculoskeletal Ultrasound Atlas. Stuttgart: Georg Thieme Verlag, 1996.

157. Gibbon WW. Musculoskeletal Ultrasound: The Essentials. London: Greenwich Medical Media, 1996.

158. Chhem RK, Cardinal E. Guidelines and Gamuts in Musculoskeletal Ultrasound. New York: John Wiley & Sons, 1999.

159. van Holsbeeck M, Introcaso JH. Musculoskeletal Ultrasound 2ed, St. Louis: Mosby-Year Book, 1999.

160. IFAA (International Federation of Associations of Anatomists) – FCAT (Federative Comimittee on Anatomical Terminology). Teminologia Anatomica, Stuttgart: Georg Thieme Verlag, 1998.

161. Backhaus M, Burmester GR, Gerber T et al. Guidelines for musculoskeletal ultrasound in rheumatology. Ann Rheum Dis 2001; 641-9.

162. Ophir J, Garra B, Kallel F et al. Elastographic imaging. Ultrasound Med Biol 2000; 26: Suppl 1, S23-S29.

163. Resnick D. Diagnosis of bone and joint disorders. Philadelphia: Saunders, 1995.

164. Bland JM, Altman DG. Measurement error. BMJ 1996; 313:744.

165. Bland JM, Altman DG. Statistical methods for assessing agreement between two methods of clinical measurement. Lancet 1986; 1:307-10.

166. Manger B, Kalden JR. Joint and connective tissue ultrasonography- a rheumatologic bedside procedure? Arthritis Rheum 1995; 38:736-42.

167. Balint P, Sturrock RD. Musculoskeletal ultrasound imaging: a new diagnostic tool for the rheumatologist? Br J Rheumatol 1997; 36:1141-2.

168. Grassi W, Cervini C. Ultrasonography in rheumatology: an evolving technique. Ann Rheum Dis 1998; 57: 268-71.

169. Wakefield RJ, Gibbon WW, Emery P. The current status of ultrasonography in rheumatology. Rheumatology 1999; 38:195-8.

170. Castriota-Scanderberg A, De Micheli V, Scarale MG, Bonetti MG, Cammisa M. Precision of sonographic measurement of articular cartilage: inter- and intraobserver analysis. Skeletal Radiol 1996; 25: 545-9.

171. McGonagle, D, Khan MA, Marzo-Ortega H, O'Connor P, Gibbon W, Emery P. Enthesitis in spondyloarthropathy. Curr Opin Rheumatol 1999; 11: 244-50.

172. Olivieri I, Barozzi L, Padula A. Enthesiopathy: clinical manifestations, imaging and treatment. Baillière`s Clin Rheumatol 1998; 12: 665-81.

173. Cruickshank B. Pathology of ankylosing spondylitis. Clin Orthop 1971; 74: 43-58.

174. Ball J. Enthesopathy of rheumatoid and ankylosing spondylitis. Ann Rheum Dis 1971; 30: 213-23.

175. McGonagle D, Gibbon W, Emery P. Classification of inflammatory arthritis by enthesitis. Lancet 1998; 352: 1137-40.

176. McGonagle D, Gibbon W, O'Connor P, Green M, Pease C, Emery P. Characteristic magnetic resonance imaging entheseal changes of knee synovitis in spondylarthropathy. Arthritis Rheum 1998; 41: 694-700.

177. Mander M., Simpson JM, McLellan A, Walker D, Goodacre JA, Dick CW. Studies with an enthesis index as a method of clinical assessment in ankylosing spondylitis. Ann Rheum Dis 1987; 46: 197-202.

178. Dawes PT, Sheeran TP, Beswick EJ, Hothersall TE. Enthesopathy index in ankylosing spondylitis. Ann Rheum Dis 1987; 46: 717.

179. Resnick D, Niwayama G. Entheses and enthesopathy. Anatomical, pathological, and radiological correlation. Radiology 1983; 146: 1-9.

180. Kenny JB, Hughes PL, Whitehouse GH. Discovertebral destruction in ankylosing spondylitis: the role of computed tomography and magnetic resonance imaging. Br J Radiol 1990; 63: 448-55.

181. Calin A, Mackay K, Santos H, Brophy S. A new dimension to outcome: application of the Bath Ankylosing Spondylitis Radiology Index. J Rheumatol 1999; 26: 988-92.

182. Secundini R, Scheines EJ, Gusis SE, Riopedre AM, Citera G, Maldonado Cocco JA. Clinico-radiological correlation of enthesitis in seronegative spondyloarthropathies (SNSA). Clin Rheumatol 1997; 16: 129-32.

183. Roberts CS, King DH, Goldsmith LJ. A statistical analysis of the accuracy of sonography of the patellar tendon. Arthroscopy 1999; 15: 388-91.

184. Olivieri I, Barozzi L, Padula A et al. Retrocalcaneal bursitis in spondyloarthropathy: assessment by ultrasonography and magnetic resonance imaging. J Rheumatol 1998; 25: 1352-7.

185. Gibbon WW, Long G. Ultrasound of the plantar aponeurosis (fascia). Skeletal Radiol 1999; 28: 21-6.

186. Dougados M, van der Linden S, Juhlin R et al. The European Spondylarthropathy Study Group preliminary criteria for the classification of spondylarthropathy. Arthritis Rheum 1991; 34: 1218-27.

187. Balint PV, Sturrock RD. Intraobserver repeatability and interobserver

reproducibility in musculoskeletal ultrasound imaging measurements. Clin Exp Rheumatol 2001; 19: 89-92.

188. Gerster JC. Plantar fasciitis and Achilles tendinitis among 150 cases of seronegative spondarthritis. Rheumatol Rehabil 1980; 19: 218-22.

189. Fornage BD. The hypoechoic normal tendon. A pitfall. J Ultrasound Med 1987; 6: 19-22.

190. Balint PV, Sturrock RD. Inflamed retrocalcaneal bursa and Achilles tendonitis in psoriatic arthritis demonstrated by ultrasonography. Ann Rheum Dis 2000; 59: 931-3.

191. van der Heijde D, Bellamy N, Calin A, Dougados M, Khan MA, van der Linden S. Preliminary Core sets for endpoints in ankylosing spondylitis. J Rheumatol 1997; 24: 2225-9

192. Clegg DO, Reda DJ, Abdellatif M. Comparison of sulfasalazine and placebo for the treatment of axial and peripheral articular manifestations of the seronegative spondylarthropathies: a Department of Veterans Affairs cooperative study. Arthritis Rheum 1999; 42: 2325-9.

193. Brandt J, Haibel H, Cornely D, Golder W, Gonzalez J, Reddig J, et

al. Succesful treatment of active ankylosing spondylitis with the anti tumor necrosis factor alpha monoclonal antibody infliximab. Arthritis Rheum 2000; 43: 1346-52.

194. van den Bosch F, Kruithof E, Baeten D, De Keyser F, Mielants H, Veys EM. Effects of a loading dose regimen of three infusions of chimeric monoclonal antibody to tumour necrosis factor alpha (infliximab) in spondyloarthropathy: an open pilot study. Ann Rheum Dis 2000; 59: 428-33.

195. Karjalainen PT, Soila K, Aronen HJ et al. MR imaging of overuse injuries of the Achilles tendon. AJR Am J Roentgenol 2000; 175:251-60

196. Spiegel TM, King W 3rd, Weiner SR, Paulus HE. Measuring disease activity: comparison of joint tenderness, swelling, and ultrasonography in rheumatoid arthritis. Arthritis Rheum 1987; 30: 1283-8.

197. Daunt AO, Cox NL, Robertson JC, Cawley MI. Indices of disease activity in psoriatic arthritis. J R Soc Med 1987; 80: 556-8.

198. D'Agostino MA, Breban M, Said-Nahal M, Dougados M. Refractory inflammatory heel pain in spondylarthropathy: a significant response to infliximab documented by ultrasound. Arthritis Rheum 2002; 46: 840-1.

199. Resnick D. Common disorders of synovium-lined joints: pathogenesis, imaging abnormalities and complications. AJR Am J Roentgenol 1988; 151: 1079-93.

200. Wilke WS, Sweeney TJ, Calabrese LH. Early, aggresive therapy for rheumatoid arthritis: concerns, descriptions and estimate of outcome. Semin Arthritis Rheum 1993; Suppl 1, 26-41.

201. Østergaard M, Stoltenberg M, Løvgreen-Nielsen P, Volck B, Sonne-Holm S, Lorenzen I. Quantification of synovitis by MRI: correlation between dynamic and static gadolinium-enhanced magnetic resonance imaging and microscopic signs of synovial inflammation. Magn Reson Imaging 1998; 16: 743-54.

202. Sugimoto H, Takeda A, Hyodoh K. Early-stage rheumatoid arthritis: prospective study of the effectiveness of MR imaging for diagnosis. Radiology 2000; 216: 569-75.

203. Sugimoto H, Takeda A, Masuyama J, Furuse M. Early-stage rheumatoid arthritis: diagnostic accuracy of MR imaging. Radiology 1996; 198: 185-92.

204. Grassi W, Tittarelli E, Blasetti P, Pirani O, Cervini C. Finger tendon involvement in rheumatoid arthritis. Arthritis Rheum 1995; 38: 786-94.

205. Rubin JM, Bude RO, Carson PL, Bree RL, Alder RS. Power Doppler US: a potentially useful alternative to mean frequency-based Color Doppler US. Radiology 1994; 190: 853-6.

206. Wårdell K, Jakobsson A, Nilsson GE. Laser Doppler perfusion imaging by dynamic light scattering. IEEE Trans Biomed Eng 1993; 40: 309-16.

207. Anderson RR, Parrish MD. The optics of human skin. J. Invest Dermatol. 1981; 77: 13-9.

208. Ferrell WR, Sturrock RD, Mallik AK, Abbot NC, Lockhart JC, Edmondson WD. Laser Doppler perfusion imaging of proximal interphalangeal joints in patients with rheumatoid arthritis. Clin Exp Rheumatol 1996; 14: 649-52.

209. Arnett FC, Edworthy SM, Bloch DA, McShane DJ, Fries JF, Cooper NS et al. The American Rheumatism Association 1987 revised criteria for the classification of rheumatoid arthritis. Arthritis Rheum 1988; 31:315-24.

210. Owsianik WD, Kundi A, Whitehead JN, Kraag GR, Goldsmith C. Radiological articular involvement in the dominant hand in rheumatoid arthritis. Ann Rheum Dis 1980; 39: 508-10.

211. Fitzgerald O, Soden M, Yanni G, Robinson R, Bresnihan B. Morphometric analysis of blood vessels in synovial membranes obtained from clinically affected and unaffected knee joints of patients with rheumatoid arthritis. Ann Rheum Dis 1991; 50: 792-26.

212. Lockhart JC, Ferrell WR, Angerson WJ. Laser Doppler perfusion imaging of synovial tissues at red and near infrared lasers. Int J Microcirc Clin Expt 1997; 17: 130-7.

213. Stone M, Bergin D, Whelan B, Maher M, Murray J, McCarthy C. Power Doppler ultrasound assessment of rheumatoid hand synovitis. J Rheumatol 2001; 28:1979-82.

214. Szkudlarek M, Court-Payen M, Strandberg C, Klarlund M, Klausen T, Østergaard M. Power Doppler ultrasonography for assessment of synovitis in the metacarpophalangeal joints of patients with rheumatoid arthritis: a comparison with dynamic magnetic resonance imaging. Arthritis Rheum 2001; 44: 2018-23.

215. Qvistgaard E, Rogind H, Torp-Pedersen S, Terslev L, Danneskiold-Samsøe B, Bliddal H. Quantitative ultrasonography in rheumatoid arthritis: evaluation of inflammation by Doppler technique. Ann Rheum Dis 2001; 60: 690-3.

216. Magarelli N, Guglielmi G, Di Matteo L, Tartaro A, Mattei PA, Bonomo L. Diagnostic utility of an echo-contrast agent in patients with synovitis using power Doppler ultrasound: a preliminary study with comparison to contrast-enhanced MRI. Eur Radiol 2001; 11: 1039-46.

217. Klauser A, Frausher F, Schirmer M et al. The value of contrast-enhanced color Doppler ultrasound in the detection of vascularization of finger joints in patients with rheumatoid arthritis. Arthritis Rheum 2002; 46: 647-53.

218. Schmidt WA, Völker L, Zacher J, Schläfke M, Ruhnke M, Gromnica-Ihle E. Colour Doppler ultrasonography to detect pannus in knee joint synovitis. Clin Exp Rheumatol 2000; 18; 439-44.

219. Shahin AA, el-Mofty SA, el-Sheikh EA, Hafez HA, Ragab OM. Power Doppler sonography in the evaluation and follow-up of knee involvement in patients with juvenile idiopathic arthritis. Z Rheumatol 2001; 60:148-55.

220. Doria AS, Kiss MHB, Lotito APN et al. Juvenile rheumatoid arthritis of the knee: evaluation with contrast-enhanced color Doppler ultrasound. Pediatr Radiol 2001; 31:524-31.

221. Giovagnorio F, Martinoli C, Coari G. Power Doppler sonography in knee arthritis –a pilot study. Rheumatol Int 2001; 20: 101-4.

222. Walther M, Harms H, Krenn V, Radke S, Faehndrich TP, Gohlke F. Correlation of power Doppler sonography with vascularity of the synovial tissue of the knee joint in patients with osteoarthritis and rheumatoid arthritis. Arthritis Rheum 2001; 44: 331-8.

223. Röntgen WC. Über eine neue Art von Strahlen. Sitzungsberichte der Physikalisch-medizinischen Gesellschaft zu Würzburg 1895; 9: 132-41.

224. Maxfield WS, Weiss TE. Technetium-99m joints images. Radiology 1969; 92:1461-6.

225. Gershon-Cohen J, Haberman-Brueschke JA, Brueschke EE. Medical thermography: a summary of current status. Radiol Clin North Am 1965; 3: 403-31.

226. Zucker-Pinchoff B, Hermann G, Srinivasen R. Computed tomography of the carpal-tunnel: a radioanatomical study. J Comput Assist Tomogr 1981; 5: 525-8.

227. Weiss KL, Beltran J, Shamam OM, Stilla RF, Levey M. High-field MR surface-coil imaging of the hand and wrist. Part I. Normal Anatomy. Radiology 1986; 160:143-6.

228. Fornage BD, Schernberg FL, Rifkin MD. Ultrasound examination of the hand. Radiology 1985; 155:785-8.

229. Griffith JF, Rainer TH, Ching AS, Law KL, Cocks RA, Metreweli C. Sonography compared with radiography in revealing acute rib fracture. AJR Am J Roentgenol 1999; 173: 1603-9.

230. Farlow R, Hayward G. Real-time ultrasonic techniques suitable for implementing non-contact NDT systems employing piezoceramic composite transducers. Insight 1994; 36: 926-35.

231. Rogovsky AJ. Development and application of ultrasonic dry contact and air contact C-scan systems for non-destructive evaluation of aerospace components. Mater Eval 1991; 763-6.

232. Kelly SP. An Air-Coupled Ultrasonic Array Scanning System for Rapid Through Transmission NDT. PhD Thesis, University of Strathclyde, 2000.

233. Hayward G, Gachagan A. An evaluation of 1-3 connectivity composite transducers for air-coupled ultrasonic applications. J Acoust Soc Am 1996; 99: 2148-57.

234. Gachagan A, Hayward G, Kelly SP, Galbraith W. Characterisation of air-coupled transducers. IEEE T Ultrason Ferr 1996; 43: 678-88.

235. Kelly SP, Hayward G, Gomez TE. An air-coupled ultrasonic matching layer employing half wavelength cavity resonance. Proceedings of IEEE Ultrasonics Symposium, Atlanta, 2001.

236. Lentle B, Aldrich J. Radiological sciences, past, present. Lancet 1997; 350: 280-5.

237. Prevoo ML, van Riel PL, van't Hof MA et al. Validity and reliability of joint indices. A longitudinal study in patients with recent onset rheumatoid arthritis. Br J Rheumatol 1993; 32: 589-94.

238. Petrie A, Sabin C. Medical statistics at a glance. Blackwell Science, 2000.

239. Altman DG, Bland JM. Measurement in medicine: the analysis of method comparison studies. Statistician 1983;32: 307-17.

240. British Standard Institution. Precision of test methods I: Guide for the determination of repeatability and reproducibility for a standard test method. 1979; BS 5497, part 1.London.

241. Kanters SDJM, Algra A, van Leeuwen MS, Banga JD. Reproducibility of in vivo carotid intima-media thickness measurements. Stroke 1997; 28:665-71.

242. Philips DS. Basic statistics for health science students. W.H. Freeman and Company, New York, 1978; 54-5.

Appendix A: Statistical equations and terminology

Binary variable: A categorical variable with two categories, also called as a dichotomous variable (238).

Bland-Altman analysis: Graphic technique to assess the agreement between two methods plotting the differences against their means (239,165).

British Standard Institution repeatability coefficient: Assuming a Normal distribution of measurement differences, we expect approximately 95% of the differences in the population to lie between $\bar{d} \pm 2_{sd}$. The upper and lower limits of this interval are called the limits of agreement (240).

where: $\bar{d}$ = mean difference

s_d = standard deviation of the differences

Categorical variable: Each individual belongs to one of a number of distinct categories of the variable (238).

Chi squared (χ^2) test: Used on frequency data. It tests the null hypothesis that there is no association between the factors that define a contingency table. Also used to test differences in proportions (238). Chi squared (χ^2) test requires at least 5 in each cells of expected frequency otherwise in case of smaller frequencies we need to use Fisher's exact test.

$$\chi 2 = \sum \frac{\left(\left| O - E \right| - \frac{1}{2} \right)}{E}$$

where: O = observed frequencies

E = expected frequencies

$\left| \right|$ = around O and E indicate that we ignore its sign

If the expected and the observed frequencies are equal means that are null hypothesis is true (238).

Cohen's kappa (κ) test: A measure of agreement between two sets of categorical measurements on the same individuals. If $\kappa = 1$ there is perfect agreement; if $\kappa = 0$, there is no better than chance agreement (238).

$$K = \frac{\left(\frac{O_d}{m} - \frac{E_d}{m} \right)}{\left(1 - \frac{E_d}{m} \right)}$$

where: m = total observed frequency

O_d = the sum of observed frequencies along the diagonal in the contingency table where observers agree.

E_d = the sum of expected frequencies along the diagonal in the contingency table where observers agree.

1 = in the denominator represents maximum agreement

Contingency table: Usually a two-way table in which the entries are the observed frequencies. They occupy the four inner cells. The total frequencies for the two row categories and those for the columns are shown at the right and at the foot, and are called marginal totals. The sum of the four marginal totals is the overall total (238).

Characteristic	e.g. Group 1	e.g. Group 2	Marginal totals
e.g. Present	a	b	a + b
e.g. Absent	c	d	c + d
Marginal totals	n_1= a + c	n_2 = b + d	n = a + b + c +d

a, b, c, d are the observed frequencies. We can calculate the proportions with characteristic as $p_1 = a/n_1$, $p_2 = b/n_2$, $p = a + b/n$ and from the observed frequencies we can calculate the expected frequencies as

$\frac{(a+c)\times(a+b)}{(a+b+c+d)}$ for the "a" cell, $\frac{(b+d)\times(a+b)}{(a+b+c+d)}$ for the "b" cell,

$$\frac{(a+c)\times(c+d)}{(a+b+c+d)}$$ for the "c" cell, $$\frac{(b+d)\times(c+d)}{(a+b+c+d)}$$ for the "d" cell.

Continuous variable: A numerical variable in which there is no limitation on the values that the variable can take other than that restricted by the degree of accuracy of the measuring technique (238).

Mean (arithmetic mean) value: A measure of location obtained by dividing the sum of the observations by the number of observations (238).

$$\bar{x} = \frac{x_1 + x_2 + x_3 + \ldots + x_n}{n}$$

Where: $\bar{x}$ = mean

$x_1, x_2\ x_3 \ldots x_n$ = observed values

n = set of observation

Median value: A measure of location that is the middle value of the ordered observations (238).

Measurement error: Repeated measurements on the same subjects varies around the true value because of measurement error. The difference between two measurements for the same subject is expected to be less than 2.77 x the within-subject standard deviation (s_w) for the 95% of pairs of observations (164).

Negative predictive value: The proportion of individuals with a negative test result who do not have the disease (238).

From the 2x2 table of frequencies:

$$\text{Negative predictive value} = \frac{d}{(c+d)}$$

Nominal variable: A categorical variable whose categories have no natural ordering (238).

Normal (Gaussian) distribution: A continuous probability distribution that is bell-shaped and symmetrical; its parameters are the mean and variance (238).

Null hypothesis (H_0): The statement that assumes no effect in the population (238).

P value: The probability of obtaining our results, or something more extreme, if the null hypothesis is true (238).

Paired observations (or data): Relate to responses from matched individuals or the same individual in two different circumstances (238).

Paired t-test: Tests the null hypothesis that the mean of a set of differences of paired observations is equal to zero (238).

$$t = \frac{(\bar{d} - 0)}{SE(\bar{d})} = \frac{\bar{d}}{s_d/\sqrt{n}}$$

Where n = sample size, must be same in the two samples

$\bar{d}$ = mean differences of variables

s_d = standard deviation of differences

SE = standard error

t = value of the paired t-test which follows the t-distribution with (n-1) degrees of freedom

Pearson's product moment correlation coefficient (r): A quantitative measure, ranging between –1 and +1, of the extent to which points in a scatter diagram conform to a straight line. This coefficient measurers only the strength of association between two variables and does not provide information about their concordance therefore does not measure the agreement between them. We will have perfect agreement only if the points lie along the line of equality, but we will have perfect correlation if the points lie along any straight line. A change in scale of measurement does not affect the correlation, but certainly affects the agreement. (165, 238 - 239).

$$r = \frac{\sum (x - \bar{x})(y - \bar{y})}{\sqrt{\sum (x - \bar{x})^2 \sum (y - \bar{y})^2}}$$

where: r = correlation coefficient

x and y = pair of values (x = variable on the horizontal axis, y = variable on the vertical axis)

$\bar{x}$ = mean of x

$\bar{y}$ = mean of y

Percent error: It is possible to express intraobserver error with discrepancies from their means in percentages. The difference of the higher value and the lower value divided by the lower value multiplied by 100 gives the individual percent error (241).

Positive predictive value: The proportion of individuals with a positive diagnostic test result who have the disease (238).

From the 2x2 table of frequencies:

$$\text{Positive predictive value} = \frac{a}{(a+b)}$$

Point biserial correlation coefficient (r_{pb}): The point correlation is used when one variable is continuous and the other variable is true dichotomy (242).

$$r_{pb} = \frac{\bar{X}p - \bar{X}t}{St} \sqrt{\frac{N_p N_t}{N_0 (N_t - 1)}}$$

where: $\bar{x}_p$ = mean area of exposure

$\bar{x}_t$ = mean area of exposure of all

s_t = standard deviation of area of exposure

N_p = number of exposed

N_0 = number of not exposed

$N_t = N_p + N_0$

r_{pb} = point biserial correlation coefficient

Power: The probability of rejecting the null hypothesis when it is false (238).

Power calculations (sample size calculation)

$$n = \frac{\left(\delta_1^2 + \delta_2^2\right) x \left(Z_{1-\alpha/2} + Z_{1-\beta}\right)}{D^2}$$

where: Z = standard normal distribution,

Z_1 = standard normal distribution in group 1

Z_2 = standard normal distribution in group 2

α = probability of Type I error (usually .05)

β = probability of Type II error (usually between .05 and .20

σ = standard deviation

σ_1 = standard deviation in group 1

σ_2 = standard deviation in group2

D = clinically relevant difference

n = calculated sample size in each group

(238)

Repeatability: The extent to which repeated measurements by the same observer in identical conditions agree (238).

Reproducibility: The extent to which the same results can be obtained in different circumstances, e.g. by two methods of measurement, or by two observers (238).

Sensitivity: The proportion of individuals with the disease who are correctly diagnosed by the test (238).

From the 2x2 table of frequencies:

$$\text{Sensitivity} = \frac{a}{(a + c)}$$

Specificity: The proportion of individuals without the disease who are correctly identified by a diagnostic test (238).

From the 2x2 table of frequencies:

$$\text{Specificity} = \frac{d}{(b + d))}$$

Standard deviation (SD): A measure of spread equal to the square root of the variance (238).

$$s = \sqrt{\frac{\sum \left(x_i - \bar{x}\right)^2}{n-1}}$$

where: s = standard deviation

x_i = values from i = 1 to n

$\bar{x}$ = mean

n = sample size

Standard error of the mean (SEM): A measure of precision of the sample mean. It is the standard deviation of the sampling distribution of the mean (238).

$$SEM = \frac{s}{\sqrt{n}}$$

where: s = standard deviation

n = number of observations

t- distibution: A continuous distribution whose shape is similar to the normal distribution and that is characterized by its degrees of freedom (238).

Type I error: Rejection of the null hypothesis when it is true (238).

Type II error: Non-rejection of the null hypothesis when it is false (238).

Unpaired (two-sample) t-test: Tests the null hypothesis that two means from independent groups are equal (238).

$$s = \sqrt{\frac{(n_1 - 1)s_1^2 + (n_2 - 1)s_2^2}{n_1 + n_2 - 2}}$$

$$t = \frac{(\bar{x}_1 - \bar{x}_2) - 0}{SE(\bar{x}_1 - \bar{x}_2)} = \frac{(\bar{x}_1 - \bar{x}_2)}{s\sqrt{\frac{1}{n_1} + \frac{1}{n_2}}}$$

Where n_1 = sample size of the first group

n_2 = sample size of the second group

x_1 = means of the first group variables

x_2 = means of the second group variables

s = is an estimate of the pooled standard deviation of the two groups

SE = standard error

t = value of the unpaired t-test which follows the t-distribution with (n_1 + n_2-2)

degrees of freedom

Variable: Any quantity that varies.

Variance: A measure of spread equal to the square of the standard deviation (238).

$$s^2 = \frac{\sum \left(x_i - \bar{x}\right)^2}{n-1}$$

Where: x_i = values from i = 1 to n

$\bar{x}$ = mean

n = sample size

Within-subject standard deviation (s_w): It is the common standard deviation of repeated measurements. Calculating s_w we need to average the variances, the squares of the standard deviations. To show that the standard deviation is unrelated to the magnitude of the measurement need to plot the individual subject's standard deviations against their means (164).